Doctoral Thesis

STRUCTURAL STUDIES OF ENDOPLASMIC RETICULUM-MITOCHONDRIA ENCOUNTER STRUCTURE (ERMES) COMPLEX

Hanbin Jeong

Department of Biological Sciences

Graduate School of UNIST

2019

STRUCTURAL STUDIES OF ENDOPLASMIC RETICULUM-MITOCHONDRIA ENCOUNTER STRUCTURE (ERMES) COMPLEX

Hanbin Jeong

Department of Biological Sciences

Graduate School of UNIST

STRUCTURAL STUDIES OF ENDOPLASMIC RETICULUM-MITOCHONDRIA ENCOUNTER STRUCTURE (ERMES) COMPLEX

A thesis/dissertation
Submitted to the Graduate School of UNIST
in partial fulfillment of the
requirements for the degree of
Doctor of Philosophy

Hanbin Jeong

12 / 11 / 2018 of submission
Approved by

Advisor
Changwook Lee

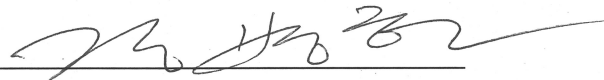# STRUCTURAL STUDIES OF ENDOPLASMIC RETICULUM-MITOCHONDRIA ENCOUNTER STRUCTURE (ERMES) COMPLEX

Hanbin Jeong

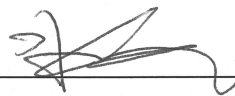This certifies that the thesis/dissertation of Hanbin Jeong is approved.
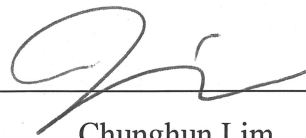
12 / 11 / 2018 of submission

Advisor: Changwook Lee

Byoung Heon Kang

Tae Joo Park

Chunghun Lim

Eunhee Kim

Abstract

The endoplasmic reticulum-mitochondria encounter structure (ERMES) is a protein complex that plays a tethering role in physically connecting ER and mitochondria membranes. The ERMES complex comprises mitochondrial distribution and morphology 12 (Mdm12), maintenance of mitochondrial morphology 1 (Mmm1), Mdm34, and Mdm10 and mediates physical membrane contact sites and nonvesicular lipid trafficking between the ER and mitochondria in yeast. Herein, we report three crystal structures of the synaptotagmin-like mitochondrial lipid-binding protein (SMP) domain of Mdm12, Mmm1, and the Mdm12-Mmm1 complex at 3.1 Å, 2.8 Å, and 3.8 Å resolution, respectively. The Mdm12 forms a dimeric SMP structure through domain swapping of the β1-strand comprising residues 1-7. Biochemical experiments reveal a phospholipid-binding site located along a hydrophobic channel of the Mdm12 structure and that Mdm12 might have a binding preference for glycerophospholipids harboring a positively charged head group. Mmm1 adopts a dimeric SMP structure augmented with two extra structural elements at the N and C termini that are involved in tight self-association and phospholipid coordination. Mmm1 binds two phospholipids inside the hydrophobic cavity, and the phosphate ion of the distal phospholipid is specifically recognized through extensive H-bonds. A positively charged concave surface on the SMP domain not only mediates ER membrane docking but also results in preferential binding to glycerophospholipids such as phosphatidylcholine (PC), phosphatidic acid (PA), phosphatidylglycerol (PG), and phosphatidylserine (PS), some of which are substrates for lipid-modifying enzymes in mitochondria. The Mdm12-Mmm1 structure reveals two Mdm12s binding to the SMP domains of the Mmm1 dimer in a pairwise head-to-tail manner. Direct association of Mmm1 and Mdm12 generates a 210-Å-long continuous hydrophobic tunnel that facilitates phospholipid transport. The Mdm12-Mmm1 complex binds all glycerophospholipids except for phosphatidylethanolamine (PE) in vitro.

Keywords

Crystal structure, Membrane contact site (MCS), ERMES (Endoplasmic reticulum-mitochondria encounter structure) complex, Mdm12 (Mitochondrial distribution and morphology protein 12), Mmm1 (Maintenance of mitochondrial morphology protein 1), Phospholipid trafficking, SMP (Synaptotagmin-like mitochondrial-lipid binding protein) domain

Table of Contents

Chapter 1. Crystal structure of Mdm12 reveals the architecture and dynamic organization of the ERMES complex

Chapter 2. Crystal structure of Mmm1 and Mdm12-Mmm1 reveal mechanistic insight into phospholipid trafficking at ER-mitochondria contact sites

List of Figures

Chapter 1. Crystal structure of Mdm12 reveals the architecture and dynamic organization of the ERMES complex

Chapter 2. Crystal structure of Mmm1 and Mdm12-Mmm1 reveal mechanistic insight into phospholipid trafficking at ER-mitochondria contact sites

List of Tables

Abbreviations

MCS	Membrane contact site
ERMES	Endoplasmic reticulum (ER)-mitochondria encounter structure
Mdm12	Mitochondrial distribution and morphology protein 12
Mdm34	Mitochondrial distribution and morphology protein 34
Mdm10	Mitochondrial distribution and morphology protein 10
Mmm1	Maintenance of mitochondrial morphology protein 1
SMP domain	Synaptotagmin-like mitochondrial-lipid binding protein domain
Gem1	GTPase EF-hand protein of mitochondria 1
TOM complex	Translocase of the outer membrane complex
vCLAMP	Vacuole and mitochondria patches
EMC	Endoplasmic reticulum membrane protein complex
PA	Phosphatidic acid
PC	Phosphatidylcholine
PE	Phosphatidylethanolamine
PG	Phosphatidylglycerol
PS	Phosphatidylserine
TEV protease	Tobacco etch virus protease
NBD	Nitrobenzoxadiazole
IPTG	Isopropyl β-D-1-thiogalactopyranoside
SEC	Size exclusion chromatography
AUC	Analytical ultracentrifugation
APCI-MS	Atmospheric pressure chemical ionization mass spectroscopy
EM	Electron microscopy
SDS-PAGE	Sodium dodecyl sulfate polyacrylamide gel electrophoresis
CN-PAGE	Clear native polyacrylamide gel electrophoresis

BN-PAGE	Blue native polyacrylamide gel electrophoresis
RMSD	Root-mean-square deviation
HEPES	4-(2-hydroxyethyl)-1-piperazineethanesulfonic acid
Se-Met	Selenomethionine
PDB	Protein data bank
MR	Molecular replacement
PEG	Polyethylene glycol
IMAC	Immobilized metal ion affinity chromatography
GST	glutathione S-transferase
MBP	Maltose binding protein
E-SYT2	Extended synaptotagmin 2
CETP	Cholesteryl ester transfer protein
GFP	Green fluorescent protein
DTT	Dithiothreitol
SAD	Single-wavelength anomalous dispersion
LDAO	Lauryldimethylamine N-oxide
BPI	Bactericidal permeability-increasing protein

Chapter 1. Crystal structure of Mdm12 reveals the architecture and dynamic organization of the ERMES complex.

1.1. Abstract

The endoplasmic reticulum–mitochondria encounter structure (ERMES) is a protein complex that plays a tethering role in physically connecting ER and mitochondria membranes. The ERMES complex is composed of Mdm12, Mmm1, and Mdm34, which have a SMP domain in common, and Mdm10. Here, we report the crystal structure of S. cerevisiae Mdm12. The Mdm12 forms a dimeric SMP structure through domain swapping of the β1-strand comprising residues 1–7. Biochemical experiments reveal a phospholipid-binding site located along a hydrophobic channel of the Mdm12 structure and that Mdm12 might have a binding preference for glycerophospholipids harboring a positively charged head group. Strikingly, both full-length Mdm12 and Mdm12 truncated to exclude the disordered region (residues 74–114) display the same organization in the asymmetric unit, although they crystallize as a tetramer and hexamer, respectively. Taken together, these studies provide a novel understanding of the overall organization of SMP domains in the ERMES complex, indicating that Mdm12 interacts with Mdm34 through head-to-head contact, and with Mmm1 through tail-to-tail contact of SMP domains.

1.2. Introduction

Eukaryotic cells are composed of membrane-bound subcellular compartments that play distinct and essential roles for cell survival. The compartments not only work independently, but also they actively cooperate to achieve their ultimate roles. Apart from communication among subcompartments achieved through vesicular trafficking, direct contact sites of subcompartment membranes have been discovered through electron microscopy (EM) [1–3]. Such membrane contact sites (MCSs) are involved in essential processes for cell survival, such as subcellular communications, ion homeostasis, metabolic pathways, and lipid biosynthesis [1–5].

Among several MCSs, ER–mitochondria direct contact sites have been extensively studied in terms of physical tethering of two membranes and their physiological relevancies, such as lipid trafficking and Ca2+ exchange [6–9]. The endoplasmic reticulum–mitochondria encounter structure (ERMES) components were first identified as molecular tethering factors in the formation of ER–mitochondrial junctions using synthetic biology screens in *S. cerevisiae* [10]. The ERMES complex consists of four proteins with different subcellular localizations. Mdm12 (mitochondrial distribution and morphology protein 12) is a soluble protein present in the cytosol, while Mmm1 (maintenance of mitochondrial morphology protein 1) and Mdm34/Mdm10 are integral membrane proteins that are anchored in the ER and mitochondrial outer membranes, respectively. Additionally, Gem1 (GTPase EF-hand protein of mitochondrial 1), a Ca2+-binding Miro GTPase, associates with ERMES and regulates the number, size, and functions of these complexes in yeast [11, 12]. In addition to its primary role in maintaining a close proximity (10–30 nm) between two membranes independently of fusion or fission, the ERMES complex also has been known to function in lipid trafficking to cooperatively synthesize phosphatidylcholine (PC) from phosphatidylserine (PS) in ER and mitochondria junctions [10, 13–15]. However, there is a conflicting report that ERMES and Gem1 do not directly affect PS trafficking [16]. Recently, a couple of redundant pathways for lipid trafficking involved in the maintenance of mitochondrial lipid homeostasis have been reported. For example, the EMC (ER–membrane protein complex) located in the ER tethers a phosphatidylethanolamine (PE) to mitochondria by interacting with a TOM (translocase of the outer membrane) [17]. The vCLAMP (vacuole and mitochondria patch) is another alternative pathway for transferring lipids to the mitochondria [18, 19]. Composite defects in these pathways result in severe disruption of mitochondrial lipid homeostasis. In addition to lipid trafficking, the Mdm12–Mmm1 complex plays an important role in β-barrel assembly of mitochondrial outer membrane proteins, and in the maintenance of mitochondrial morphology and mtDNA [6, 20]. Furthermore, the ERMES complex has been repeatedly implicated in essential activities for cell survival such as mitophagy, inheritance, mtDNA inheritance, and mitochondrial dynamics [12, 21–25].

Primary structure analyses of ERMES components reveal that Mdm12, Mmm1, and Mdm34 share a synaptotagmin-like mitochondrial-lipid-binding protein (SMP) domain, although their sequences are not closely related to each other [13]. In particular, full-length Mdm12 contains SMP domains across its entire sequence, while SMP domains in Mmm1 and Mdm34 account for half of the C-terminus and N-terminus, respectively. The remaining halves of the Mmm1 and Mdm34 protein sequences are predicted to be unstructured and not conserved among species, and the C-terminus of Mdm34 is known to be anchored into the outer mitochondrial membrane [26]. Structural studies demonstrated that the SMP domain adopts a dimer configuration rather than existing solely as a monomer [27–29]. The association of SMP domains might act as the driving force in the assembly of ERMES components and maintain intact membrane proximity. Biochemistry experiments combined with a negative-staining EM structure revealed that Mdm12–Mmm1 forms a hetero-tetramer through the direct association of SMP domains, generating an arch-shaped structure with dimensions of ~210 × 45 × 35 Å [30]. However, despite its importance in ER–mitochondria contact, no high-resolution structures of the ERMES complex are available. Therefore, the molecular details of how the SMP domains in the ERMES complex are organized to tether two organelles, and how ERMES recognizes certain lipids and facilitates their trafficking, remain unknown.

In this study, we determined the crystal structures of full-length Mdm12 and ΔMdm12 (Δ74–114) and elucidated the molecular details of the contact regions for self-association of SMP domains and of lipid coordination in Mdm12. Furthermore, we suggest that two interfaces between SMP domains, head-to-head and tail-to-tail, provide a mechanistic understanding of the assembly and organization of the ERMES tetrameric complex at a molecular level.

1.3. Results

1.3.1. The oligomeric state of full-length Mdm12 and Mmm1

We prepared the Mdm12 protein from *S. cerevisiae* by expression in *E. coli* bacterial cells. Interestingly, the *S. cerevisiae* Mdm12 migrated differently on size-exclusion columns, depending on the presence or absence of N-terminus hexa-histidine (His$_6$) tag plus TEV cleavage site (ENLYFQS) for full-length Mdm12 proteins. Full-length Mdm12 without His$_6$ eluted from the column at a volume corresponding to approximately the mass of the Mdm12 dimer. On the other hand, His6–Mdm12 eluted from the column at a mass corresponding to the Mdm12 monomer (Figure 1.1A and B). The TEV cleavage site existing between His6 tag and Mdm12 was not vulnerable to proteases, suggesting that the N-terminus including the TEV cleavage site of Mdm12 was somehow masked by the protein itself. To further investigate the oligomeric state of Mdm12 and measure the molecular weights in solution, we conducted analytical ultracentrifugation with native Mdm12 and His$_6$-Mdm12 proteins. Consistent with gel-filtration chromatography, Mdm12 and His6-Mdm12 were measured as 58.3 kDa (dimer) and 34.5 kDa (monomer), respectively (Figure 1.1C and Figure 1.2). From this observation, we propose that the N-terminus of Mdm12 could be critically involved in self-association and that the extra amino acid sequences consisting of the His$_6$ tag and TEV cleavage sequence might disturb the dimerization of the protein.

Mmm1 from *S. cerevisiae* was eluted in the void volume fraction during gel-filtration column chromatography, indicating that by itself Mmm1 is aggregated in solution (Figure 1.1B). However, when we co-expressed Mmm1 with Mdm12 in BL21 (DE3) bacterial cells, the complex displayed a monodisperse profile on the gel-filtration column, with an estimated molecular weight of around 200 kDa, suggesting that the Mdm12–Mmm1 complex exists as a hetero-tetramer in solution. This result was confirmed by analytical ultracentrifugation (Figure 1.1C, M.W. 122.7 kDa) and is consistent with previous data [30].

A

B

C

	Mdm12	His6–Mdm12	Mdm12 + tMmm1
Theoretical M.W. (kDa)	30.7	33.0	61.4
Estimated M.W. (kDa)	58.3	34.5	122.7
Estimated M.W. / Theoretical M.W.	1.90	1.05	2.00
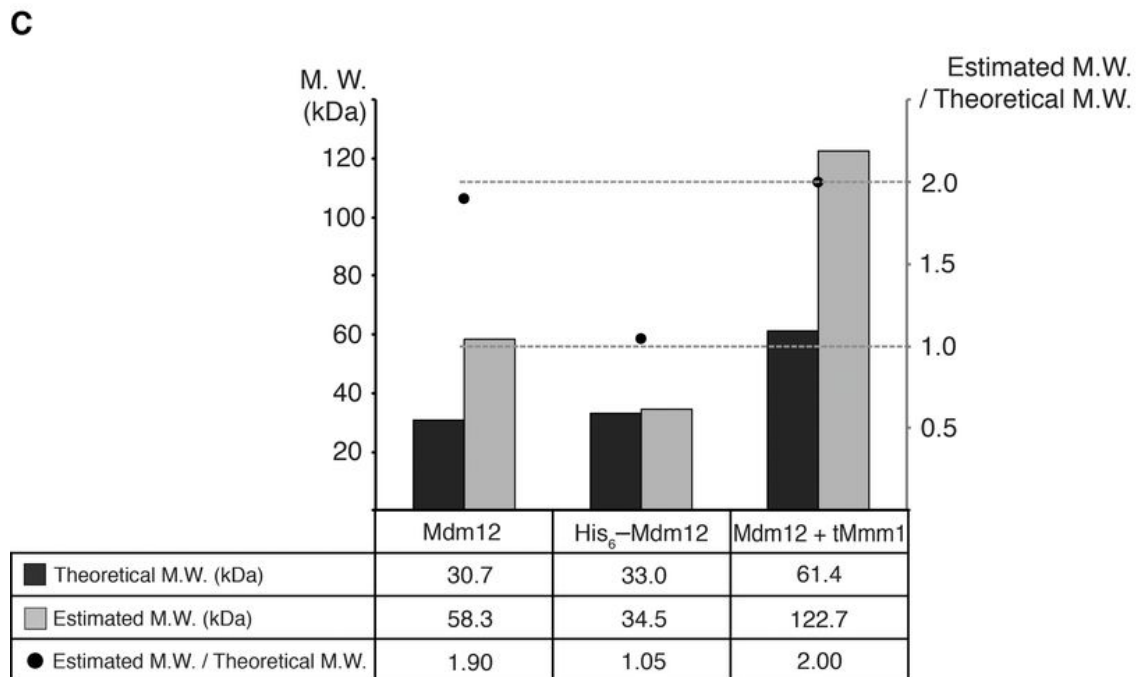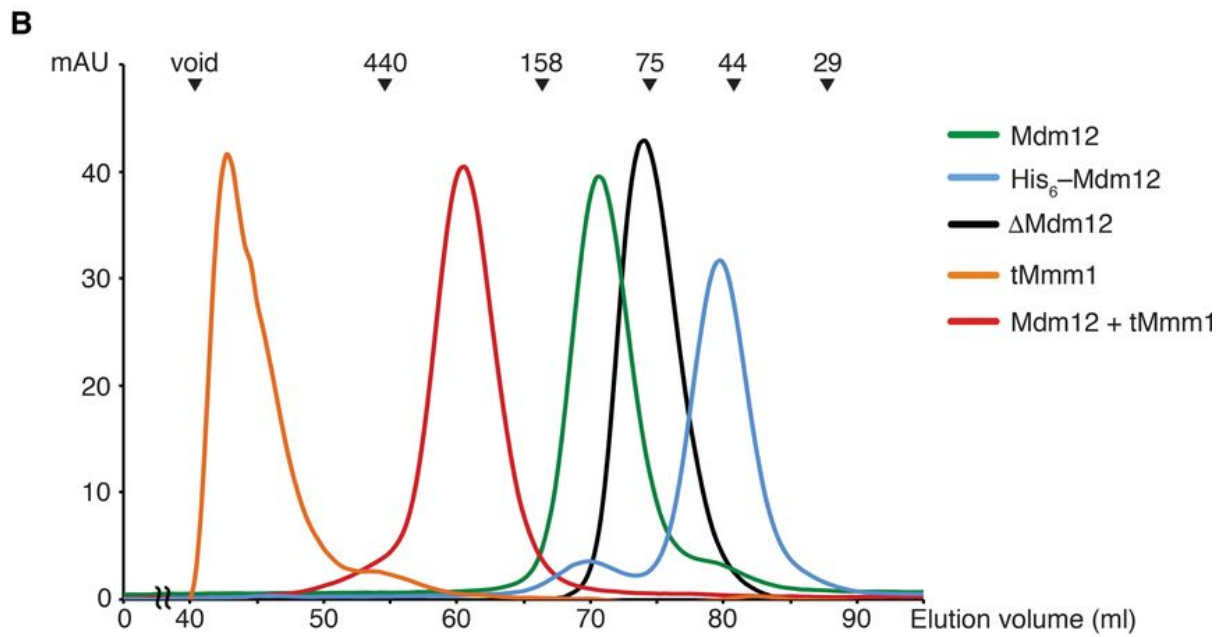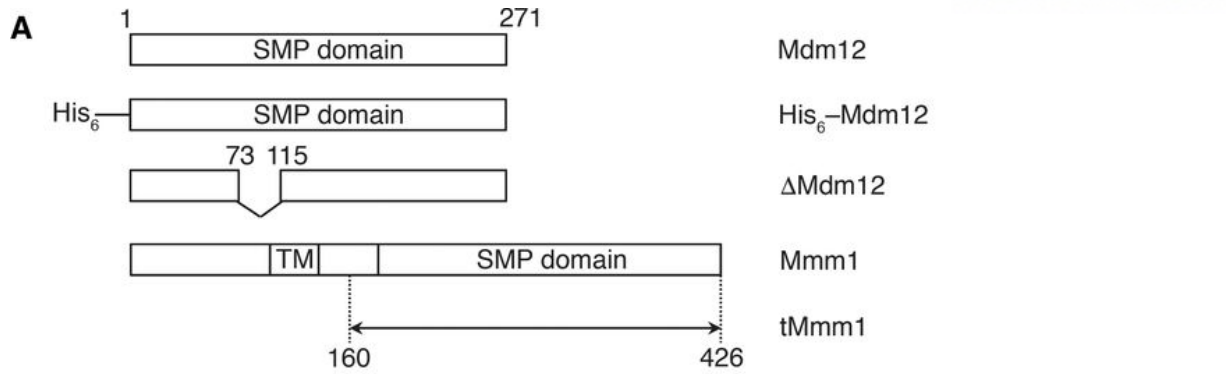
Figure 1.1. Mdm12 and Mmm1 organization

A) Schematic diagrams showing the domain structures of Mdm12 and Mmm1 used in this study.

B) Size-exclusion chromatography (SEC) experiments of Mdm12, tMmm1, and the Mdm12–tMmm1 complex comparing the molecular size of these proteins in solution. The proteins indicated were injected into a Superdex 200 column (GE Healthcare) with a buffer containing 25 mM Tris–HCl (pH 7.5), 150 mM NaCl, and 5 mM DTT. The standard molecular masses for the SEC experiments (top) are shown for relative molecular weight comparison (blue dextran, void; ferritin, 440 kDa; aldolase, 158 kDa; conalbumin, 75 kDa; ovalbumin, 44 kDa; and carbonic anhydrase, 29 kDa).

C) Graph indicating the molecular weights of Mdm12, His$_6$–Mdm12, and the Mdm12–tMmm1 complex in solution as measured by analytical ultracentrifugation.
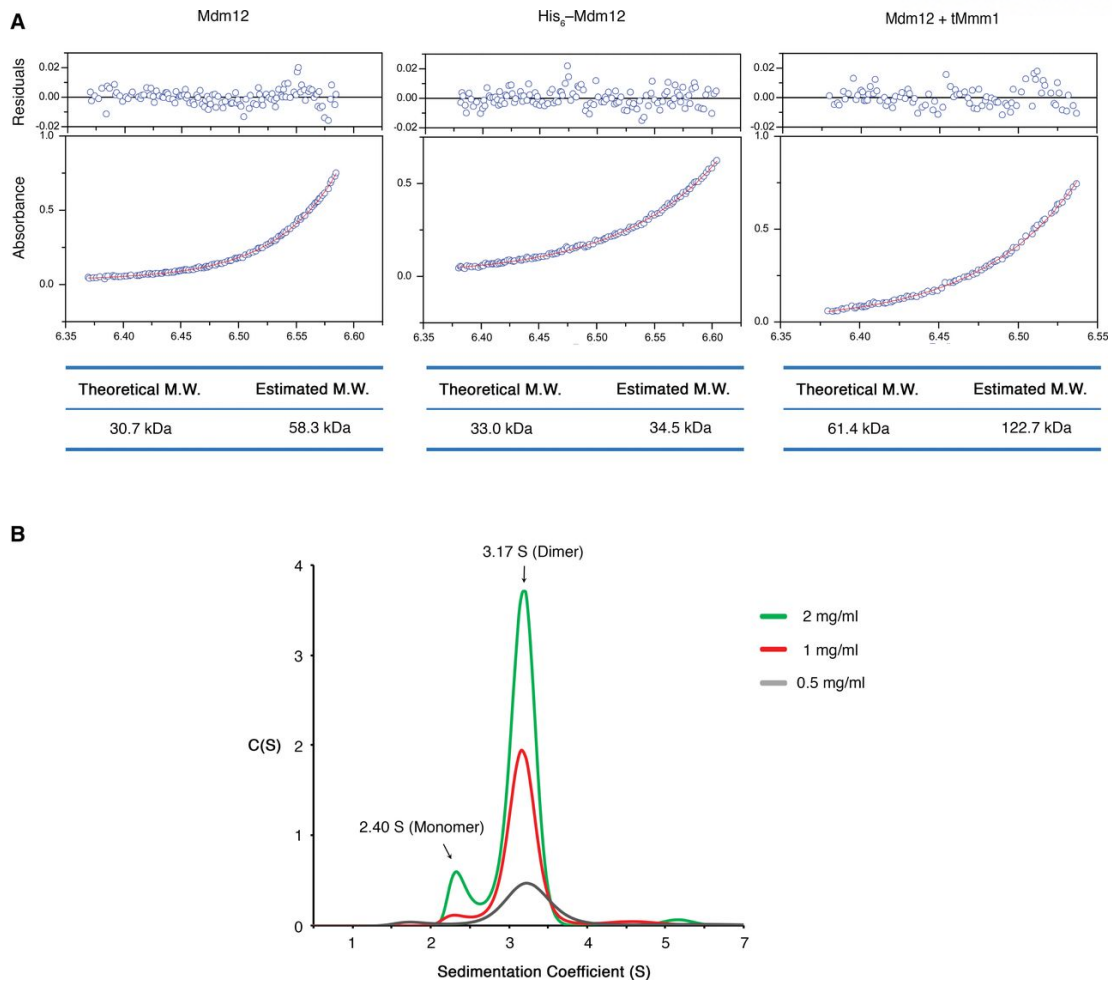
Figure 1.2. Analytical ultracentrifugation experiments

A) Sedimentation equilibrium fitting results following analytical ultracentrifugation of wild-type Mdm12 (left), N-terminus hexahistidine-tagged Mdm12 (His$_6$–Mdm12, middle), and the Mdm12–Mmm1 complex (right). The lower panel depicts the fitted overlay (red line) to the experimental data (blue circles). The upper panel depicts the residuals.

B) Sedimentation velocity analytical ultracentrifugation profiles of wild-type Mdm12. Self-oligomerization of wild-type Mdm12 was analyzed at various concentrations (0.5, 1, and 2 mg/ml) at 20,124 g. Peak sedimentation coefficient values of 2.40 S and 3.17 S correspond to monomer and dimer, respectively.

1.3.2. Crystal structure determination for S. cerevisiae Mdm12

Full-length Mdm12 proteins from *S. cerevisiae* were crystallized under various conditions. The best crystals grew in a $P2_12_12$ space group and diffracted to 3.1 Å resolution at a synchrotron source. The initial electron density map was calculated to 3.5 Å resolution from Se-Met-derivatized crystals using a single-wavelength anomalous diffraction (SAD) experiment, and the structure was phase extended and refined to 3.1 Å resolution with native crystal with R_{work}/R_{free} values of 21.2/26.5%. Statistics for data collection and refinement are presented in Table 1.

1.3.3. Overall structure of Mdm12

The molecular models of Mdm12 are presented in Figure 1.3A–D. As observed by size-exclusion chromatography, the full-length Mdm12 forms dimers in the crystals with the asymmetric unit containing two Mdm12 dimers (four Mdm12 monomers in total) related to twofold symmetry. The four Mdm12 molecules are almost identical with a RMSD of < 0.3 Å. The crystal structure reveals that the Mdm12 dimer adopts an elongated tubular structure with dimensions of 40 Å × 60 Å × 110 Å (Figure 1.3A). The Mdm12 monomer consists of three structural elements: (i) β1-dimerization center; (ii) β-barrel with incomplete and highly twisted β-strands and three α-helices, which are comparably organized as shown in most synaptotagmin (SMP) domain-containing proteins [27–29]; and (iii) proline rich region, which protrudes from the SMP domain from the middle of the last strand of the β-barrel (Figure 1.3B and Figure 1.4). The truncated cone-shaped structure of the Mdm12 monomer forms an extensive hydrophobic channel through the elongated cavity, which was reported to provide a binding channel for particular fatty acids (discussed below) in previous studies [27–29]. Two Mdm12 molecules are arranged in a twofold symmetry and associate with each other through domain swapping of the N-terminus β-strand (β1) comprising residues 1–7 as detailed below. Overall, the Mdm12 dimer structure resembles that of members of the TULIP family such as E-SYT2 (extended synaptotagmin 2, RMSD: 5.71), CETP (cholesteryl ester transfer protein, RMSD: 4.47), and BPI (bactericidal/permeability-increasing protein, RMSD: 4.26) despite the absence of any significant sequence similarity among them [27–29]. Notably, BPI and CETP exist as monomers containing two separate SMP domains that show no significant sequence conservation between them.

No electron density was observed for residues 74–114 of Mdm12, suggesting that this region might be highly flexible. Furthermore, these residues are not conserved in several Mdm12 orthologs. We obtained another orthorhombic crystal from the construct excluding the disordered region (Δ74–114, referred to as ΔMdm12 hereafter) in full-length Mdm12. The crystals of ΔMdm12 grew in a $P2_12_12_1$ space group and diffracted to 3.6 Å resolution. The structure of ΔMdm12 was solved by

molecular replacement using the full-length Mdm12 structure as the search model and refined to 3.6 Å resolution. ΔMdm12 also crystallized as a dimer, and the structures and twofold arrangement of Mdm12 and ΔMdm12 are almost identical with a RMSD of 0.5 Å.
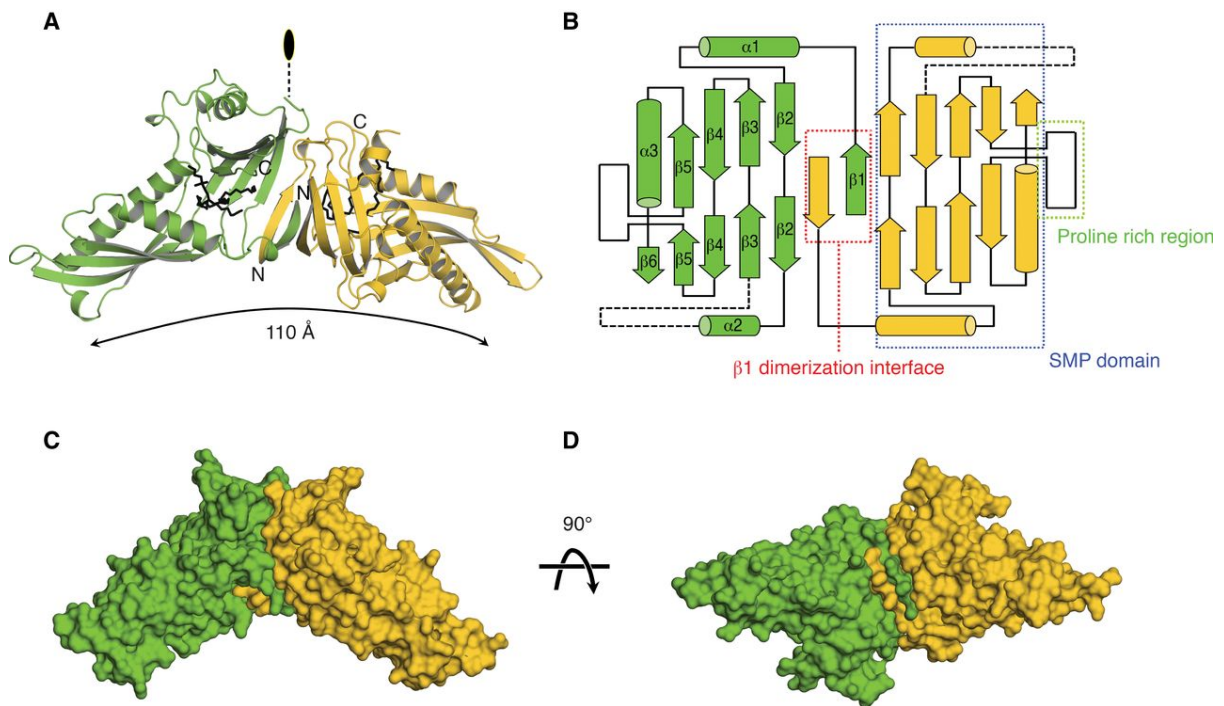
Figure 1.3. Overall structure of Mdm12

A) Ribbon diagram of the yeast Mdm12 dimer. The crystal structure of full-length Mdm12 was determined by SAD and refined with native data to 3.1 Å resolution. Lipids bound to Mdm12 are drawn with black stick models.

B) Schematic diagram indicating the secondary structure elements and their organization in Mdm12. Three structural elements of Mdm12 are highlighted in different colored boxes.

C, D) Surface representations of the Mdm12 dimer are shown in different orientations.
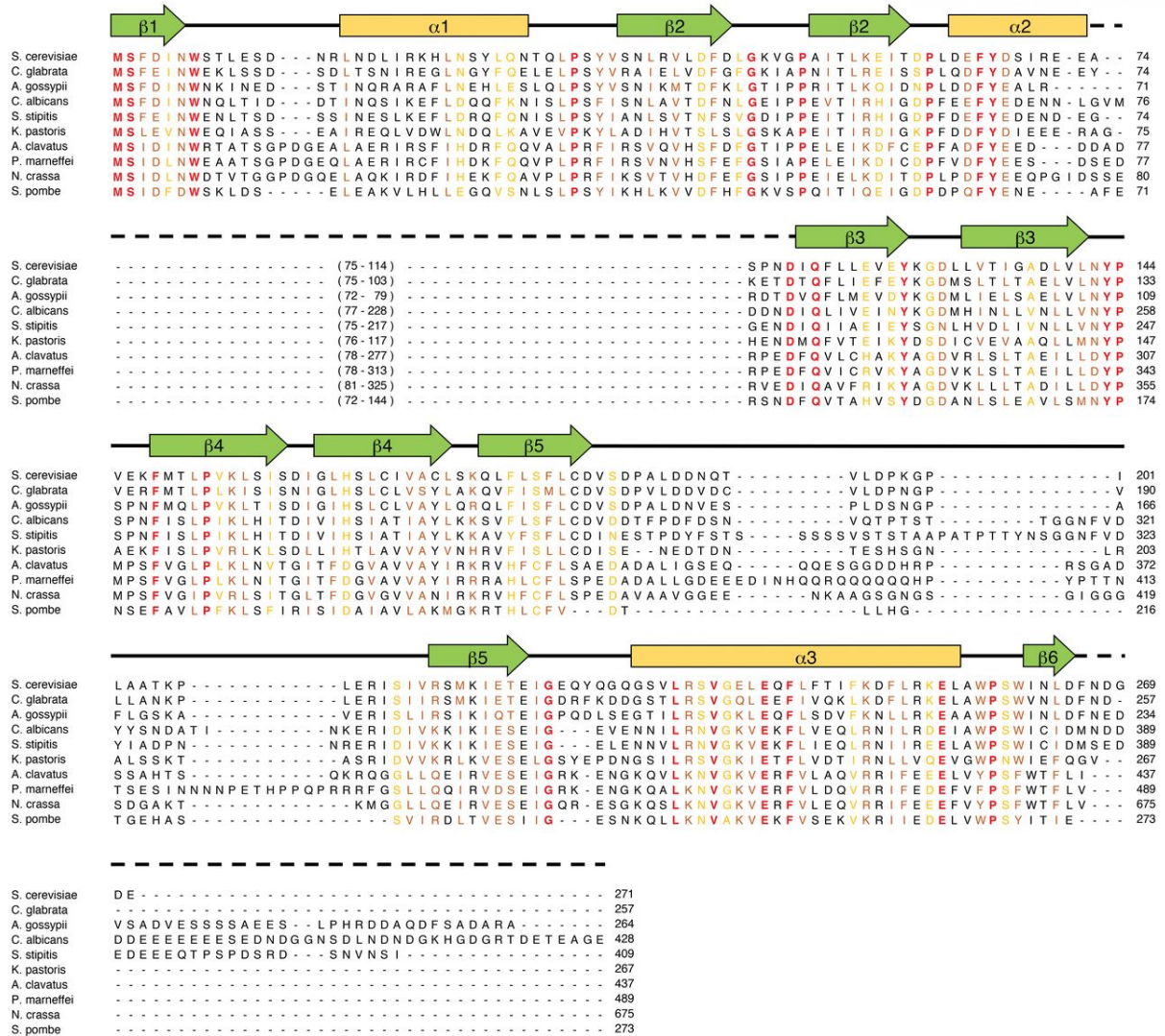
Figure 1.4. Sequence conservation of Mdm12

Sequence alignment of Mdm12 orthologs in fungi. The secondary structure elements are indicated above the sequences with helices, strands, loops, and disordered regions represented by arrows, cylinders, solid lines, and dashed lines, respectively. The absolutely conserved and highly similar sequences are highlighted in red and yellow, respectively.

1.3.4. The highly conserved β1-strand of Mdm12 forms the dimeric interface for self-association

The N-terminus of Mdm12 is highly conserved among Mdm12 orthologs (Figure 1.5A). In the Mdm12 dimer, residues 1–7 from one monomer fold into a β-strand that inserts itself between β1 and β2 from the second monomer, running antiparallel with β1 and parallel with β2 in the twofold center of the Mdm12 dimer. They are systematically associated with each other by forming a hydrogen bond network among main chains of the protein between β1 (residues 4–7) and β2 (residues 53–56) from counter molecules, and two β1 (residues 1–6) strands from two molecules (Figure 1.5A). The buried surface area caused by the dimerization of Mdm12 is around 1,400 Å2. E-SYT2 makes a twofold dimerization interface between two separate SMP domains using a highly conserved helix (residues 167–180) located at the beginning of each SMP domain (Figure 1.5C). The dimeric interface of Mdm12 closely resembles the twofold-like interface of CETP and BPI involving two SMP domains, an interface consisting of the central β-sheets comprising six antiparallel β-strands (Figure 1.5C). However, it is a distinctive feature of Mdm12 that the dimer is formed through domain swapping of the central β-strand located between the two SMP domains.

To further investigate whether the role of the β1-strand in the dimerization of Mdm12 as observed in the crystal structure also applied to Mdm12 in solution, we generated a point mutant (I5P) aimed at disrupting the β1-strand structure. In the dimer, the main chain of I5 forms H-bonds with the main chain of M1 from the second Mdm12 molecule, and its side chain makes van der Waals interactions with the hydrophobic side chains of M1, F3, W7, and I54 in the second molecule. As expected, both gel-filtration and analytical ultracentrifugation experiments revealed that the I5P mutant could not form a homo-dimer (Figure 1.5B), supporting the critical involvement of the highly conserved β1-strand in Mdm12 homo-dimerization in solution.
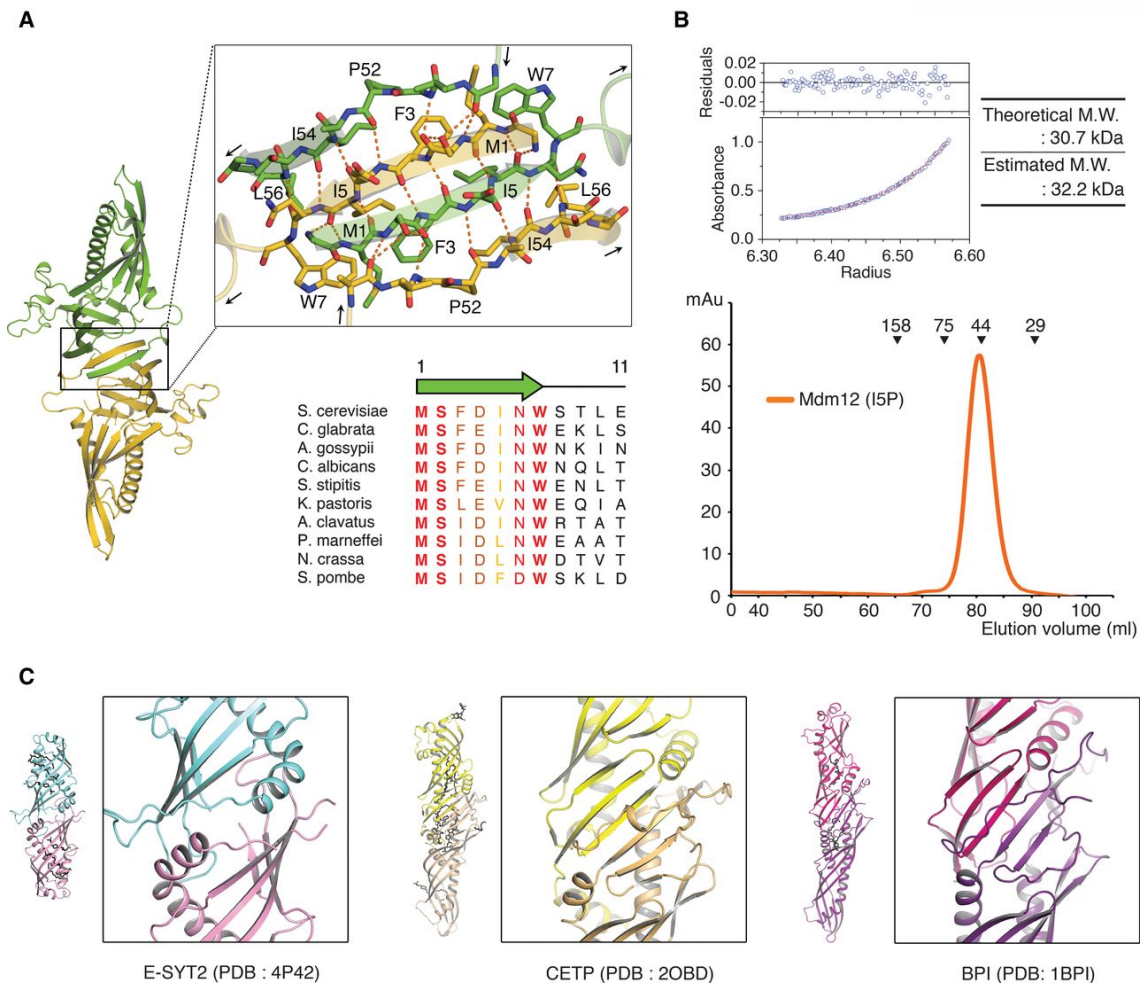
Figure 1.5. Dimer interface of Mdm12

A) Ribbon diagram showing the twofold dimerization interface of Mdm12. Oxygen and nitrogen atoms are shown in red and blue, respectively. The orange dotted lines indicate intermolecular hydrogen bonds between two protomers of Mdm12. The sequence alignment of yeast Mdm12 orthologs is shown to highlight the sequence conservation in the N-terminus β1-strand. Ten orthologs are aligned from residues 1–11. Absolute and highly conserved residues are indicated in red and orange, respectively.

B) The molecular weight of the Mdm12 (I5P) mutant was measured by size-exclusion chromatography (below) and ultracentrifugation (top) as in Fig 1B and C.

C) Ribbon diagram showing the structures of the SMP domain in E-SYT2, CETP, and BPI for the comparison of dimeric interfaces among SMP domains. Note that CETP and BPI are not dimers but monomers containing two tandem SMP domains.

1.3.5. The SMP domain of Mdm12 binds phospholipid

Initial electron density maps clearly displayed a lipid-like molecule inside the hydrophobic channel of the Mdm12 monomer (Figure 1.6A and B). We were unable to identify the bound phospholipid using only electron density maps because of (i) the mid-range resolution (~3.1 Å) of this structure and (ii) the disordered electron density corresponding to the head group of phospholipid. However, it was previously reported that the recombinant Mdm12 proteins expressed in bacteria bind PE (~80%) and PG (~15%) species [30]. Therefore, we inferred that the diacyl glycerophospholipid bound to Mdm12 might be a PE or PG. To identify the phospholipids present in the Mdm12 structure, we performed denaturing quantitative APCI-MS using purified Mdm12 expressed in *E. coli*. The major phospholipid bound to Mdm12 was observed to have an m/z of 704.5 (Figure 1.7B), which identified the molecule as PE, consistent with a previous lipidomic analysis in which PE (33:1) with an m/z of 704.5 was the predominant phospholipid co-purified with Mdm12 expressed in bacteria [30]. We built a PE (1,2-dioleoyl-sn-glycero-3-phosphoethanolamine) into the diacyl-like ligand density (Figure 1.6A), and the lipid-bound Mdm12 structure was well refined with native diffraction data. Ligand positioning is almost identical among three Mdm12 molecules within the asymmetric unit, except in one Mdm12 molecule, where the hydrocarbon chain of lipid is displaced and the head region is disordered (Figure 1.7A). This displacement might be the result of crystal packing because the hydrophobic cavity of this molecule was slightly shrunk through the formation of close contacts with the symmetry-related molecules in the crystal.

Based on our crystal structure, the head group of phospholipid is exposed into the solvent and makes no direct contacts with neighboring residues of Mdm12, indicating that Mdm12 might have no clear selectivity for specific phospholipids. However, the fatty acyl chain of PE was tightly coordinated by the hydrophobic side chains of neighboring amino acids including I20, F45, L47, L177, F179, F251, L256, I262, and L264 (Figure 1.6C). We tested the ability of phospholipids to bind directly to the SMP domain of Mdm12 *in vitro*. We used the fluorescently labeled PE (7-nitro-benz-2-oxa-1,3-diazol-4-yl-1,2-dipalmitoyl-sn-glycero-3-phosphoethanolamine, referred to as NBD-PE) and full-length Mdm12 purified from *E. coli* to measure their binding, as previously described [29, 30]. Mdm12 proteins incubated with NBD-PE were run onto native PAGE to remove unbound NBD-PE, and NBD-PE-bound Mdm12 was quantified with fluorescence detection. Figure 1.6D and E shows that Mdm12 binds NBD-PE in a concentration-dependent manner. Unexpectedly, while around half of the full-length Mdm12 appeared as a dimer (46% of total Mdm12), the other half ran as a monomer (54%) in the native PAGE, as compared with Mdm12 (I5P) that migrated only as a monomer. The monomer and dimer distribution of Mdm12 observed in native PAGE was not correlated with NBD-PE incorporation (Figure 1.6D and Figure 1.8B). More surprisingly, monomeric Mdm12 had a higher

14

affinity for NBD-PE than did dimeric Mdm12. Interestingly, the I5P mutant showed the highest affinity for NBD-PE, suggesting that the N-terminal β1-strand of Mdm12 might be involved in regulating lipid trafficking, including access. Indeed, the structure shows the lipid-binding region, including the head group, to be very close to the dimerization interface. The dimerization of Mdm12 could thus sterically occlude lipid access, and the perturbation of the β1-strand by mutation therefore increased the affinity for NBD-PE (Figure 1.8).

Next, to validate the lipid coordination shown in our Mdm12 structure, we generated a construct harboring mutations in L256 and I262, both mutated to tryptophan residues. Our rationale was that the bulky side chain of tryptophan introduced by these mutations would occupy the hydrophobic cavity and generate a steric hindrance for lipid interaction. Compared with wild-type Mdm12 (I5P), the affinities of I262W and the L256W/I262W double mutants for NBD-PE were reduced by twofold and fourfold, respectively (Figure 1.6F). In this experiment, the Mdm12 (I5P) mutant was used as a reference to compare the effects of I262W and L256W/I262W because it migrated as a monomer during native PAGE.

A

mFo-DFc   Final model

B

C

D

E

F
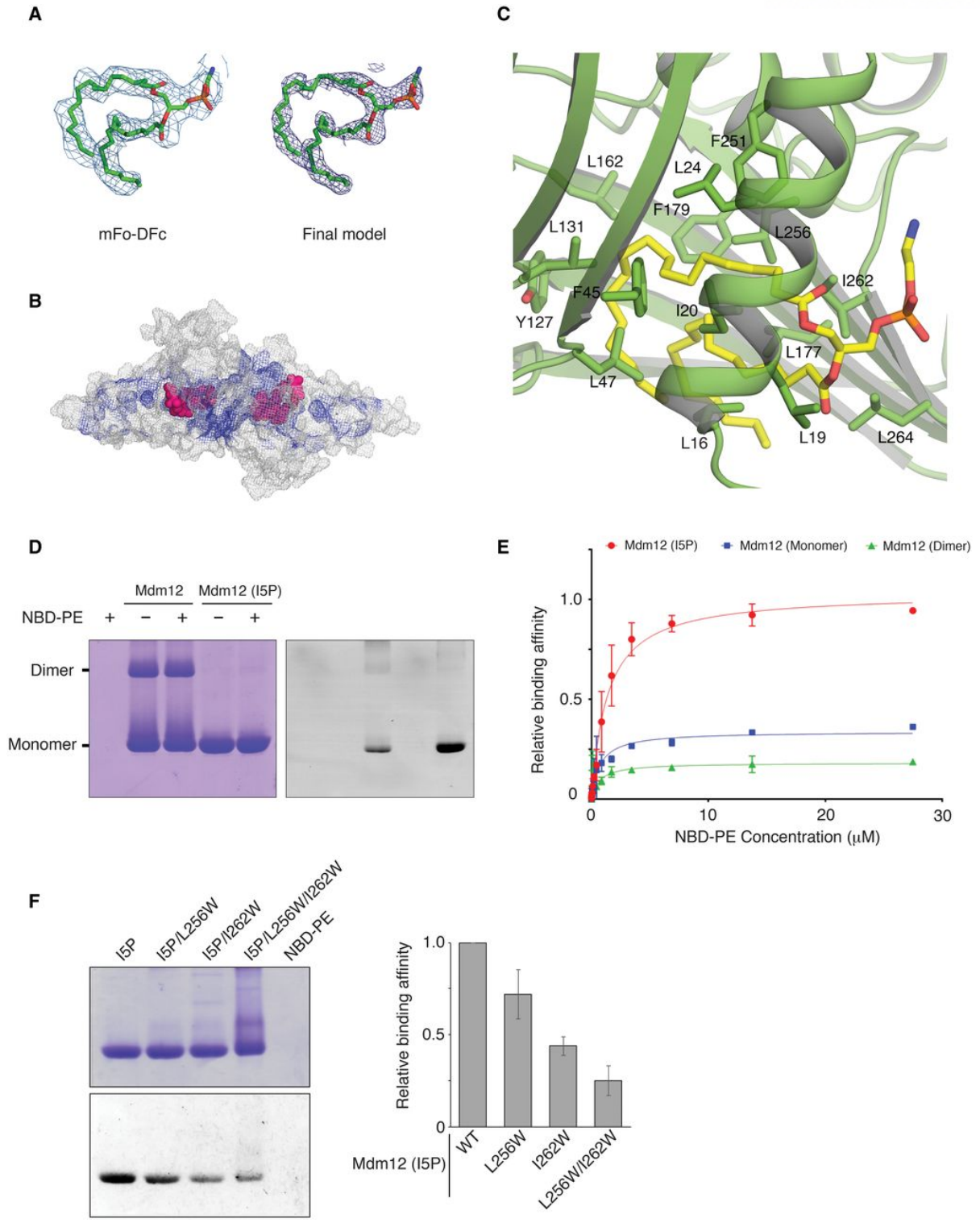
Figure 1.6. Mdm12 binds lipid through the SMP domain

A) Simulated annealing omit map (Fo-Fc, contoured at 1.5σ) showing the molecule bound to Mdm12 (left). The final model for the bound PE is shown as in stick representation. The electron density (2Fo-Fc) calculated in the final model is shown with the stick model of PE in the right (3.1 Å resolution, contoured at 0.8σ).

B) Surface representation of the Mdm12 dimer. Hydrophobic amino acids lining the Mdm12 channel are indicated by a blue mesh. Lipids built in Mdm12 are in space-filling representation.

C) Ribbon diagram showing lipid coordination by Mdm12. Mdm12 residues and lipid fatty acids are colored in green and yellow, respectively.

D) Mdm12 binds NBD-PE. Wild-type and monomeric (I5P mutant) Mdm12 were incubated with NBD-PE and separated from free NBD-PE in native PAGE. Coomassie staining (left) and fluorescent (right) detection indicates that Mdm12 directly interacts with NBD-PE *in vitro*.

E) Quantitative data showing binding affinities for NBD-PE by Mdm12. The binding affinities of Mdm12 (monomer/dimer shown in native PAGE and I5P mutant) for NBD-PE was measured with a NBD-PE concentration-dependent manner. All experiments were carried out three times, and the means ± SD are given.

F) Mdm12 mutants (L256W, I262W, and L256W/I262W double mutants) were incubated with NBD-PE and subjected to native PAGE. Because wild-type Mdm12 separates as both monomer and dimer on native PAGE, the purely monomeric form (I5P) of Mdm12 was used as the wild type for clarity. The graph in the right indicates the quantities measured in the experiments. The bar shows the relative amounts of the band ratio (fluorescence/Coomassie). Values represent the means and SD from three independent experiments.
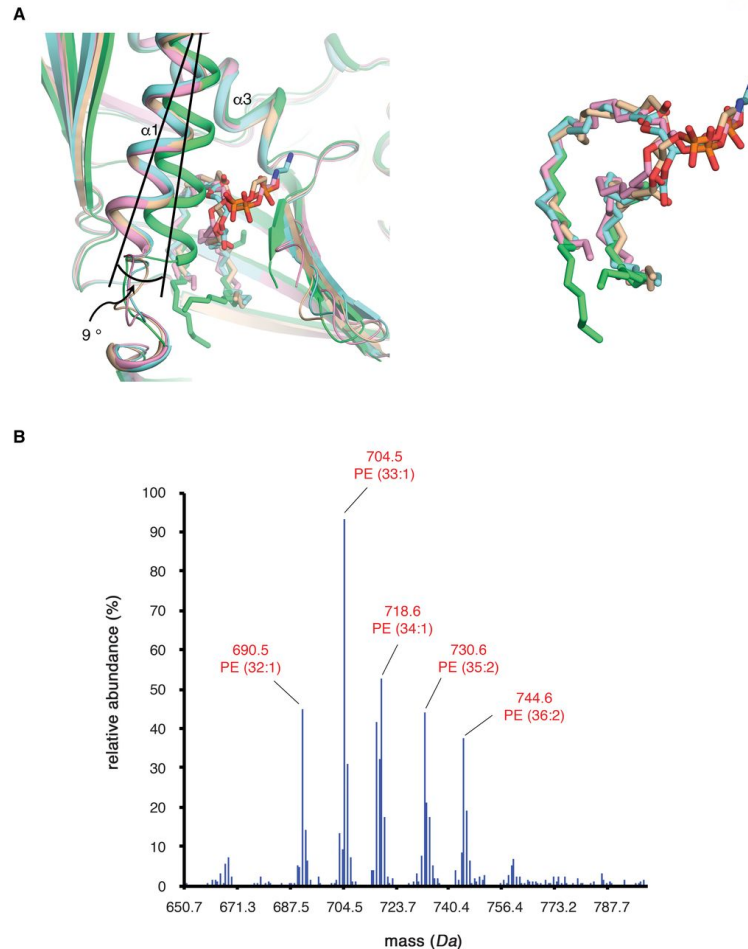
Figure 1.7. Structural comparison of lipids bound to Mdm12 in the crystallographic asymmetric unit and lipids identified from APCI-MS analysis

A) Ribbon diagram showing the overlay of the lipids bound to the SMP domains of the four Mdm12 molecules in the asymmetric unit. Four Mdm12 molecules and the hydrocarbon chains of bound lipids are identically colored in pink, green, cyan, and yellow. Oxygen and nitrogen atoms in lipids are colored in red and blue, respectively. The α1-helices and bound lipids in the three Mdm12 molecules (pink, cyan, yellow) precisely align with each other. However, the α1-axis of one Mdm12 (green) molecule is tilted around 9 degrees owing to crystal packing. The displaced α1-helix induces a break in coordination of the lipid hydrocarbon chain, and the head group of the lipid is disordered in the structure. Right figure shows only the lipids bound to Mdm12 for clarity.

B) Quantitative profiling of phospholipids bound to Mdm12 purified from E. coil using APCI-MS (see Materials and Methods section for details). The most abundant species bound to Mdm12 had a mass of 704.5 Da and was identified as PE (33:1), consistent with a previous report [30].

18

A

Head group

Proximal

Distal

Head group

Mdm12

E-SYT2

B

NBD-PE (μM)   0   0.1   1.7   27

Mdm12 (WT)-Dimer

Mdm12 (WT)-Monomer

Mdm12 (I5P)

C   **D**

Mdm12   E-SYT2
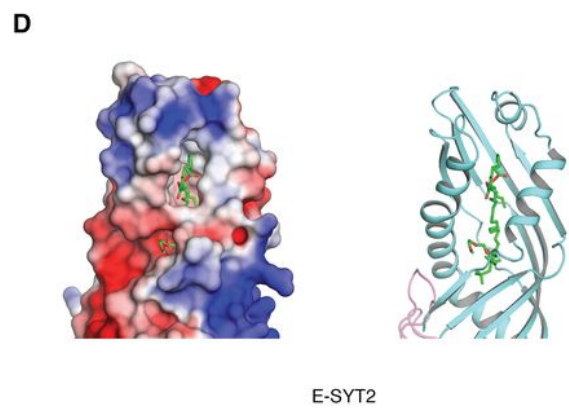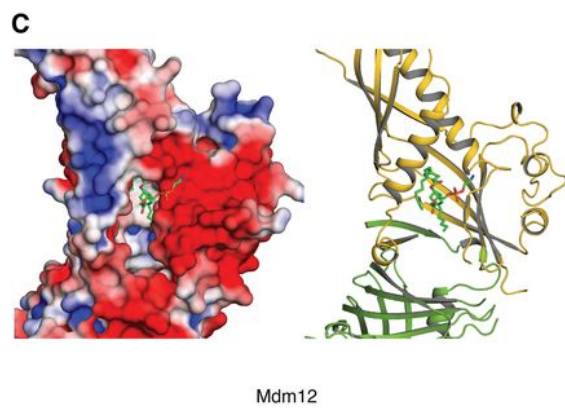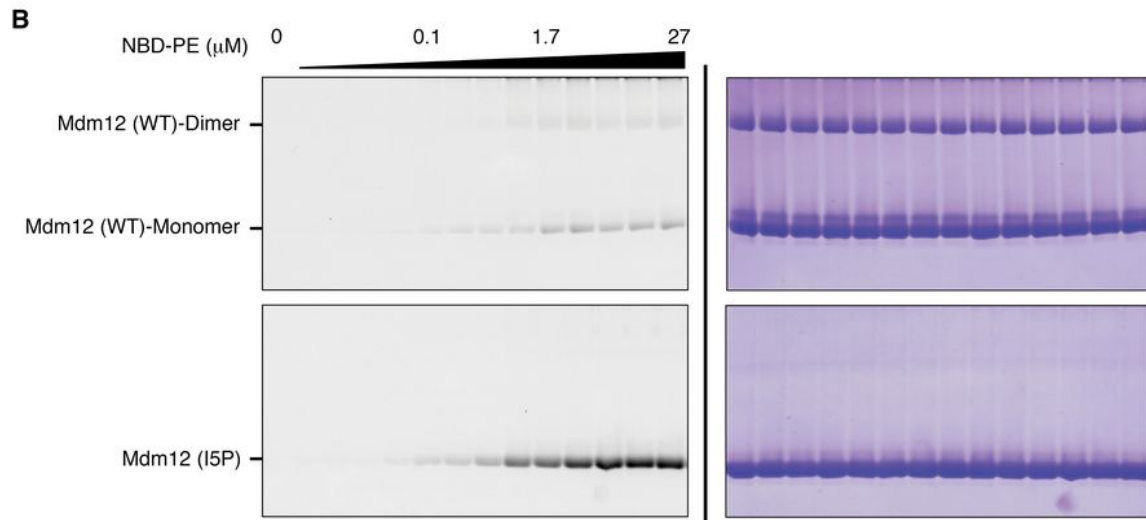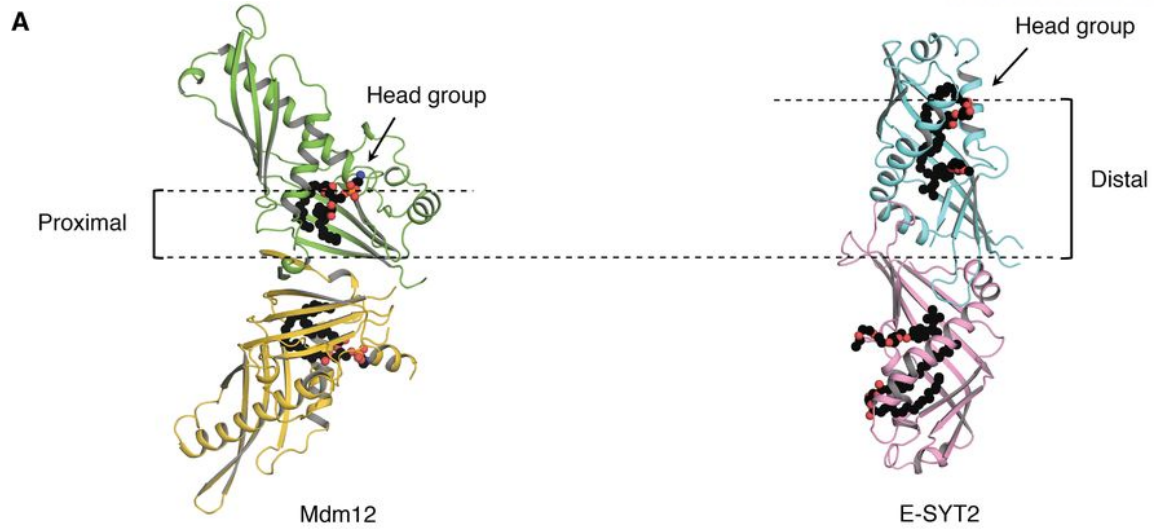
Figure 1.8. Mdm12 preferentially binds phospholipids with a positively charged head group at the dimerization interface

A) Figure highlights that the lipid-binding site of Mdm12 is proximal to the dimerization interface. Views are along the twofold rotation axis. The bound lipids are shown as spheres. The hydrocarbon, oxygen, and nitrogen are colored in black, red, and blue, respectively. Lipids bound to Mdm12 are located in close proximity to the dimerization interface, in contrast to E-SYT2 where there is a clear separation between the two sites. As the dimerization interface of Mdm12 would be similar to the Mdm12–Mdm34 interface (see the text), the proximal position of lipids could be advantageous in facilitating the translocation of lipids between the two proteins.

B) Binding affinities of Mdm12 (monomer/dimer [top] and the I5P mutant [bottom]) for NBD-PE. Coomassie-stained (right) and fluorescently labeled (left) native PAGE gels are shown.

C, D) Surface charge distribution around the lipid-binding regions in Mdm12 and E-SYT2. Ribbon diagrams (right) show their orientations. Surface charges were calculated as in Figure 1.9A.

1.3.6. Mdm12 has a clear preference for positively charged phospholipids

We further investigated the structure to determine whether Mdm12 might have a preference for certain phospholipids under native conditions. Interestingly, the surface for Mdm12 in which the phospholipid head group is placed represents a negative charge according to analysis of the surface electrical potential [31] (Figure 1.9A). The negative electric potential comes from mainly the C-term dipole end of helix 3, the main chain carbonyl oxygen of the loop comprising residues 250–255, and negatively charged side chains from E65, E73, E255, and D265. An investigation using the ConSurf [32] server revealed that these residues of Mdm12 are highly conserved among different species. We propose that Mdm12 might have a higher affinity for phospholipids with positive charges, such as PC or PE, than for negatively charged lipids. This hypothesis is supported by previous biochemical studies, which show that Mdm12 has a higher affinity for PC and PE than for PA and PS [30]. To measure quantitatively and kinetically the natural lipid-binding ability of Mdm12, we carried out lipid replacement experiments as previously described [29, 30]. NBD-PE-preloaded Mdm12 (GST-tagged at the C-terminus) was incubated with a series of phospholipids in a dose-dependent manner, and the amount of NBD-PE replaced by non-labeled phospholipids was estimated by measuring the decrease in fluorescence. Figure 1.9B shows that PC and PG have the highest affinity for Mdm12 among the phospholipids tested, consistent with a previous report in which PC was confirmed as a bona fide ligand of Mdm12 purified from yeast *in vitro* [30]. Interestingly, acidic phospholipids such as PA and PS were unable to replace NBD-PE, even when present at a high concentration (~0.25 mM). To investigate the involvement of negatively charged amino acids in phospholipid selection, we engineered the E255R mutant of Mdm12 and measured its binding affinity for PC. Interestingly, the binding affinity of the E255R mutant for PC was reduced by ~1.4-fold compared with the wild-type protein, which supports our suggestion that the negatively charged surface of Mdm12 underpins its preference for positively charged phospholipids (Figure 1.9B).

In E-SYT2, no apparent weighted surface charge for the hydrophilic head group of lipid is apparent (Figure 1.8C), which is consistent with data demonstrating that E-SYT2 has no preference for specific phospholipids. However, while E-SYT2 might recruit other proteins for their lipid selectivity [29], no additional proteins have yet been suggested to provide lipid selectivity in the ERMES complex. Taken together, we propose that Mdm12 might have a preference for binding of positively charged phospholipids through its negatively charged surface.
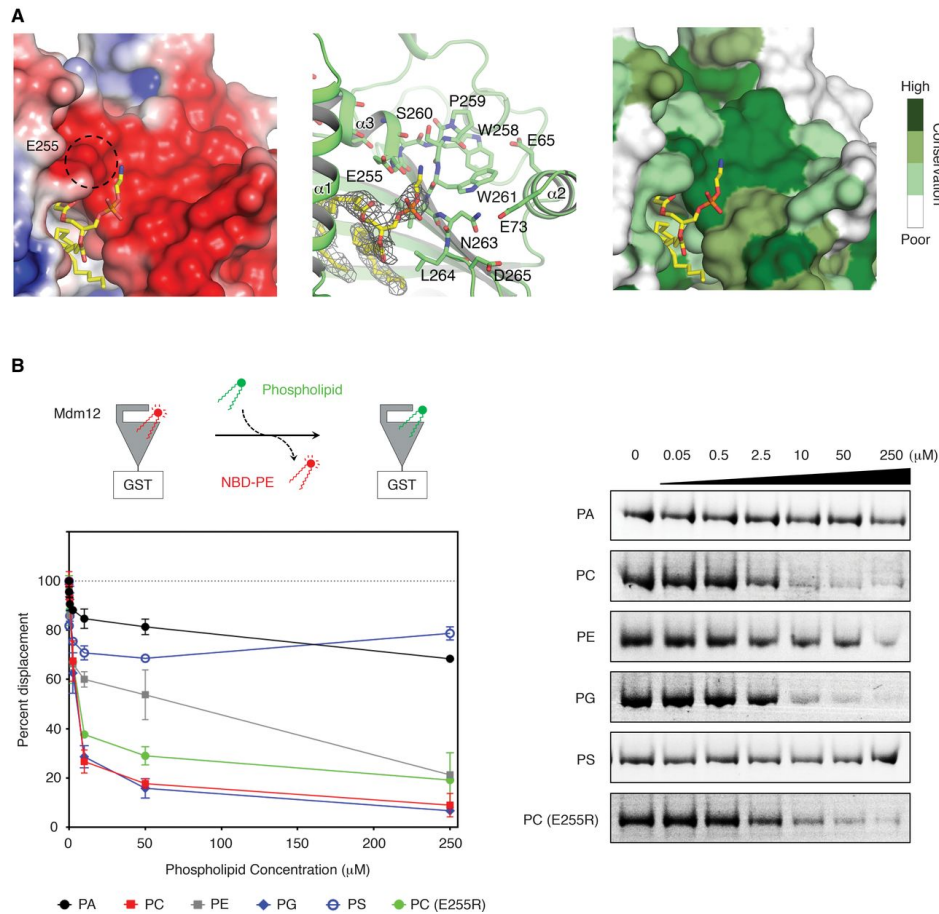
Figure 1.9. Glycerophospholipid selectivity of Mdm12

A) Structural views suggesting that Mdm12 might have a preference for certain phospholipids. The surface representation of Mdm12 positioned around the binding site for the head group of PE is shown with charge distribution (left) and the sequence conservation (right) in the same orientation. Surface electrostatics and sequence conservation were calculated using an APBS program [31] with the nonlinear Poisson–Boltzmann equation and contoured at $\pm$ 3 kT/e, and ConSurf website (consurf.tau.ac.il) [32] with 34 different yeast orthologs, respectively. The ribbon diagram shown in the middle indicates the overall orientation of Mdm12.

B) Lipid displacement experiments to identity the natural ligands of Mdm12 in vitro (see Materials and Methods section for details). NBD-PE-preloaded Mdm12-GST was mixed with a series of glycerophospholipids at different concentrations, and displacement of NBD-PE by non-labeled ligand was estimated from the decrease in fluorescence. Means $\pm$ SD are shown (n = 3 independently performed experiments).

1.3.7. Putative architecture of Mdm12–Mmm1 complex

In the crystal asymmetric unit, there are four Mdm12 molecules (Figure 1.10A). In addition to the N-terminus dimerization interface (referred to as "head"), two Mdm12 dimers make another twofold rotation arrangement through the highly conserved C-terminal helices (referred to as "tail"), resulting in an extended arch-shaped structure with a 200 Å long dimension. Here, two Mdm12 dimers self-associate through a tail-to-tail junction, burying a surface accessible area of around 765.8 Å2 (Figure 1.10C). We initially considered that the tail-to-tail junction of the SMP domain shown in the Mdm12 structure might represent a crystal contact, not a biological one, based on previous biochemical experiments demonstrating that Mdm12 forms a homo-dimer in solution. The structure of ΔMdm12 lacking residues 74–114 has the same arrangements of the molecules in the asymmetric unit, although ΔMdm12 crystals are differently packed from wild-type Mdm12 (Figure 1.10B). Crystals of ΔMdm12 contain six ΔMdm12 molecules in the asymmetric unit, and three ΔMdm12 dimers are organized through a tail-to-tail junction in a similar fashion to wild-type Mdm12. Previous biochemical data show that Mdm12 interacts with Mmm1 in a 1:1 ratio stoichiometry, and four molecules are depicted in an elongated organization as a series of Mdm12-(Mmm1)$_2$-Mdm12 [30]. We propose a new model in which Mmm1 forms a homo-dimer through a head-to-head interaction of each SMP domain in the center, and a hetero-dimer with Mdm12 through a tail-to-tail interaction of their respective SMP domains. Consistent with the hypothesis, the size-exclusion chromatography experiment of Mmm1–Mdm12 (Δ1–10) revealed that the N-terminus-truncated Mdm12 retained its ability to interact with Mmm1, suggesting that the N-terminus of Mdm12 is not involved in the interaction with Mmm1 (Figure 1.10D). Based on these results, we suggest that the tail-to-tail contact of two SMP domains from the Mdm12 tetramer and ΔMdm12 hexamer, as shown in the two crystal structures, might provide a novel structural binding interface from two SMP domains between Mmm1 and Mdm12.

A

Full-length Mdm12

B

Mdm12 (Δ74–114)

C

α2

Proline rich region

α1

α3

α3

α1

Proline rich region

α2

F245 L208   R253

Q242   K206

E241   T205   E65

R235

α3   α2

D

mAu

void   440   158   75   44   29

20

15

10   Mdm12 (11–271) + tMmm1

5

66

45   Mdm12 (11–271)

29   tMmm1 (160–426)

0   40   50   60   70   80   90

Elution volume (ml)
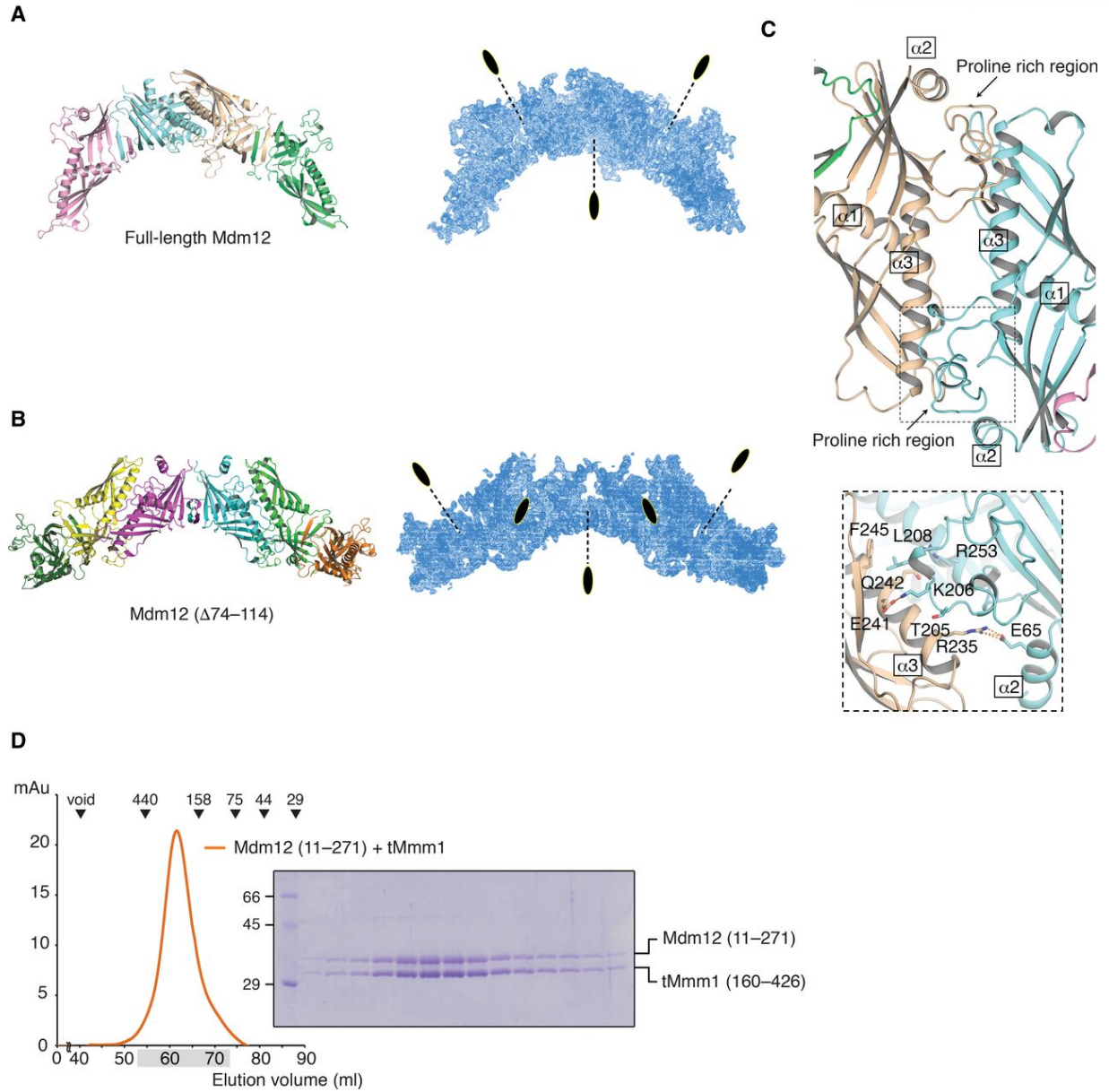
Figure 1.10. The Mdm12/ΔMdm12 molecules in the asymmetric unit provide an insight into the organization of the Mdm12–Mmm1 binary complex

A) Overall structure (left) and electron density (right) of Mdm12 in the asymmetric unit. Four molecules (two Mdm12 dimers) are organized with twofold rotation symmetry. The twofold axes are indicated with a black dotted line.

B) Overall structure (left) and electron density (right) of ΔMdm12 in the asymmetric unit. Six ΔMdm12 molecules (three Mdm12 dimers) are arranged with twofold rotation symmetry as shown above.

C) Ribbon diagram showing a twofold interface (tail-to-tail) in two crystal structures (see text for details).

D) Size-exclusion chromatography revealing that the N-terminus-truncated version of Mdm12 (residues 11–271) retains the ability to interact with Mmm1. The experiment was performed as in Figure 1.1B. Eluted fractions indicated by shading were subjected to SDS–PAGE followed by Coomassie Blue staining.

1.4. Discussion

In this study, we have elucidated the crystal structure of Mdm12 and the organization of SMP domains from self-associated molecules in crystal asymmetric unit. To ensure the correct organization of ERMES components and eventually the facilitation of direct contact between the two organelles, the interactions among the SMP domains of the different ERMES components are of critical importance. A potential model for the formation of the Mdm12–Mmm1–Mdm34 ternary complex is represented in Figure 1.11A and C. Similar to most SMP domains, Mmm1 forms a homo-dimer through the head region of its SMP domain, while the tail region of Mmm1 forms a hetero-dimer with Mdm12 through the highly conserved tail region of its SMP domain. Since both the biochemical data and EM structure showed that Mdm12–Mmm1 forms a hetero-tetramer rather than a hetero-hexamer, accommodating the organization of the Mdm12–Mmm1 complex in our model would first require the dissociation of the Mdm12 homo-dimer. The results of native PAGE described above showed that Mdm12 alone exists in a dynamic monomer/dimer equilibrium, and the crystal structure revealed that Mdm12 self-associates through its N-terminus. Given that the interaction of Mdm12 with Mmm1 occurs through tail-to-tail contact of their respective SMP domains, the exposed head region of the Mdm12 monomer would then be free to associate with the SMP domain of Mdm34, which is one of the core components in the ERMES complex. Interestingly, the N-terminal sequences of Mdm34 (residues 1–7, sequence "MSFRFNE") are highly conserved among other species and are precisely aligned with those in Mdm12 (MSFDINW) (Figure 1.11B), suggesting that (i) the N-terminus (residues 1–7) of Mdm34 might fold into a β-strand, and (ii) the Mdm34 might form a complex with Mdm12 using this β-strand through head-to-head contact as seen in the Mdm12 dimer. To test whether the β1-strand of Mdm12 is involved in the interaction with the Mdm34 SMP domain, the full-length or the N-terminus-truncated Mdm12 was incubated with the SMP domain of Mdm34 (residues 1–188) fused with MBP and analyzed using a MBP pull-down assay. Full-length Mdm12 interacted with the Mdm34 SMP domain, while the truncated Mdm12 did not (Figure 1.12A). We also demonstrated a direct interaction between Mdm12 and the N-terminal fragment of Mdm34 comprising residues 1–22 tagged with GST by co-expressing the two proteins and a GST pull-down assay (Figure 1.12A). The I5P homologous mutant of Mdm34 (residues 1–22, F5P) lost its ability to interact with Mdm12. The data support our proposed model that the interaction between Mdm12 and Mdm34 would be very similar to that seen in the Mdm12 dimer interface, namely the domain-swapped structure of β1-strands from two SMP domains.

A previous structural study identified a unique contact site comprising an α-helix in the SMP domain of E-SYT2 that was required for its homo-oligomerization [29]. From our crystal structures

26

and biochemical experiments, we propose two novel interfaces (head-to-head and tail-to-tail) for contact among SMP domains in ERMES components (Figure 1.11A and C). Mdm12 in particular, a soluble component, acts as a bridge to physically connect two membrane-anchored components, Mmm1 in the ER and Mdm34 in mitochondria, by providing both head- and tail-interacting surfaces through its SMP domain. The observed self-association of Mdm12 was unexpected; however, it is necessary to further test how the self-association of Mdm12 could be related to biological functions such as lipid trafficking. We observed that the self-oligomerization of Mdm12 is dynamic between monomers and dimers from the native PAGE of full-length Mdm12, and the Mdm12 monomer has even higher affinity for NBD-PE than the Mdm12 dimer (Figure 1.6D and E). In the same vein, it is necessary to examine whether the self-association of Mdm12 might have a negative effect on the lipid trafficking or the organization of the ERMES tetramer complex by inhibiting the interaction with Mdm34.

The structure of the Mdm12 dimer interface and the pairwise sequence alignment between Mdm12 and Mdm34 in N-terminus residues 1–7 reveals that the Mdm12–Mdm34 interaction would be mediated by the crossover of their N-terminus β-strand as shown in the Mdm12 dimer interface. The highly conserved N-terminus sequences of Mdm34 would have the ability to form homo- and hetero-complexes with Mdm12. The dimeric conformation of Mdm34 has been already verified by size-exclusion chromatography with Mdm34 SMP (residues 1–188), and the GST- or GFP-fused SMP domain of Mdm34 [30]. The interactions occurring through the flexible β-strand among the Mdm12 dimer, Mdm34 dimer, and Mdm12–Mdm34 complex appear to be relatively weak, a characteristic that could be associated with the dynamics for the assembly and disassembly of membrane contact mediated by the ERMES complex. The dynamics of the SMP domain also might be important in lipid trafficking, as shown with the Mdm12 monomer that has a higher affinity for lipids than the Mdm12 dimer. Likewise, the association between Mdm12 and Mdm34 might be implicated in lipid trafficking. We observed that the glycerophospholipid-binding site is located very close to the dimerization interface of Mdm12, a distinctive feature for lipid binding by the SMP domain shared by other TULIP family proteins including E-SYT2 (Figure 1.8A). The proximity of the lipid interaction and dimerization sites in Mdm12 could enable a direct and more efficient transfer of lipids from Mdm12 to Mdm34. Our structure thus provides indirect evidence for lipid translocation from Mdm12 to Mdm34 or in the reverse direction. We also observed that self-association of Mdm12 inhibits lipid access and incorporation, maybe because new lipids cannot be introduced into the ERMES complex when it is intact, assembled, and transferring lipids. Gem1 has been characterized as a regulator of ERMES activity [11]. The weak interactions and dynamics of ERMES components might contribute to the regulation of membrane contact and lipid trafficking by this small GTPase. Further studies will be required to test this hypothesis.

The self-association of Mmm1 could be mediated by a helix, as in the case of the E-SYT2 SMP domain (Figure 1.5C and 1.12C). The sequences of Mmm1 encoding the first helix in the SMP domain (residues 198–210) are well aligned with those of E-SYT2 and are predicted to fold into an α-helix, suggesting that Mmm1 might form a homo-dimer through this helical interface (Figure 1.12B–D). Given that the SMP domains in Mmm1 and E-SYT2 are located in the middle of the protein primary sequences, and that the association of Mdm12–Mmm1 is stronger than that of Mdm12–Mdm34, control of the assembly of the ERMES complex would likely occur through regulation of the Mdm12–Mdm34 complex, which involves the N-terminus β-strands of the two proteins. Future work will be required to address this biological hypothesis. A high-resolution structure of the ERMES tetramer complex including Mdm10 would be required to elucidate in molecular detail how the tetramer cooperatively and efficiently facilitates direct contact with the membrane and lipid exchange. In the absence of such a structure, our study provides a first understanding of the molecular mechanisms involved in the recognition of lipids by Mdm12 as well as of the dynamics and organization of the ERMES complex in its entirety.
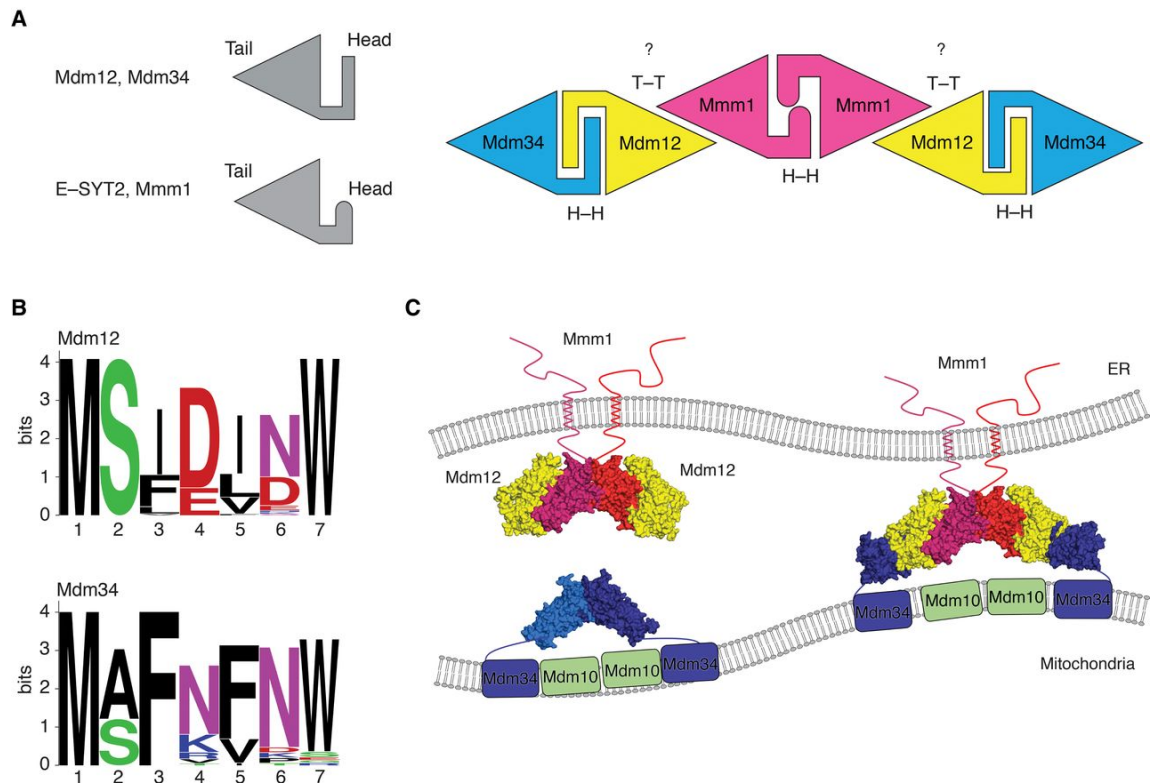
Figure 1.11. Putative architecture of the Mdm12–Mmm1–Mdm34 ternary complex

A) Schematic representation of the SMP domains of Mdm12 and E-SYT2 showing different head structures depending on the presence of helix or strand. Based on our structural and biochemical data, we modeled Mdm12–Mmm1–Mdm34 ternary complex according to the organization of their respective SMP domains using head or tail regions. Two major contact regions among SMP domains are highlighted: H-H (head-to-head) and T-T (tail-to-tail) contacts.

B) Sequence alignment between Mdm12 and Mdm34 along the N-terminal region (residues 1–7) critical for self-association or hetero-interaction. Each of the Mdm12 and Mdm34 sequences is displayed as a WebLogo [38] representation to highlight sequence conservation. The sequences for Mdm12 and Mdm34 were analyzed using 34 and 60 orthologs, respectively.

C) Schematic diagram showing the putative organization of the Mdm12 (yellow)–Mmm1 (red)–Mdm34 (blue)–Mdm10 (green) tetramer. Mmm1 forms a homo-dimer with a head-to-head contact in the center, capped on each end by a Mdm12 monomer through a tail-to-tail contact. Mdm12 associates with Mdm34 through a head-to-head contact. The hexameric SMP model was derived from the structure of six ΔMdm12 molecules within the asymmetric unit.

A

MBP pull-down | Input

MBP alone	+	−	−	+	−	−	−
MBP–Mdm34 (1–188)	−	+	+	−	+	−	−
Mdm12	+	+	−	−	−	+	−
Mdm12 (11–271)	−	−	+	−	−	−	+

66
45
29
20

Mdm12

1 11   271
Mdm12 [SMP domain]

1   22   188   459
Mdm34 [SMP domain]

Mdm34 (1–22)–GST	WT	WT	F5P	F5P
Mdm12	·	WT	WT	I5P

66
45
29
20
—Mdm12

B

H1a   H1b   S1

Mmm1 189 N V D V H P A E S L D W F N V L V A Q I I Q Q F R S E A W H R D N I L H S L N D F I G R K S P D L P E Y L D T I K I T E L D T G D D F P I F 258
E-SYT2 158 W V H F P D T E R A E W L N K T V K H M W P - - - - F I C Q F I E K L F R E T I E P A V R G A N T H L S T F S F T K V D V G Q Q - P L R 220

S2   S3   S4   S5

Mmm1 249 S N C R I Q Y S P N S G N K K L E A K I D I D L N D H L T L G V E T K L L L N Y P K P G I A A L P I N L V V S I V R F Q A C L T V S L T N A 318
E-SYT2 221 I N G V K V Y T E N V D K R Q I I L D L Q I S F V G N C E I D L E I K R - - Y F C R A G V K S I Q I H G T M R V I L E P L I G D M P L V G - 287

S6   S7   H2   H3

Mmm1 309 E E F A S T S N G S S S E N G M E G N S G Y F L M F S F S P E Y R M E F E I K S L I G S R S K L E N I P K I G S V I E Y Q I K K W F V E R C 378
E-SYT2 288 - - - - - - - - - - - - - - - - - - A L S I F F L R K P L L E I N W T G L T N - - - - L L D V P G L N G L S D T I I L D I I S N Y L 331

S8

Mmm1 369 V E P R F Q F V R L P S M W P R S K N T R E E K P T E L 426
E-SYT2 332 V L P N R I T V P L V S E - - - - - - - - - - - - - - - - 344

C

H1b
H1a
H1a
H1b

D

Conf :

Pred :   H1a   H1b

Pred : CCCCCCCCHHHHHHHHHHHHHHHHCHHHHHHHHHHHHHHHHCCCCCCCCCC
Mmm1 : NVDVHPAESLDWFNVLVAQIIQQFRSEAWHRDNILHSLNDFIGRKSPDLPEY
       189   240

Legend :

⬭ = helix   Conf :] ▂▃▅▆[= confidence of prediction
                              −   +

⬈ = strand

— = coil   Pred : predicted secondary structure

30

Figure 1.12. The Mdm12–Mdm34 interaction might be mediated through the N-terminus and the N-terminus of the SMP domain in Mmm1 might resemble that in E-SYT2

A) MBP pull-down experiment (left) showing that the SMP domain of Mdm34 interacts with full-length Mdm12 but not with N-terminus-truncated Mdm12 (residues 11–271). GST pull-down experiment (right) indicates that the N-terminal fragment (residues 1–22) of Mdm34 can interact with the Mdm12. The constructs used in the experiments are shown above.

B) Sequence alignment of SMP domains in Mmm1 and E-SYT2. The relatively conserved sequences are highlighted in red. The secondary structure elements are indicated above the sequences with helices and strands as arrows and cylinders, respectively, based on the crystal structure of E-SYT2 [29]. The N-terminus of Mmm1 that is predicted to form an α-helix (H1a) and make a twofold interface for Mmm1 self-association is indicated by a red square [39]. The sequences corresponding to H1a are highly conserved in E-SYT2 and Mmm1.

C) Ribbon diagram of SMP domain of E-SYT2 highlighting the twofold interface. The color scheme is the same as in (A).

D) Secondary structure prediction of the N-terminus of Mmm1 comprising residues 189–240. Explanations of the different symbols are given in the box.

Table 1.1. Data collection and refinement statistics

	Mdm12		ΔMdm12
Dataset	Native	Se-SAD	Native
PDB accession #			
X-ray source	Beamline 5C, PAL	Beamline 5C, PAL	Beamline 5C, PAL
Temperature (K)	100	100	100
Space group	$P2_12_12$	$P2_12_12$	$P2_12_12_1$
Cell parameters a, b, c (Å)	142.59, 219.07, 73.10	142.59, 219.02, 73.27	109.24, 148.24, 212.39

Data processing

Wavelength (Å)	0.97933	0.97928	0.97957
Resolution (Å)	35.0-3.10 (3.15-3.10)	50.0-3.50 (3.55-3.50)	50.0-3.60 (3.66-3.60)
R_{merge} (%)[a]	11.0 (84.5)	14.3 (65.8)	14.2 (67.9)
CC1/2	0.995 (0.626)	0.994 (0.841)	0.995 (0.648)
I/σ	19.9 (2.22)	20.6 (3.98)	11.1 (2.21)
Completeness (%)	99.6 (100.0)	99.8 (100.0)	99.7 (100.0)
Redundancy	5.3 (5.3)	6.4 (6.6)	3.6 (3.7)
Measured reflections	221431	190622	146540
Unique reflections	41953	29933	40722

Refinement statistics

Data range (Å)	35.0-3.10		50.0-3.60
Reflections	41909		40628
Nonhydrogen atoms	7202		10572
R.m.s. Δ bonds (Å)[b]	0.005		0.007
R.m.s. Δ angles (°)[b]	1.058		1.232
R-factor (%)[c]	21.19		23.26
R_{free} (%)[c, d]	26.88		28.62
Ramachandran plot, residues in			
Most favored regions (%)	92.4		87.6
Additional allowed regions (%)	7.2		11.0
Generously allowed regions (%)	0.4		1.4
Disallowed regions (%)	0		0

*Highest resolution shell is shown in parenthesis.

[a] $R_{merge} = 100 \times \sum_h \sum_i | I_i(h) - \langle I(h)\rangle | / \sum_h \langle I(h)\rangle$, where $I_i(h)$ is the ith measurement and $\langle I(h)\rangle$ is the weighted mean of all measurements of $I(h)$ for Miller indices h.

[b] Root-mean-squared deviation (r.m.s. Δ) from target geometries.

[c] R-factor $= 100 \times \sum|F_P - F_{P(calc)}|/\sum F_P$.

[d] R_{free} was calculated with 5% of the data.

1.5. Materials and Methods

1.5.1. Cloning and protein production

The DNA fragments encoding full-length Mdm12, truncated Mmm1 (residues 160–426), and Mdm34 (residues 1–188) were amplified by PCR using *S. cerevisiae* genomic DNA as a template, and cloned into pET28b-SMT3 vector with BamHI/SalI restriction sites, pCDF-Duet vector with NdeI/XhoI sites, and pMBP-Parallel1 fusion vector with EcoRI/SalI sites, respectively. For production of Mdm12 proteins, the plasmids were transformed into E. coli strain BL21 (DE3) cells, and proteins were expressed by induction with 0.4 mM IPTG at 18°C for 18 h after cell density reached an A_{600} of 0.5–0.6. The harvested cells were lysed in 25 mM sodium phosphate (pH 7.8), 400 mM sodium chloride, 4 mM β-mercaptoethanol, 1 mM phenylmethylsulfonyl fluoride (PMSF) at 4°C. Mdm12 was purified by Ni^{2+}-immobilized affinity chromatography (IMAC) followed by ULP1 cleavage of the SMT3 tag overnight during dialysis against 25 mM Tris–HCl (pH 7.5), 100 mM NaCl, 5 mM β-mercaptoethanol at 4°C. The non-cleaved Mdm12 were removed by another round of Ni^{2+}-IMAC, and the Mdm12 collected from the flow-through was concentrated and applied onto a Superdex 200 column (GE Healthcare) equilibrated with buffer A containing 25 mM Tris–HCl (pH 7.5), 150 mM NaCl, 5 mM dithiothreitol. For selenomethionine-derivatized protein, the Mdm12 plasmid was transformed and expressed in B834 (DE3) grown in M9 minimal media plus selenomethionine. Prior to crystallization experiments, the proteins were concentrated by ultrafiltration to 10 mg/ml and flash frozen in liquid nitrogen for storage. For the Mdm12–tMmm1 complex, two plasmids containing pCDF-Duet with Mdm12 (no-tag) and pET28b-SMT3-tMmm1 were transformed into BL21 (DE3) and expressed and purified as above. All mutants including point mutants and deletion mutant (5′-E_{73}-GGSGG (extra sequences)-S_{115}-3′, for ΔMdm12) were generated by PCR-based methods, and the mutations were confirmed by sequencing.

1.5.2. Crystallization and SAD structure determination

Native and Se-Met-derivatized crystals of Mdm12 of maximum diffraction quality were grown in different crystallization conditions. Native crystals were grown in a well solution containing 2.9 M sodium formate, 100 mM ADA (pH 7.5), 5 mM DTT at 4°C by hanging-drop vapor diffusion. Crystals were cryoprotected by soaking them in a well solution plus 30% glycerol. Diffraction data at 3.1 Å resolution were collected at the Pohang synchrotron at 100 K and processed with HKL2000 [33]. Se-Met-derivatized crystals were grown in a crystallization buffer consisting of 12% polyethylene glycol (PEG) 3350, 100 mM bis tris propane (BTP) pH 6.5, and 200 mM magnesium sulfate at room temperature. Crystals were cryoprotected by soaking them into a well solution plus

30% ethylene glycol, and 3.5 Å resolution Se-SAD data were collected at the same synchrotron beamline and processed as above. Phase determination with the SAD dataset was carried out using Phenix, and excellent electron density was produced with a figure-of-merit of 0.4 [34]. The final model was refined to R/R_{free} values of 0.212/0.265 with native data via successive rounds of model building and refinement using Coot and Phenix [34, 35]. The final model includes four molecules of Mdm12 without any disallowed geometry. The following residues were not modeled owing to disordered electron density: residues 74–113 and 268–271 in the first copy, residues 73–113 and 267–271 in the second copy, residues 74–112 and 268–271 in the third copy, and residues 74–117 and 266–271 in the fourth copy.

ΔMdm12 was crystallized using the hanging-drop method by mixing 1 μl of 15 mg/ml ΔMdm12 proteins with 1 μl of crystallization buffer comprising 1.2 M ammonium sulfate, 100 mM Tris–HCl (pH 8.5), 100 mM lithium sulfate at room temperature. A complete dataset was collected to a resolution of 3.6 Å at the same beamline and processed with HKL2000 as above. Using the Mdm12 structure as a search model, a molecular replacement solution was determined using Phaser [36]. Refinement and model building were performed with Phenix and Coot, respectively. The final model contains six Mdm12 (Δ74–114) molecules in the asymmetric unit without any disallowed geometry. The following residues were not modeled owing to the presence of disordered electron density: residues 268–271 in the first copy, residues 73 and 265–271 in the second copy, residues 73 and 268–271 in the third copy, residues 268–271 in the fourth copy, residues 267–271 in the fifth copy, and residues 266–271 in the sixth copy. The coordinates and structure factors have been deposited in the Protein Data Bank under accession codes 5GYD (native Mdm12) and 5GYK (ΔMdm12).

1.5.3. Size-exclusion chromatography

To measure the relative molecular weights and oligomerization in solution, Mdm12 with or without His-tag, tMmm1, Mdm12–tMmm1 complex were prepared in buffer A at 4°C. Proteins were applied to a Superdex 200 16/60 column (GE Healthcare).

1.5.4. Lipid-binding assays and lipid displacement experiments

For the lipid-binding assay, 1 μl of 10 mg/ml wild-type and mutant (I5P, I5P/L256W, I5P/I262W, and I5P/L256W/I262W) Mdm12 proteins was mixed with 1 μl of 1 mg/ml 16:0 NBD-PE (1,2-dipalmitoyl-sn-glycero-3-phosphoethanolamine-N-[7-nitro-2-1,3-benzoxadiazol-4-yl], purchased from Avanti Polar Lipids) in a total reaction volume of 20 μl of buffer A for 2 h on ice. After reaction, the products were diluted with the sample buffer consisting of 25 mM Tris–HCl (pH 6.8), 20%

glycerol, and 0.01% Bromophenol blue, and subjected to 12% native PAGE. The reaction products were detected with fluorescence (ImageQuant LAS 4000, GE Healthcare) followed by Coomassie Blue staining. Signal intensities were quantified with ImageJ software, and statistical analysis of the results was performed using Excel 2015.

For lipid displacement experiments, the C-terminal GST-tagged Mdm12 (Mdm12-GST) was incubated with a twofold molar excess of NBD-PE for 2 h on ice with 0.3 mM N,N-dimethyldodecylamine N-oxide (LDAO, Sigma-Aldrich). To remove excess unbound NBD-PE, Mdm12-GST was mixed with glutathione sepharose 4B (GE Healthcare) beads and washed three times with buffer A supplemented with 0.3 mM LDAO. NBD-PE bound to Mdm12-GST was eluted with buffer A containing 10 mM reduced glutathione and concentrated to a final concentration of 0.5 mg/ml. Mdm12-GST (20 μl) preloaded with NBD-PE was mixed with 1 μl of phospholipids dissolved in methanol. Reactions were incubated for 2 h on ice and analyzed by native PAGE as described above. All phospholipids were purchased from Avanti Polar Lipids: PA (1,2-dioleoyl-sn-glycero-3-phosphate; DOPA), PC (1,2-dioleoyl-sn-glycero-3-phosphocholine; DOPC), PE (1,2-dioleoyl-sn-glycero-3-phosphoethanolamine; DOPE), PG (1,2-dioleoyl-sn-glycero-3-phospho-(1′-rac-glycerol); DOPG), and PS (1,2-dioleoyl-sn-glycero-3-phospho-L-serine; DOPS).

1.5.5. Pull-down experiments

For the pull-down experiment shown in Figure 1.12A, 200 μg of MBP-tagged Mdm34 (residues 1–188) purified from *E. coli* was mixed with 5 μl of beads of amylose resin (NEB) in a total reaction volume of 500 μl. The beads were washed three times with buffer A. Purified wild-type or mutant Mdm12 (300 μg) was added to the beads and incubated for 2 h at 4°C. The beads were washed again three times with buffer A, and the proteins were analyzed by 12% SDS–PAGE followed by Coomassie Blue staining.

The Mdm34 fragment (residues 1–22, wt or mutants)-GST fusion proteins were co-expressed with full-length Mdm12. Proteins were incubated with 5 μl of a 50% (v/v) slurry of glutathione sepharose 4B beads (GE Healthcare) for 60 min at 4°C. Beads were washed twice with buffer A. Proteins were eluted with SDS sample buffer and analyzed by SDS–PAGE.

1.5.6. Analytical ultracentrifugation

The molecular masses of Mdm12, His$_6$–Mdm12, Mdm12 (I5P), and the Mdm12–tMmm1 complex were analyzed by equilibrium methods using a Beckman An-60 Ti rotor in a Beckman

Optima XL-A analytical ultracentrifuge at 15°C. Proteins at a concentration of 10–20 μM were prepared in buffer B comprising 25 mM Tris–HCl (pH 7.5), 200 mM NaCl, and 5 mM β-mercaptoethanol. The buffer density, viscosity, and sample partial specific volumes were calculated using SEDNTERP (http://sednterp.unh.edu) [37]. Data were evaluated using a nonlinear least-squares curve-fitting algorithm (XL-A data analysis software). The measurements were fit to a single species model using the Origin 6.03 software (Beckman Coulter, Inc.). Sedimentation velocity experiments were performed at 15°C and 20,124 g using two-channel 12-mm path length aluminum centerpieces loaded with 400 μl of sample and 420 μl of buffer B. Separate experiments were conducted with various concentrations of Mdm12 (0.5, 1, and 2 mg/ml). Scans were collected in 10-min intervals using continuous scan mode with a radial spacing of 0.003 cm. Data were analyzed using the continuous c(s) distribution in the SEDFIT program for fitting the frictional ratio, meniscus, and time-invariant noise.

1.5.7. APCI-MS

Purified Mdm12 was desalted using a HiTrap desalting column (GE healthcare) equilibrated with ultrapure grade water. Desalted Mdm12 (50 μl) was mixed with 950 μl of acetonitrile and incubated with vigorous vortexing for 1 h at room temperature. All analyses were performed with a Bruker HCT ion-trap mass spectrometer (Bruker Daltonics, Bremen, Germany) equipped with an atmospheric pressure chemical ionization (APCI) source. For direct infusion, samples were infused with a syringe pump (KD Scientific) at a flow rate of 240 μl/h. The APCI source was operated in positive mode with a drying gas (N2) flow of 5 l/min, nebulizer pressure of 30 psi, drying gas temperature of 250°C, vaporizer temperature of 400°C, capillary voltage of 4.5 kV, and corona current of 4,000 nA. The scanning mass to charge range was 430–1,000 m/z, with a scanning speed of 26,000 m/z per s. To control the instrument, a Compass 1.3 for HCT/esquire (EsquireControl Version 6.2) was employed, and an ESI Compass 1.3 for HCT/esquire (DataAnalysis Version 4.0) was used for data evaluation (both obtained from Bruker Daltonics).

1.6. Reference

[1] Robertson JD (1960) The molecular structure and contact relationships of cell membranes. *Prog Biophys Mol Biol* 10:343

[2] Mannella CA, Buttle K, Rath BK, Marko M (1998) Electron microscopic tomography of rat-liver mitochondria and their interactions with the endoplasmic reticulum. *BioFactors* 8:225–228

[3] Csordás G, Renken C, Várnai P, Walter L, Weaver D, Buttle KF, Balla T, Mannella CA, Hajnóczky G (2006) Structural and functional features and significance of the physical linkage between ER and mitochondria. *J Cell Biol* 174:915–921

[4] Elbaz Y, Schuldiner M (2011) Staying in touch: the molecular era of organelle contact sites. *Trends Biochem Sci* 36:616–623

[5] Helle SC, Kanfer G, Kolar K, Lang A, Michel AH, Kornmann B (2013) Organization and function of membrane contact sites. *Biochim Biophys Acta* 1833:2526–2541

[6] Kornmann B, Walter P (2010) ERMES-mediated ER-mitochondria contacts: molecular hubs for the regulation of mitochondrial biology. *J Cell Sci* 123:1389–1393

[7] Lang A, Peter ATJ, Kornmann B (2015) ER–mitochondria contact sites in yeast: beyond the myths of ERMES. *Curr Opin Cell Biol* 35:7–12

[8] Rowland AA, Voeltz GK (2012) Endoplasmic reticulum–mitochondria contacts: function of the junction. *Nat Rev Mol Cell Biol* 13:607–625

[9] Kornmann B (2013) The molecular hug between the ER and the mitochondria. *Curr Opin Cell Biol* 25:443–448

[10] Kornmann B, Currie E, Collins SR, Schuldiner M, Nunnari J, Weissman JS, Walter P (2009) An ER-mitochondria tethering complex revealed by a synthetic biology screen. *Science* 325:477–481

[11] Kornmann B, Osman C, Walter P (2011) The conserved GTPase Gem1 regulates endoplasmic reticulum–mitochondria connections. *Proc Natl Acad Sci USA* 108:14151–14156

[12] Murley A, Lackner LL, Osman C, West M, Voeltz GK, Walter P, Nunnari J (2013) ER-associated mitochondrial division links the distribution of mitochondria and mitochondrial DNA in yeast. *eLife* 2:e00422

[13] Kopec KO, Alva V, Lupas AN (2010) Homology of SMP domains to the TULIP superfamily of lipid-binding proteins provides a structural basis for lipid exchange between ER and mitochondria. *Bioinformatics* 26:1927–1931

[14] Toulmay A, Prinz WA (2012) A conserved membrane-binding domain targets proteins to organelle contact sites. *J Cell Sci* 125:49–58

[15] Lahiri S, Toulmay A, Prinz WA (2015) Membrane contact sites, gateways for lipid homeostasis. *Curr Opin Cell Biol* 33:82–87

[16] Nguyen TT, Lewandowska A, Choi JY, Markgraf DF, Junker M, Bilgin M, Ejsing CS, Voelker DR, Rapoport TA, Shaw JM (2012) Gem1 and ERMES do not directly affect phosphatidylserine transport from ER to mitochondria or mitochondrial inheritance. *Traffic* 13:880–890

[17] Lahiri S, Chao JT, Tavassoli S, Wong AK, Choudhary V, Young BP, Loewen CJ, Prinz WA (2014) A conserved endoplasmic reticulum membrane protein complex (EMC) facilitates phospholipid transfer from the ER to mitochondria. *PLoS Biol* 12:e1001969

[18] Hönscher C, Mari M, Auffarth K, Bohnert M, Griffith J, Geerts W, van der Laan M, Cabrera M, Reggiori F, Ungermann C (2014) Cellular metabolism regulates contact sites between vacuoles and mitochondria. *Dev Cell* 30:86–94

[19] Elbaz-Alon Y, Rosenfeld-Gur E, Shinder V, Futerman AH, Geiger T, Schuldiner M (2014) A dynamic interface between vacuoles and mitochondria in yeast. *Dev Cell* 30:95–102

[20] Meisinger C, Pfannschmidt S, Rissler M, Milenkovic D, Becker T, Stojanovski D, Youngman MJ, Jensen RE, Chacinska A, Guiard B (2007) The morphology proteins Mdm12/Mmm1 function in the major b-barrel assembly pathway of mitochondria. *EMBO J* 26:2229–2239

[21] Böckler S, Westermann B (2014) Mitochondrial ER contacts are crucial for mitophagy in yeast. *Dev Cell* 28:450–458

[22] Friedman JR, Lackner LL, West M, DiBenedetto JR, Nunnari J, Voeltz GK (2011) ER tubules mark sites of mitochondrial division. *Science* 334:358–362

[23] Hobbs AEA, Srinivasan M, McCaffery JM, Jensen RE (2001) Mmm1p, a mitochondrial outer membrane protein, is connected to mitochondrial DNA (mtDNA) nucleoids and required for mtDNA stability. *J Cell Biol* 152:401–410

[24] Meeusen S, Nunnari J (2003) Evidence for a two membrane–spanning autonomous mitochondrial DNA replisome. *J Cell Biol* 163:503–510

[25] Frederick RL, McCaffery JM, Cunningham KW, Okamoto K, Shaw JM (2004) Yeast Miro GTPase, Gem1p, regulates mitochondrial morphology via a novel pathway. *J Cell Biol* 167:87–98

[26] Youngman MJ, Hobbs AEA, Burgess SM, Srinivasan M, Jensen RE (2004) Mmm2p, a mitochondrial outer membrane protein required for yeast mitochondrial shape and maintenance of mtDNA nucleoids. *J Cell Biol* 164:677–688

[27] Beamer LJ, Carroll SF, Eisenberg D (1997) Crystal structure of human BPI and two bound phospholipids at 2.4 angstrom resolution. *Science* 276:1861–1864

[28] Qiu X, Mistry A, Ammirati MJ, Chrunyk BA, Clark RW, Cong Y, Culp JS, Danley DE, Freeman TB, Geoghegan KF (2007) Crystal structure of cholesteryl ester transfer protein reveals a long tunnel and four bound lipid molecules. *Nat Struct Mol Biol* 14:106–113

[29] Schauder CM, Wu X, Saheki Y, Narayanaswamy P, Torta F, Wenk MR, De Camilli P, Reinisch KM (2014) Structure of a lipid-bound ExtendedSynaptotagmin indicates a role in lipid transfer. *Nature* 510:552

[30] AhYoung AP, Jiang J, Zhang J, Khoi Dang X, Loo JA, Zhou ZH, Egea PF (2015) Conserved SMP domains of the ERMES complex bind phospholipids and mediate tether assembly. *Proc Natl Acad Sci USA* 112:E3179–E3188

[31] Baker NA, Sept D, Joseph S, Holst MJ, McCammon JA (2001) Electrostatics of nanosystems: application to microtubules and the ribosome. *Proc Natl Acad Sci USA* 98:10037–10041

[32] Ashkenazy H, Erez E, Martz E, Pupko T, Ben-Tal N (2010) ConSurf 2010: calculating evolutionary conservation in sequence and structure of proteins and nucleic acids. *Nucleic Acids Res* 38:W529–W533

[33] Otwinowski Z, Minor W (1997) Processing of X-ray diffraction data collected in oscillation mode. *Methods in enzymology*, Carter CW Jr. (ed) pp 307–326. New York: Academic Press

[34] Adams PD, Afonine PV, Bunkoczi G, Chen VB, Davis IW, Echols N, Headd JJ, Hung LW, Kapral GJ, Grosse-Kunstleve RW et al (2010) PHENIX: a comprehensive Python-based system for macromolecular structure solution. *Acta Crystallogr D Biol Crystallogr* 66:213–221

[35] Emsley P, Lohkamp B, Scott WG, Cowtan K (2010) Features and development of Coot. *Acta Crystallogr D Biol Crystallogr* 66:486–501

[36] McCoy AJ, Grosse-Kunstleve RW, Adams PD, Winn MD, Storoni LC, Read RJ (2007) Phaser crystallographic software. *J Appl Crystallogr* 40:658–674

[37] Harding SE, Horton JC (1992) Analytical ultracentrifugation in biochemistry and polymer science. Cambridge: Royal Society of Chemistry

[38] Crooks GE, Hon G, Chandonia J-M, Brenner SE (2004) WebLogo: a sequence logo generator. *Genome Res* 14:1188–1190

[39] Jones DT (1999) Protein secondary structure prediction based on position-specific scoring matrices. *J Mol Biol* 292:195–202

Chapter 2. Crystal structures of Mmm1 and Mdm12-Mmm1 reveal mechanistic insight into phospholipid trafficking at ER-mitochondria contact sites.

2.1. Abstract

The endoplasmic reticulum (ER)-mitochondria encounter structure (ERMES) comprises mitochondrial distribution and morphology 12 (Mdm12), maintenance of mitochondrial morphology 1 (Mmm1), Mdm34, and Mdm10 and mediates physical membrane contact sites and nonvesicular lipid trafficking between the ER and mitochondria in yeast. Herein, we report two crystal structures of the synaptotagmin-like mitochondrial lipid-binding protein (SMP) domain of Mmm1 and the Mdm12–Mmm1 complex at 2.8 Å and 3.8 Å resolution, respectively. Mmm1 adopts a dimeric SMP structure augmented with two extra structural elements at the N and C termini that are involved in tight self-association and phospholipid coordination. Mmm1 binds two phospholipids inside the hydrophobic cavity, and the phosphate ion of the distal phospholipid is specifically recognized through extensive H-bonds. A positively charged concave surface on the SMP domain not only mediates ER membrane docking but also results in preferential binding to glycerophospholipids such as phosphatidylcholine (PC), phosphatidic acid (PA), phosphatidylglycerol (PG), and phosphatidylserine (PS), some of which are substrates for lipid-modifying enzymes in mitochondria. The Mdm12–Mmm1 structure reveals two Mdm12s binding to the SMP domains of the Mmm1 dimer in a pairwise head-to-tail manner. Direct association of Mmm1 and Mdm12 generates a 210-Å-long continuous hydrophobic tunnel that facilitates phospholipid transport. The Mdm12–Mmm1 complex binds all glycerophospholipids except for phosphatidylethanolamine (PE) in vitro.

2.2. Introduction

Membrane contact sites (MCSs) play an essential role in subcellular communication by exchanging cellular materials and information [1, 2]. Among the various endoplasmic reticulum (ER)-mediated MCSs reported to date [3], the ER-mitochondria contact site has been the most extensively studied, and an involvement in ion homeostasis, mitochondrial dynamics such as membrane fission and fusion, and cooperative lipid synthesis has been reported [4–9]. Most importantly, lipid trafficking occurring at the ER-mitochondria MCS is essential for the biogenesis of the mitochondrial membrane, since mitochondria are not connected with the vesicular transport machinery, and essential lipids required for the composition of mitochondrial membrane must therefore be supplied directly from the ER [10–12].

Formation of the MCS is the result of direct interaction between protein components located at two distinct subcompartments to be adjoined. In yeast, ER-mitochondria contact sites are primarily mediated by the ER-mitochondria encounter structure (ERMES) complex that comprises four proteins: the cytosolic component mitochondrial distribution and morphology 12 (Mdm12); the ER membrane protein maintenance of mitochondrial morphology 1 (Mmm1); and two mitochondria outer membrane proteins, Mdm34 and Mdm10 [13]. Additionally, mitochondria anchoring Gem1, a Ca^{2+}-binding small GTPase, directly associates with the ERMES complex and regulates its size and number [14–16]. ERMES components are also regulated by Rsp5 E3 ubiquitin ligase, and ubiquitination is required for efficient mitophagy [17].

Accumulated evidence suggests that Mdm12, Mmm1, and Mdm34 share a synaptotagmin-like mitochondrial lipid-binding protein (SMP) domain [7, 18–20], suggesting that the ERMES complex not only tethers two connecting membranes but also acts as a transfer vehicle to exchange phospholipids between the ER and mitochondria [21]. Indeed, ERMES mutants have an altered phosphatidylserine (PS)-to-phosphatidylethanolamine (PE) conversion rate [13, 22], suggesting that the ERMES complex might be critically involved in phospholipid trafficking at ER-mitochondria contact sites, although its direct involvement in converting PS to PE still remains contentious [23]. Recent studies have highlighted alternative lipid trafficking pathways involving vacuoles, which reciprocally supply mitochondria with phospholipids [24–26]. Furthermore, the ER membrane protein complex (EMC) comprising conserved Emc1–Emc6 proteins performs a comparable role in lipid transfer from the ER to mitochondria by mediating tethering between these organelles [26]. In addition to lipid trafficking, other functions of the ERMES complex have been reported, including mitochondrial protein assembly [27] and import [28], maintenance of mitochondrial DNA [15, 29, 30], mitochondria inheritance [31], and mitophagy [17, 32–34].

Previously, we determined the crystal structure of *Saccharomyces cerevisiae* Mdm12 at 3.1 Å resolution and revealed that Mdm12 forms a dimeric SMP structure that binds phospholipids inside a hydrophobic channel, with a preference for glycerophospholipids harboring a positively charged head group [20]. Another study determined a 17 Å resolution electron microscopy (EM) structure of the Mdm12–Mmm1 (SMP domain) complex, revealing an elongated tubular structure with an Mdm12-Mmm1-Mmm1-Mdm12 arrangement [19, 35]. Despite these structure studies, the molecular-level mechanism by which the SMP domains of Mdm12, Mmm1, and Mdm34 are directly organized and facilitate phospholipid trafficking without consuming energy at the ER-mitochondria contact site remains unknown. Additionally, exactly how Mmm1, an ER component of the ERMES complex, recognizes specific phospholipids in the ER membrane remains elusive, as does the mechanism by which phospholipids selected by Mmm1 are transported into Mdm12, as a direct binding partner of the ERMES complex.

In the present study, we determined crystal structures of the Mmm1 SMP domain and the Mdm12–Mmm1 binary complex, and discuss the resultant molecular-level insight into how the Mmm1 SMP domain contributes to the organization of the ERMES components, as well as phospholipid trafficking.

2.3. Results

2.3.1. Structure Determination of Mmm1.

The Mmm1 protein is predicted to comprise a single transmembrane domain near its N terminus that anchors it to the ER membrane, an unstructured region consisting of around 50 residues, and an SMP domain at the C terminus (Figure 2.1A and Figure 2.2). The N-terminal region of Mmm1 is located in the ER lumen, while the SMP domain is localized in the cytosol and directly interacts with Mdm12, a cytosolic component of the ERMES complex. Despite significant effort to purify Mmm1 proteins, size-exclusion chromatography (SEC) experiments revealed that the SMP domain of *S. cerevisiae* Mmm1 (scMmm1) aggregated in solution unless in a complex with Mdm12 [20]. Extensive screening for solubility and homogeneous dispersal in solution for Mmm1 orthologs, together with limited proteolysis analysis, revealed that the Mmm1 SMP domain of *Zygosaccharomyces rouxii* (zrMmm1, residues 190–444) was soluble even when not complexed with Mdm12 (Figure 2.1B). The SMP domain of zrMmm1 shares 76% sequence identity with that of scMmm1. The zrMmm1 proteins eluted from the gel-filtration column at a volume corresponding to the molecular weight of a dimer, suggesting that the recombinantly expressed zrMmm1 SMP domain forms a homodimer in solution. Interestingly, the SEC experiment confirmed that zrMmm1 was able to interact with scMdm12 when coexpressed in *Escherichia coli* cells despite the organismal discrepancy (Figure 2.1B). Diffraction-quality crystals of zrMmm1 were grown in the $P3_{2}21$ space group at 4 °C over a period of 1 week, and the structure was solved using selenomethionine-substituted crystals by the single-wavelength anomalous dispersion method (Figure 2.3). The final model of zrMmm1 was refined with data from native crystals to 2.8 Å resolution.
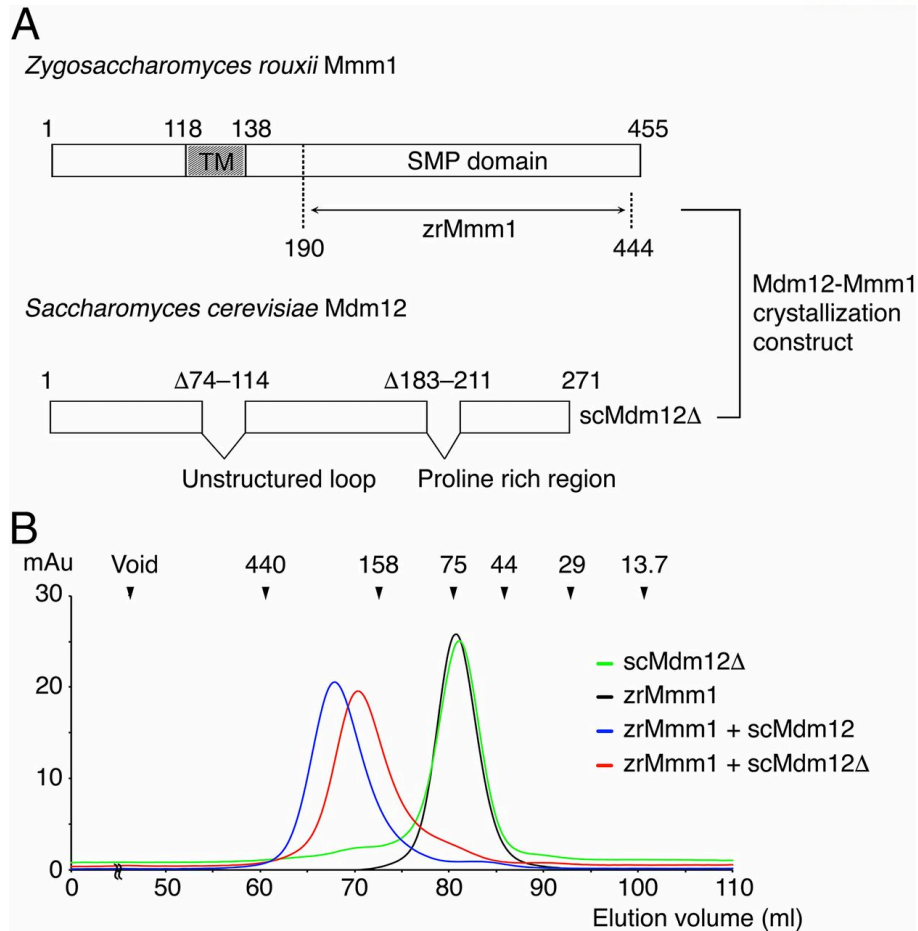
Figure 2.1. Domain structure and direct interaction of Mmm1 and Mdm12.

(A) Diagrams showing the domain structure of Z. rouxii Mmm1 and *S. cerevisiae* Mdm12. Mmm1 has a transmembrane (TM) domain in the middle of the protein chain that is required for anchoring the ER membrane, and the SMP domain is at the C terminus. Full-length scMdm12 covers the overall SMP domain. The Mmm1 construct used in this study is indicated with an arrow (*Z. rouxii* Mmm1 residues 190–444, referred to as zrMmm1). To obtain diffraction-quality crystals of the Mdm12–Mmm1 complex, two unstructured regions were omitted in the scMdm12 construct (Δ74–114 and Δ183–211, referred to as scMdm12Δ).

(B) SEC profiles of scMdm12Δ (green), zrMmm1 (black), and complexes of zrMmm1 and scMdm12 (blue) and zrMmm1 and scMdm12Δ (red). Experimental details are provided in Materials and Methods. Protein standards used in the experiment are indicated above the chromatogram. mAu, milliabsorbance unit.

```
Z. rouxii     M E S N Y T G M D G - - - - - - - - - - - - - - - N W A L N G T V S V G N G T L I S V D E F L H N A L P M H L Q A L F Q D G N S Q G P L L T M E D L E K A I E F K   66
C. glabrata   M V S A L E V K S - - - - - - - - - - - - - - - - - - - I K D - S N E T L I S L D D Y I R N T L P S Q L H E I L L E E F Q - - - - - N Q D F S R G Q D V S N   53
S. cerevisiae M T D S E N E S T - - - - - - - - - - - - - - - - - - E T - - - D S L M T F D D Y I S K E L P E H L Q R L I M E N - - - - - - - L K G S T T N D L K Q   47
A. gossypii   M K G V E N T L S Q S E S V N R G Y N G W M G M E S E T S A R A T H S S E Q M I S L E E Y V R E M L P M H L Q K L L M E R - - - - - - - - - - - I I E A E Q T G   69
N. crassa     M - - - - - - - - - - - - - - - - - - - - - - - - - - - - - - - - - - - - - - - - - - - - - - - - - - - - - - - - - - - - - - - - - - - - - - - - - - - -    1
K. lactis     M E M S E L L A S E V V S S G P D Y - A K K S V D G L N M T A A N G T N D T L M T D E Y L N K S L P L H L E Q L I L D - - - - - - - - - - - - A N Q K E L F D   67
V. polyspora  M N N L D N L A G - - - - - - - - - - - - - - - N M S N L T I Q Q G K G N E T L I S L D E Y V N N I L P S H L K K I F S D N - - - - - - L R E N Y Q I P R E F F E   59
S. stipitis   M A D L E T S D L S - - - - - - - - - - - - - - - - - - R V L P S - S N L L S L E Q - L Q E Q L K R H R D E L F Q Q - - - - - - - - - - - - Q Q D S H V L G   46
```

Transmembrane region

```
Z. rouxii     R A S Q E L V N D N V L A P D G L F V E L L R Q Q E K T - - L P R L I S A T S N T Q G S F S S W S F A Q G L I V G Q V S V V L V L I F F I K F F I F S D S S T K   144
C. glabrata   S T H D Q M I D H T L E L T S D L L R N - - - A L D K Q L M E V Q S R T L P V R Q S N Q L I S W S F A Q G L I I G Q L S V V I F L I F F V K F F I F T D A S S K   130
S. cerevisiae T S N N S E F N V S K N G S F K G L D D A I Q A L Q M Q S V L H P S S L G S L A T S S K F S G W S F A Q G F F V G Q L S I V L L F I F F L K F F I F S D E P S K   127
A. gossypii   A A H T S V F A A P T G V A A Q - - - - - - - - - - - - - Y P A M G P P M L P G Q T F S S R S F A E G L V V G Q L S V I V V L I F F I K F F I F S D G P A K   134
N. crassa     - - - - - - - - - - - - - - - - - - - - - - - A D I C P S R S E P T L S F T Q G L I L G Q L S V V L L L A A F I K F F I F G D P P S P   45
K. lactis     S A A K S L L S S T L L A K Q Q - - - - - - - - - - - - - Q S L Q I A P I Q P Q S S F S S Q S F A E G L I V G Q L S V I V A L I F V I K F F V F S E G G T K   132
V. polyspora  S A E L S G I N N K I D Q E I Q K Y S H L L K G L S N N - - G Q T S F G S Y L S N S N S F S G W S F I E G F I I G Q F S V I V L I F I K F F V F S D G S S S   137
S. stipitis   S K P D D S L N N N Y L L S H Q - - - - - - - - - - - - - - - Y H D S Q V Y I P S N - - - - T W S F T Q G L I V G Q L S V V F V I V I F I K F F V F A E S S P A   107
```

α1
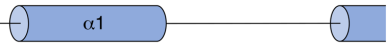
```
Z. rouxii     T N P N P A K N S S S T N S L S G L S S E S R S F I S P H F F T S I M N R K G N E Q A E S N - D D E N E R S R Q I D D I L E K T Y Y N V D T H P A E S L D W F N   223
C. glabrata   M D - - - - - - - N P L P S K V S K S Y L K N - - R R - E S S S I K D K R K G V L V K E E S G E T D L H G S L Q L N D I L E K T Y Y N V D T H S A E S L D W F N   200
S. cerevisiae S - - - - - K N P K P A A S R H R S K F K E Y P F I S R E F L T S L V R K G A K Q H Y E L N E E A E N E H L Q E L A L I L E K T Y Y N V D V H P A E S L D W F N   202
A. gossypii   T G G G G G S S A E S R S S G F T G S P L T S - - T T S R L L T E T H G R K G K E G T E F A E D S E N E R T R Q I N A I L E K T Y Y V D V E T H S P E S L D W F N   212
N. crassa     E - - - V V A S I R A T D R R S R T L A H K K S I L S L R E T N A L Q L V Q N P A L N K K H V L R P G P P I L T I G S I L S K T Y Y K V D S H Q P E S L D W F N   122
K. lactis     T - - - - - - - A T A K S V G S A S S F M D S - - T K N S I L S T I I K R G G H D G L E V D - D K D N E K S R Q I N S I L E K T Y Y N V E T H S P E S L D W F N   202
V. polyspora  N S S N P K P S L N S R S D R T S F S Y K S N S M L S N F F S S I M K R G G K T H Y E T D - - I D S G N T N R L N T I L E K V Y Y D V D T H P S E S L D W F N   215
S. stipitis   L - - - - - - - - A K S S I T K D A S V V I V K - - R D K K D Q S S S D D A D P D D D S E T T - - A S N - - - A K V A A I L E K T Y Y D V D N H S P E S L D W F N   173
```

α2   α3   β1   β1
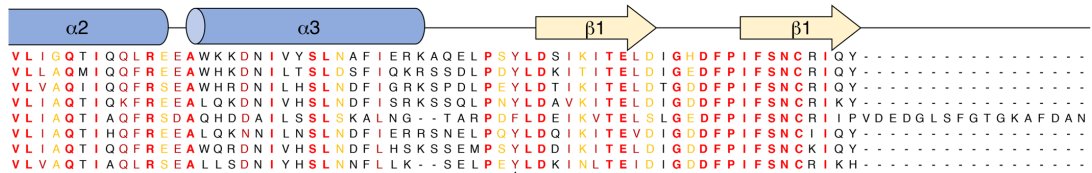
```
Z. rouxii     V L I G G Q T I Q Q L R E E A W K K D N I V Y S L N A F I E R K A Q E L P S Y L D S I K I T E L D I G H D F P I F S N C R I Q Y - - - - - - - - - - - - - - -   286
C. glabrata   V L L A Q M I Q Q F R E E A W H K D N I L T S L D S F I Q K R S S D L P D Y L D K I T I T E L D I G E D F P I F S N C R I Q Y - - - - - - - - - - - - - - -   263
S. cerevisiae V L V A Q I I Q Q F R S E A W H R D N I L H S L N D F I G R K S P D L P E Y L D T I K I T E L D T G D D F P I F S N C R I Q Y - - - - - - - - - - - - - - -   265
A. gossypii   V L I A Q T I A Q F R S D A Q H D D A I L S S L S K A L N G - - T A R P D F L D E I K V T E L S L G E D F P I F S N C R I K Y - - - - - - - - - - - - - - -   275
N. crassa     V L I A Q T I A Q F R S D A Q H D D A I L S S L S K A L N G - - T A R P D F L D E I K V T E L S L G E D F P I F S N C R I P V D E D G L S F G T G K A F D A N   200
K. lactis     V L I A Q T I H Q F R E E A L Q K D N I V H S L N D F I E R R S N E L P Q Y L D Q I K I T E V D I G D D F P I F S N C I Q Y - - - - - - - - - - - - - - -   265
V. polyspora  V L I A Q T I Q Q F R E E A W Q R D N I V H S L N D F L H S K S S E M P S Y L D D I K I T E L D I G D D F P I F S N C K I Q Y - - - - - - - - - - - - - - -   278
S. stipitis   V L V A Q T I A Q L R S E A L L S D N I Y H S L N N F L L K - - S E L P E Y L D K I N L T E I D I G D D F P I F S N C R I K H - - - - - - - - - - - - - - -   234
```

Y261

β2   β2   β3   β3
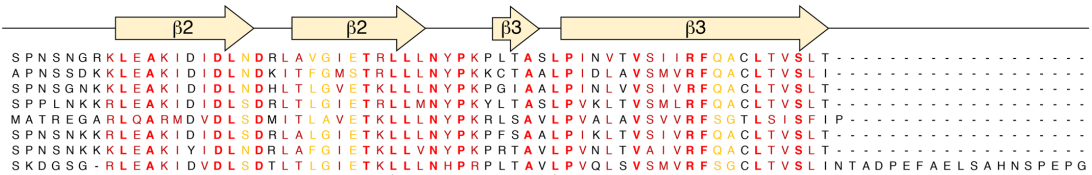
```
Z. rouxii     S P N S N G R K L E A K I D I D L N D R L A V G I E T R L L L N Y P K P L T A S L P I N V T V S I I R F Q A C L T V S L T - - - - - - - - - - - - - - -   347
C. glabrata   A P N S S D K K L E A K I D I D L N D K I T F G M S T R L L L N Y P K P G I A A L P I D L A V S M V R F Q A C L T V S L I - - - - - - - - - - - - - - -   324
S. cerevisiae S P N S G N K K L E A K I D I D L N D H L T L G V E T K L L L N Y P K P G I A A L P I N L V V S I V R F Q A C L T V S L T - - - - - - - - - - - - - - -   326
A. gossypii   S P P L N K K R L E A K I D I D L S D R L T L G I E T K L L M N Y P K Y L T A S L P V K L T V S M L R F Q A C L T V S L T - - - - - - - - - - - - - - -   336
N. crassa     M A T R E G A R L Q A R M D V D L S D M I T L A V E T K L L L N Y P K R L S A V L P V A L A V S V V R F S G T L S I S F I P - - - - - - - - - - - - - - -   262
K. lactis     S P N S N K K R L E A K I D I D L S D R L A L G I E T K L L N Y P K P F S A A L P I K L T V S I V R F Q A C L T V S L T - - - - - - - - - - - - - - -   326
V. polyspora  S P N S N K K K L E A K I Y I D L N D R L A F G I E T K L L V N Y P K P R T A V L P V N L T V A I V R F Q A C L T V S L T - - - - - - - - - - - - - - -   339
S. stipitis   S K D G S G - R L E A K I D V D L S D T L T L G I E T K L L L N H P R P L T A V L P V Q L S V S M V R F S G C L T V S L I N T A D P E F A E L S A H N S P E P G   313
```

L315   G loop   L327

β4   β4

```
Z. rouxii     - - - - - - - - - K A E E F V P T S P E S V D E - - - - - - - - D D N D G Y F L M F S F A P E Y R M E F E T Q S L I G A R S K L E N I P K I G S L   403
C. glabrata   - - - - - - - - - T A E E L E F T T G N K I D D - - - - - - - - N E K N G Y V L V F S F T P E Y K I D F D I K S L I G S R S K L E N I P K I S N I   380
S. cerevisiae - - - - - - - - - N A E E F A S T S N G S S S E N G - - - - - M E G N S G Y F L M F S F S P E Y R M E F E I K S L I G S R S K L E N I P K I S G V   385
A. gossypii   - - - - - - - - - T A E E F V P T M A A T T D T D - - - - - - A G D S E G H Y L V F S F S P D Y R M E F D I K S L I G A R S K L E N I P K I S S L   394
N. crassa     - - - - - - - - - - - - - - - - - S N P S - - - - - - - - N N E P A K M I F T L D D Y R L D F S I R S L L G S R L Q D V P K I A Q L   306
K. lactis     - - - - - - - - - T D E Q F V P T S E E T N D D E - - - - - M G N D K G Y Y L M F S F N P E Y R M E L E V K S L I G S R S K L E N I P K I A S L   384
V. polyspora  - - - - - - - - - N A E D F V P T T K E T A S S - - - - - - - Q D D D G Y F L M F S F G P E Y K M D F D I E S L I G A R S K L Q N I P K I S S V   395
S. stipitis   E P M S R S H S A G S P G G D S S H D E V I S T P D S S S H T A Q R K H S K D D P N D G T A L M F S F S P D Y R L E F T V K S L I G A R A K L Q D V P K I S S L   393
```

α4   β5   β6

```
Z. rouxii     V E Y Q I K K W F V E R C V E P R F Q F I K L P S V W P R S K N T R E G K A D V D E S E P G R E T H Y - - - - - - - - - -   454
C. glabrata   I E Y N I K K W F A E R C V E P R F Q S V K L P G M W P R S K N T R E E V I H K T E D E S S S K T P H S - - - - - - - -   431
S. cerevisiae I E Y Q I K K W F V E R C V E P R F Q F V R L P S M W P R S K N T R E E K P T E L - - - - - - - - - - - - - - - -   426
A. gossypii   V E Y Q I K K W F M D R C V E P R F Q F V K L P S M W P R S K N T R E E K S D M Q E E D P S R A P E - - - - - - - -   444
N. crassa     V E S R L H R W F D E R C V E P R F Q F E I A L P N M W P R K K N T R G G D E T I S D V E R S M S K A K G V D I A K D V R E E A R K E I E A E A H G G A D R V P D   386
K. lactis     I E Y Q I S K W F V E R C V E P R F Q F V K L P S M W P R S K N T R K E K T D T D D S V S V K S N D - - - - -   434
V. polyspora  I E Y H I K K W F V E R C V E P R F Q C I R L P S M W P R S K N T R E E K V D T D D V P L S K A E - - - - - - -   444
S. stipitis   I E N R L R A W F I E R C I E P R F Q V V R L P S L W P R R K N T R E Q V T N K N G D K V E D G S N - - - - - -   443
```

C-string

```
Z. rouxii     - - - - - - - - - - - - - - - - - - - - - - - - - - - -   454
C. glabrata   - - - - - - - - - - - - - - - - - - - - - - - - - - - -   431
S. cerevisiae - - - - - - - - - - - - - - - - - - - - - - - - - - - -   426
A. gossypii   - - - - - - - - - - - - - - - - - - - - - - - - - - - -   444
N. crassa     S L R Y R H R P R A D E E F P G A G S M P G S M P G S M P   415
K. lactis     - - - - - - - - - - - - - - - - - - - - - - - - - - - -   434
V. polyspora  - - - - - - - - - - - - - - - - - - - - - - - - - - - -   444
S. stipitis   - - - - - - - - - - - - - - - - - - - - - - - - - - - -   443
```

Figure 2.2. Sequence alignment of Mmm1 homologs in yeast species.

The figure shows full-length Mmm1 sequences among yeast homologs, including those of *Zygosaccharomyces rouxii*, *Candida glabrata*, *Saccharomyces cerevisiae*, *Ashbya gossypii*, *Neurospora crassa*, *Kluyveromyces lactis*, *Vanderwaltozyma polyspora*, and *Scheffersomyces stipitis*. The sequence conservation at each amino acid is shaded in a color gradient from yellow (70% similarity) to red (100% identity). The secondary structure assigned by the crystal structure of zrMmm1 (residues 190–444) is indicated above the sequences as blue cylinders (α-helices), yellow arrows (β-strands), black lines (loop regions), and black dots (disordered residues). Putative transmembrane domains required for anchoring the ER membrane are highlighted with a dotted box. Two conserved and significant residues (L315 and L327) involved in the interaction with Mdm12 are indicated below the sequences.

2.3.2. Structure of the zrMmm1 SMP Domain.

Crystals of zrMmm1 contained one zrMmm1 molecule in the asymmetric unit. However, zrMmm1 forms a tight dimer with a crystal symmetry-related molecule via a twofold rotation arrangement. The dimeric organization of zrMmm1 was confirmed by previous biochemical experiments, and is consistent with other SMP domain structures [20, 36–38]. Overall, the dimeric zrMmm1 SMP structure resembles a compact diamond with dimensions of $50 \times 60 \times 120$ Å, and each component consists of four helices and six extended and twisted antiparallel β-strands that assemble into a typical SMP structure with an extended hydrophobic channel (Figure 2.4A and Figure 2.2 and 2.3). In a previous study, we suggested that the N terminus (residues 198–214) of the Mmm1 SMP domain dimer might be involved in the twofold interface and might be structurally similar to that of E-SYT2 based on sequence similarity [20]. Consistent with our prediction, the twofold interface of the zrMmm1 dimer is composed of two helices in a face-to-face arrangement reminiscent of that in the E-SYT2 structure (Figure 2.4B, interface I and Figure 2.5A). In particular, three hydrophobic residues (Leu219, Trp221, and Phe222) stabilize the twofold axis through van der Waals interactions.

Upon comparing the SMP domains of E-SYT2 and Mdm12, it was immediately apparent that two extra structural elements absent in the Mdm12 and E-SYT2 domains are present at the N and C termini of zrMmm1 (Figure 2.4B and Figure 2.5). These structural elements presumably make an important contribution to the tight association between subunits of the zrMmm1 dimer, since over 3,400 $Å^2$ of solvent-accessible surface area is buried upon self-association. The N terminus of zrMmm1 adopts an α-helix (α1) and a well-ordered loop that contacts the head region of the other molecule of the dimer (interface II). In particular, the N-terminal helix comprising residues 196–207 wraps around the twofold axis helix of the opposing molecule in an antiparallel domain-swapped manner (Figure 2.4B, interface II). The highly conserved C terminus of zrMmm1 exhibits a long, extended loop that crosses over the two molecules and essentially mediates the self-association of the zrMmm1 dimer, as well as phospholipid binding (Figure 2.4 B and C, interface III). In more detail, the extended loop consisting of residues 425–432 forms an antiparallel β-strand–like strap structure that zips up the opposing twofold central helices, and eventually covers the concave surface at the center of the dimeric SMP domain (Figure 2.4B, interface III). This loop also contains the absolutely conserved Trp430 and Arg432 residues that are essential for the recognition of phospholipids, as discussed below. Additionally, the C terminus of zrMmm1 adopts a short 310 helix (residues 433–435), followed by antiparallel β-strands, and is incorporated between β5 and an 11-residue loop (residues 347–357) from the opposing molecule of the dimer through the formation of an extensive hydrogen-bonding network (Figure 2.4B, interface IV).

In summary, the extensive interfaces that are lacking in E-SYT2 and Mdm12 provide the driving force for the tight self-association observed in the zrMmm1 dimer. Consistently, SEC and native PAGE revealed that the dynamic distribution between monomer and dimer observed for Mdm12 and the SMP domain of E-SYT2 was not a feature of zrMmm1 [20].
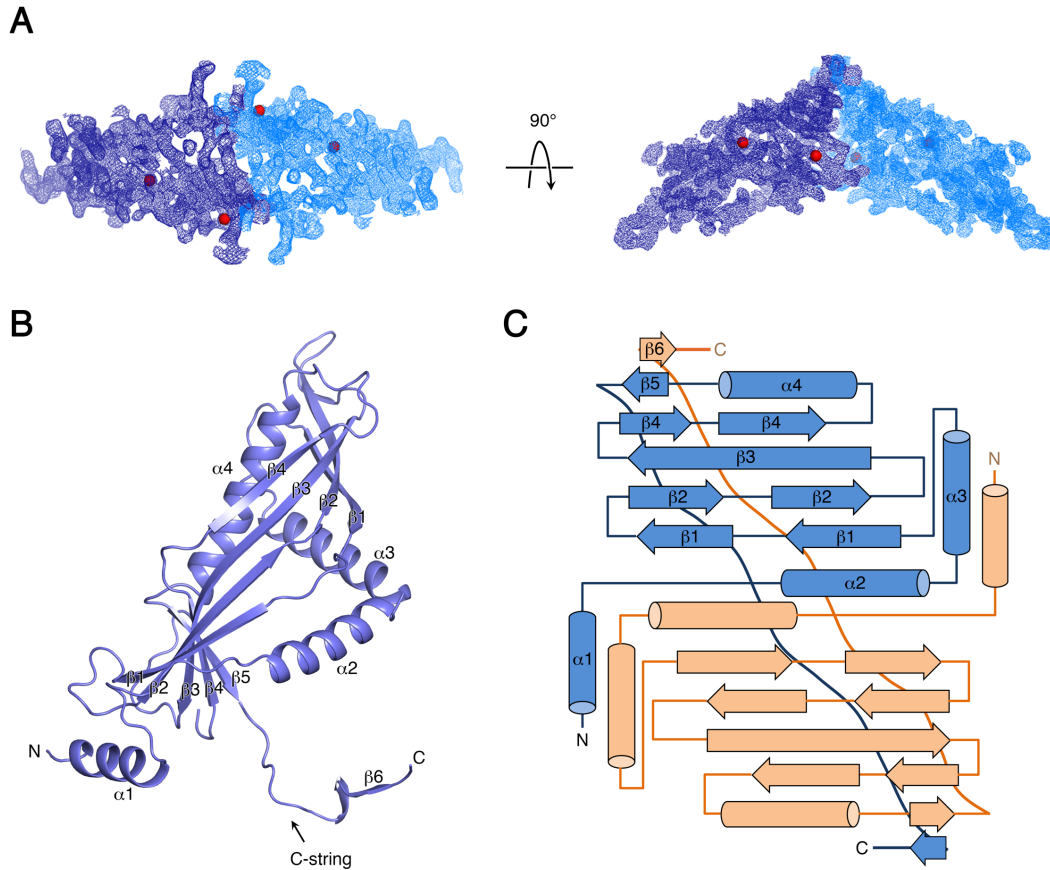
Figure 2.3. Structural analysis of the zrMmm1 SMP domain.

(A) Experimental electron density map (contoured at the 1.0 σ level at 3.1 Å resolution) for zrMmm1 in the dimeric SMP configuration. Crystals of zrMmm1 have one molecule of zrMmm1 in the asymmetric unit. Two protomers of zrMmm1 are organized by crystallographic symmetry in the $P3_221$ space group. The map was calculated using single-wavelength anomalous diffraction phases after density modification. Red spheres represent selenium atoms found by the Phenix program [45].

(B) Overall structure of the SMP domain of zrMmm1, showing the four α-helices and six β-strands.

(C) Schematic diagram showing the secondary structure elements and their organization in the zrMmm1 dimer.
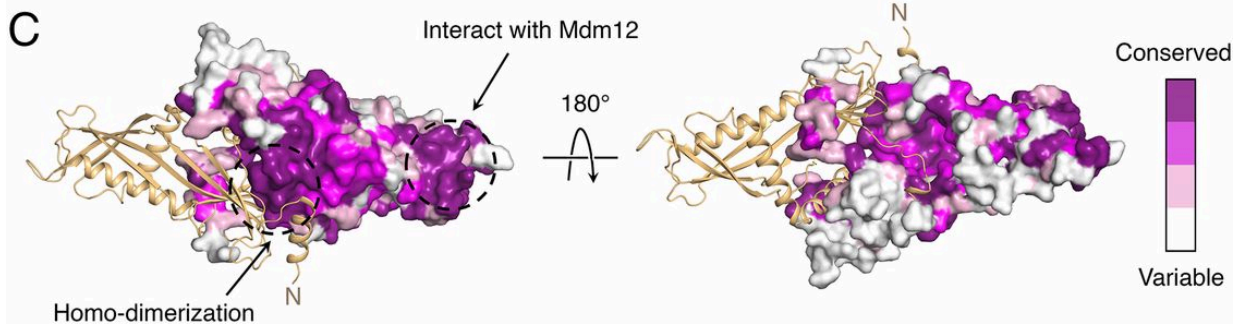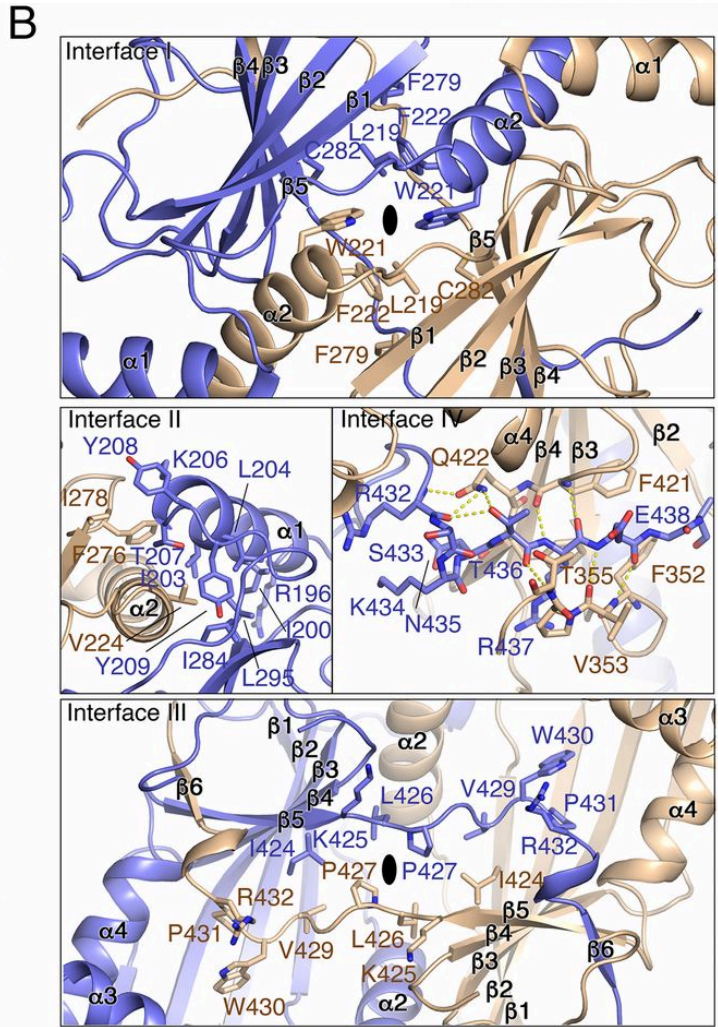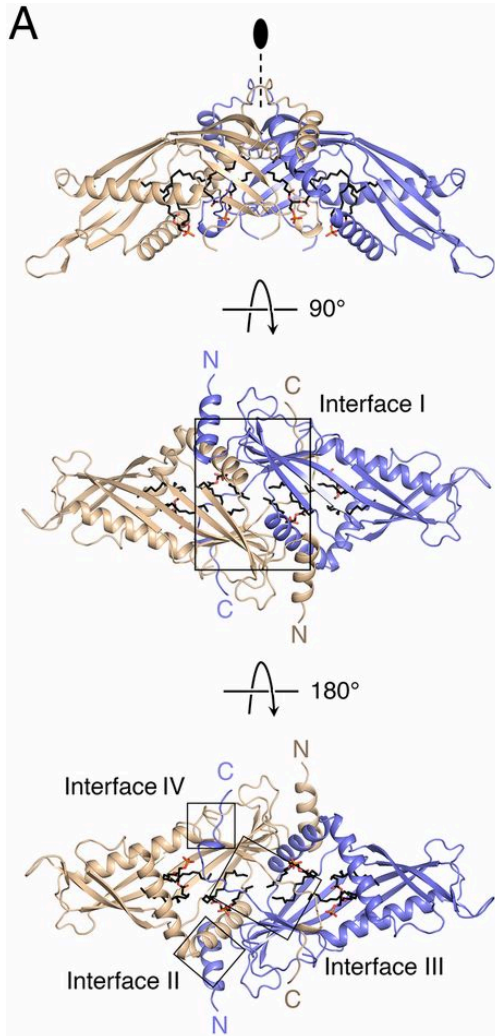
Figure 2.4. Crystal structure of the zrMmm1 SMP domain.

(A) Ribbon diagrams of zrMmm1 viewed in three orientations. The crystal structure of the SMP domain of zrMmm1 was determined by Se single-wavelength anomalous dispersion phasing and refined to 2.8 Å resolution. The protein adopts a dimeric SMP structure consisting of four helices and six strands in each monomer. Phospholipids bound to zrMmm1 are shown in black stick representation. Four dimeric interfaces for self-association are highlighted with black boxes.

(B) Close-up view of the highlighted boxes (interfaces I–IV). Key residues that contribute to the self-association of zrMmm1 are shown in ball-and-stick representation. Oxygen and nitrogen atoms are colored red and blue, respectively. Yellow dotted lines indicate intermolecular H-bonds.

(C) Molecular surface view of zrMmm1. The surface is colored according to sequence conservation from white (variable) to dark purple (conserved) as calculated by the Consurf server (consurf.tau.ac.il) [42] using 35 different yeast orthologs. To show the orientation of zrMmm1, one molecule of the zrMmm1 dimer is drawn in ribbon representation. Highly conserved regions indicated by dotted circles are essential for self-association or interaction with Mdm12.

2.3.3. The zrMmm1 Dimer Binds Glycerophospholipids.

The crystal structure revealed that recombinant zrMmm1 expressed in bacteria contained glycerophospholipids bound in the hydrophobic channel formed from the SMP domain (Figure 2.6A). Based on the observed electron density, we concluded that two glycerophospholipids were bound to each zrMmm1 molecule in two distinct regions: One phospholipid binds at the dimeric interface (proximal), and the other molecule is located in the middle (distal) part of the SMP channel. As mentioned above, the zrMmm1 dimer formed from symmetry-related molecules in the crystal, and the two phospholipids superimposed precisely over the two molecules of the zrMmm1 dimer, suggesting that the phospholipids are specifically recognized by zrMmm1 and were not the result of nonspecific binding. The head groups of two glycerophospholipids are located within a concave surface generated by helices α2–α4, and are solvent-exposed and disordered in the structure, suggesting that zrMmm1 does not possess clear selectivity for particular phospholipids, consistent with Mdm12 and E-SYT2 [20, 38] (Figure 2.6 B and C and Figure 2.5). However, unlike in other SMP domain proteins, the phosphate group and carboxyl oxygen of the distal phospholipid can be clearly seen in the structure, and are systematically coordinated by the conserved Arg253, Arg415, Trp411, Trp430, Arg432, and Ser433 through an extensive hydrogen-bonding network (Figure 2.6C). Among these, three residues (Trp430, Arg432, and Ser433) are from the opposing molecule in the dimer, suggesting that lipid coordination in zrMmm1 requires homodimerization.

To examine if zrMmm1 shows preferential binding to certain phospholipids in solution, we performed lipid displacement experiments using 1,2-dioleoyl-sn-glycero-3-phosphoethanolamine-N-(7-nitro-2-,3-benzoxadiazol-4-yl) (NBD)-PE, as reported in our previous study [20]. First, we confirmed the binding between NBD-PE and purified zrMmm1 using native PAGE and fluorescence detection (Figure 2.6D), and found that NBD-PE bound to zrMmm1 could be easily displaced by phosphatidylglycerol (PG), phosphatidic acid (PA), PS, or phosphatidylcholine (PC), but only relatively weakly by PE, even at high concentrations (Figure 2.6D). However, the NBD-PE on Mmm1 could not be displaced by the nonphospholipid cholesterol, ergosterol, or ceramide, even at high concentrations (Figure 2.6D). Based on these results, we conclude that zrMmm1 can bind efficiently to any glycerophospholipid. A previous structural study suggested that Mdm12 binds preferentially to PC or PE, both of which have a positively charged head group in common, via their negatively charged surfaces [20]. Analysis of the electrostatic surface potential of zrMmm1 using the Adaptive Poisson–Boltzmann Solver (APBS) program [39] revealed a strong positively charged region in the vicinity of the bound phospholipid head group (Figure 2.6B). Unlike Mdm12, the positively charged residues of zrMmm1 might be critically responsible for screening phospholipids themselves, not for the selection of certain head groups of phospholipids.

Next, we mutated key residues involved in lipid coordination and measured binding between zrMmm1 mutants and NBD-PE using blue native PAGE and fluorescence methods. As shown in Figure 2.6E, R415E, W411A, and W430A variants completely lost the ability to bind NBD-PE, while the negative control R379E could still bind NBD-PE. Interestingly, two bands consistent with the monomer and dimer of zrMmm1 were observed with the R415E and W430A mutants, supporting our structural analysis and conclusion that self-association of zrMmm1 is required for lipid conjugation, and suggesting that lipid binding might enhance the stability of the dimeric form.
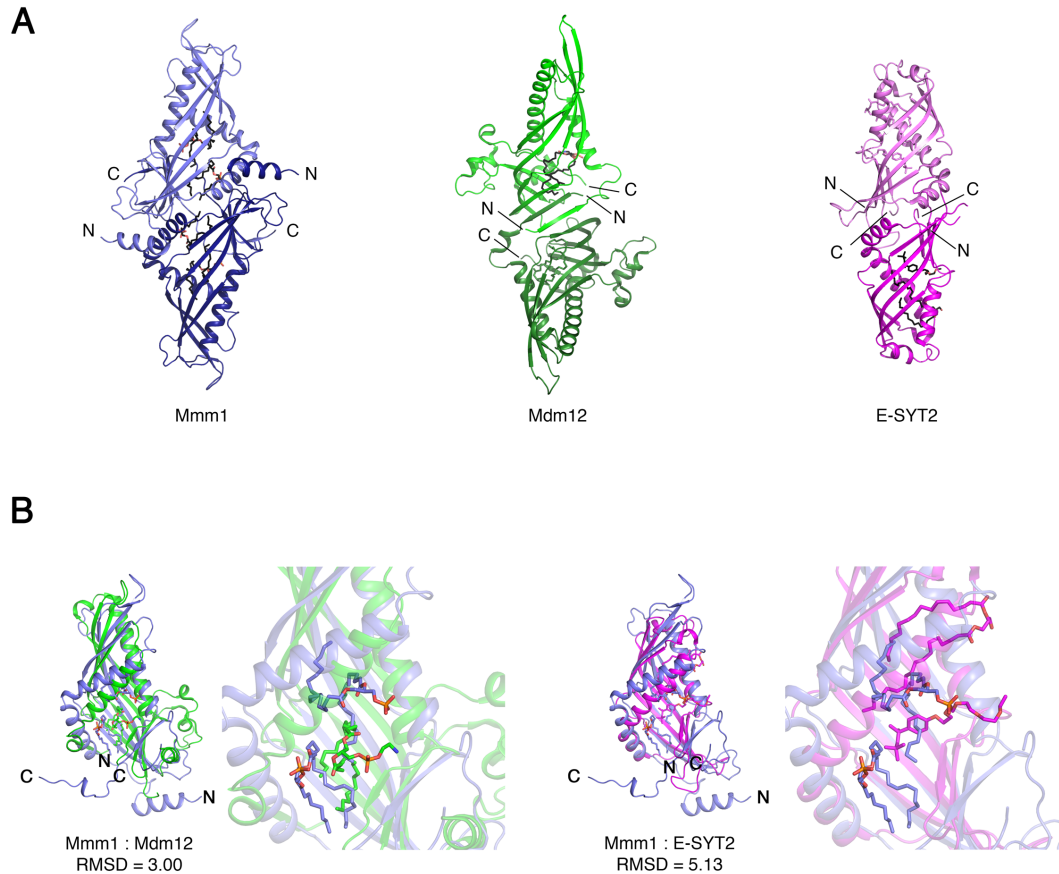
Figure 2.5. Structural comparison of the SMP domains of zrMmm1, Mdm12, and E-SYT2.

(A) Ribbon diagrams showing the overall structure of the SMP domain of zrMmm1, Mdm12 [Protein Data Bank (PDB) ID code 5GYD], and E-SYT2 (PDB ID code 4P42) in the same orientation. The zrMmm1, E-SYT2, and Mdm12 are colored blue, red, and green, respectively.

(B) Structural comparison of the zrMmm1 SMP domain (blue) aligned with those of *S. cerevisiae* Mdm12 (green, rmsd of 3.0 Å) and Homo sapiens E-SYT2 (red, rmsd of 5.13 Å). Phospholipid molecules bound to each protein are shown in ball-and-stick representation.

Figure 2.6. zrMmm1 binds to glycerophospholipids.

(A, Left**)** Overall structure of zrMmm1 (gray) bound to two phospholipids (black) viewed from the concave surface of the SMP domain. One molecule of zrMmm1 binds two phospholipids in two distinct regions, 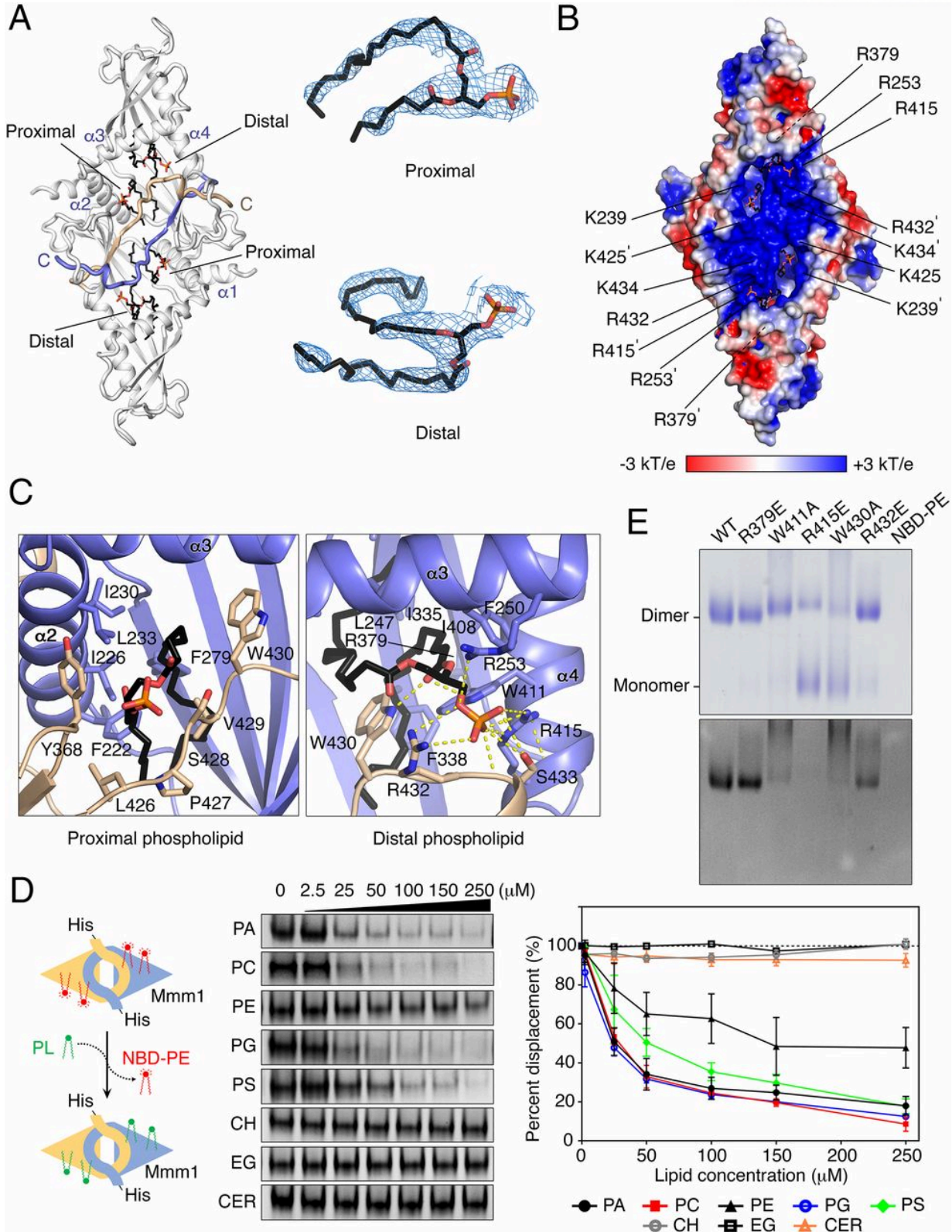referred to as proximal and distal phospholipids (details are provided in the main text). Highly conserved C-terminal loops in the zrMmm1 dimer that are important for specific and tight lipid conjugation are colored yellow and blue.

(A, Right**)** Molecular structures of the two phospholipids bound to zrMmm1 are shown with Fo-Fc electron density difference maps calculated in the absence of phospholipids (2.8 Å resolution, contoured at 2.0 σ).

(B) Electrostatic surface representation of zrMmm1 viewed in the same orientation as in A. The electrostatic potential was calculated with the APBS program [39], and colored from −3 (red) to +3 (blue) kT/e (k, Boltzmann's constant; T, temperature; e, charge of an electron).

(C) Ribbon diagram showing a close-up view of the coordination of bound phospholipids (black) by the SMP domains of the zrMmm1 dimer (blue and yellow). The dimeric organization of zrMmm1 is clearly essential for the specific interactions with the phosphate ion of the distal phospholipid.

(D) *In vitro* phospholipid displacement experiment using fluorescently labeled NBD-PE (details are provided in Materials and Methods). (Left and Center) NBD-PE preloaded His-zrMmm1 was incubated with natural phospholipid ligands (PA, PC, PE, PG, and PS) and nonphospholipid ligands (CER, ceramide; CH, cholesterol; EG, ergosterol) at increasing concentrations, and the quantity of NBD-PE displaced by natural ligands was measured as the diminishment in NBD-PE fluorescence. (Right) Graph indicates quantification data. Experiments were performed in triplicate. Means ± SD are shown.

(E) To probe interactions between wild-type (WT) or mutant (R379E, W411A, R415E, W430A, and R432E) zrMmm1 and phospholipids, proteins indicated in each lane were incubated with NBD-PE for 2 h on ice. Mixtures were separated by blue native PAGE, and binding was analyzed by Coomassie staining (Top) and fluorescence detection (Bottom).

2.3.4. Structure Determination of the Mdm12–Mmm1 Complex.

Mmm1 specifically interacts with the Mdm12 component of the ERMES complex (19, 20). In our previous study, we proposed a putative model for the Mdm12–Mmm1 complex involving dimerization via the SMP domains in a tail-to-tail manner. In this model, the conserved long C-terminal helices of the SMP domains lie adjacent to each other in a twofold rotation arrangement, resulting in an extended arch-shaped structure [20]. However, one of the concerns raised from this model was the lack of direct evidence for the tail-to-tail junction, and contacts between the self-associated Mdm12 molecules could be an artifact of crystallization (i.e., the result of crystal contacts rather than physiologically relevant molecular interfaces). Additionally, the potential interface between Mdm12 and Mmm1 in this model is exposed to solvent, suggesting that it is energetically unfavorable for hydrophobic glycerophospholipids to cross the solvent region in the Mdm12 and Mmm1 interface.

To further investigate how phospholipids could be transferred through the SMP domains of Mdm12 and Mmm1, we determined the crystal structure of the Mdm12–Mmm1 complex. Initially, we obtained crystals of the S. cerevisiae Mdm12–Mmm1 complex and hybrid complex of scMdm12–zrMmm1, but all were of low crystallographic quality. Through extensive screening, we eventually obtained diffraction-quality crystals of truncated scMdm12Δ, in which both the unstructured loop (residues 74–114) and proline-rich region (residues 184–211) were excluded, in complex with zrMmm1 (Figure 2.1A). The ability of scMdm12Δ to interact with zrMmm1 was assessed by SEC experiments (Figure 2.1B). However, crystals only diffracted to low resolution (~5 Å). To overcome this, we attempted dehydration of crystals using a higher percentage of precipitant, and the diffraction quality was dramatically improved (details are provided in Materials and Methods). Dehydrated crystals of the scMdm12Δ–zrMmm1 complex diffracted to 3.8 Å synchrotron radiation, and the structure was determined by the molecular replacement method. Crystals contained one heterotetramer organized in an scMdm12Δ-zrMmm1-zrMmm1-scMdm12Δ arrangement in the asymmetric unit (Figure 2.7A). The Mdm12 modification needed for crystallization did not affect the overall structure or binding to Mmm1 compared with wild-type Mdm12 (rmsd of 1.5 Å for all Cα atoms). The overall conformation of zrMmm1 and scMdm12Δ was not significantly changed upon formation of the complex (rmsd of 0.9 Å and rmsd of 1.5 Å, respectively). No apparent electron density corresponding to the hydrocarbon chain of glycerophospholipids was observed in the complex structure except for the phosphate group of phospholipids, but this might be due to the relatively low resolution of the complex structure or to treatments such as crystal dehydration.
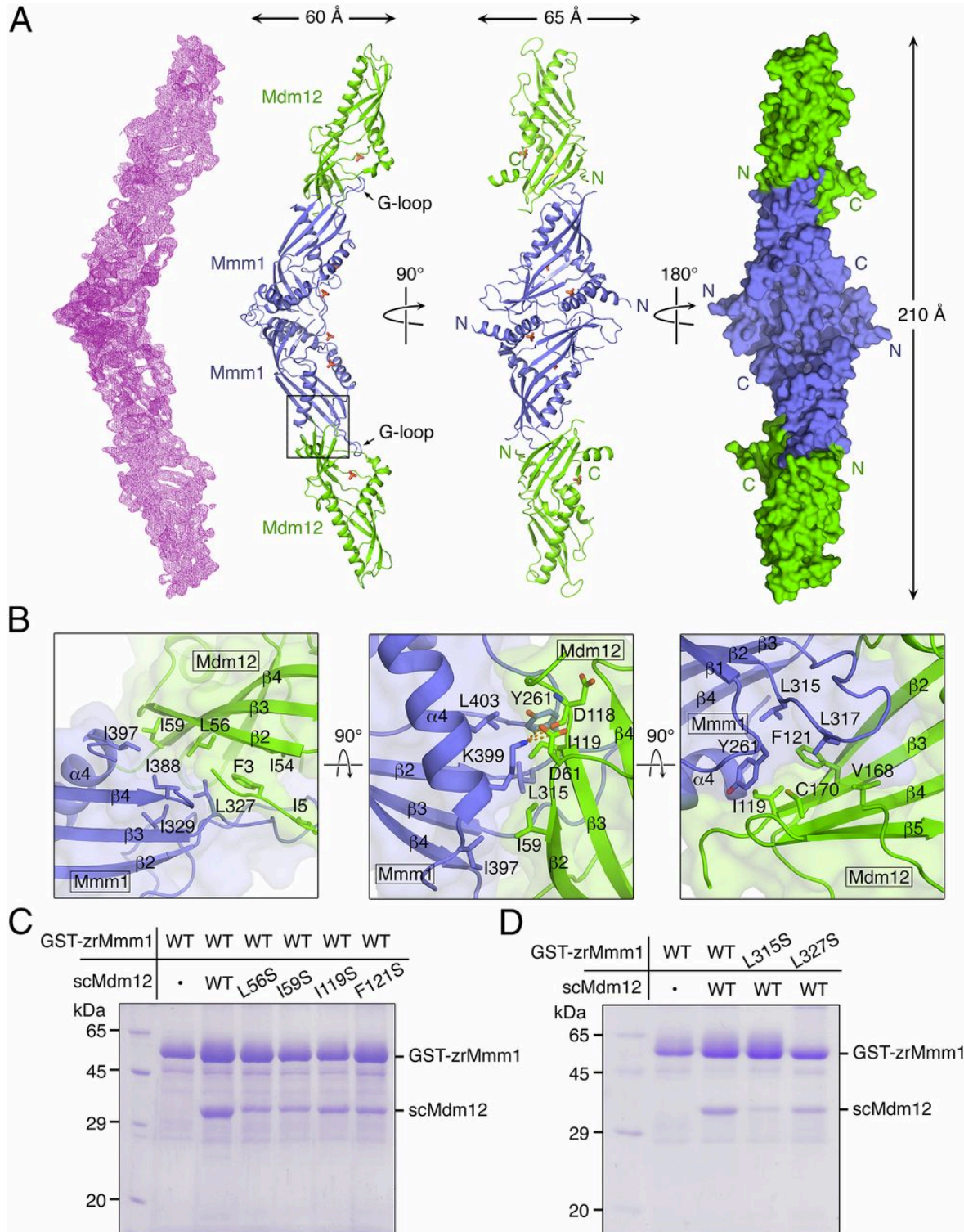
Figure 2.7. Overall architecture of the scMdm12Δ–zrMmm1 complex.

(A) Figures showing the overall architecture of the scMdm12Δ (green)–zrMmm1 (blue) complex. The structure of the scMdm12Δ–zrMmm1 complex was determined by the molecular replacement method and refined to 3.8 Å resolution. The 2Fo-Fc electron density map (Left, calculated with data to 3.8 Å resolution and contoured at 1.0 σ) and the surface representation of the crystallographic asymmetric unit of the scMdm12Δ–zrMmm1 complex (Right) are shown. Phosphate ions are shown as ball-and-stick models with red for oxygen and orange for phosphorus atoms.

(B) Binding interface between zrMmm1 and scMdm12Δ in three orientations. Residues involved in the interaction are shown in ball-and-stick representation.

(C) Role of scMdm12 residues in the interaction with zrMmm1 assessed through GST pull-down experiments using scMdm12 mutants (L56S, I59S, I119S, and F121S).

(D) SDS/PAGE showing the results of a reciprocal test of the effect of mutations in zrMmm1 (L315S and L327S) on the interaction with scMdm12. WT, wild type.

2.3.5. Architecture and Organization of the scMdm12Δ–zrMmm1 Complex.

The overall structure of the scMdm12Δ–zrMmm1 complex closely resembles the EM structure described in a previous study [19] (Figure 2.8A). The scMdm12Δ–zrMmm1 complex adopts an elongated curved and tubular structure with dimensions of $60 \times 65 \times 210$ Å. The zrMmm1 dimer is located at the center, with scMdm12Δ monomers bound at each end (Figure 2.7A and Figure 2.8A). Consistent with the previously reported model [19], scMdm12Δ and zrMmm1 are organized in a head-to-tail manner, with the N terminus of scMdm12Δ (referred to as the head) that is proximal to the dimeric interface in the scMdm12 dimer associating with the distal end (referred to as the tail) of the homodimeric interface of the zrMmm1 SMP domain. The interaction between scMdm12Δ and zrMmm1 appears to be strong, and buries 1,012 Å^2 of surface-accessible surface area. The truncated residues of the unstructured loop and proline-rich region of Mdm12 are not involved in the interaction. In the crystal structure of Mdm12 alone, the N terminus (residues 1–7) adopts a β-strand that is involved in self-association by forming a domain-swapped structure with the opposing molecule of the dimer [20]. However, no such conformation of Mdm12 was observed in the complex structure. Rather, the N terminus of scMdm12Δ forms an extended loop structure and lies adjacent to the β2 strand of scMdm12Δ itself.

The highly conserved β2 and β3 strands, the extended hairpin loop [referred to as the guide loop (G-loop)] generated between β2 and β3, and the α4 helix of zrMmm1 contribute to interactions with the β2 and β3 strands of scMdm12Δ (Figure 2.7B). In particular, the hydrophobic amino acids Leu315, Leu317, Leu327, Ile388, and Ile397 in zrMmm1 form extensive and coordinated nonpolar contacts with the side chains of Phe3, Ile5, Leu56, Ile59, Ile119, Phe121, and Cys170 of scMdm12Δ (Figure 2.7B). In addition, Lys399 of zrMmm1 forms a salt bridge and H-bonds with the side chain of Asp61 and the main chain of Asp118 of scMdm12Δ. To confirm whether these residues are involved in the interaction, we generated a series of zrMmm1 mutants and scMdm12 proteins (with GST fused at the N terminus of zrMmm1) and examined their binding ability using GST pull-down experiments. Single-residue mutants of scMdm12 (L56S, I59S, I119S, and F121S) lost appreciable affinity for zrMmm1 (Figure 2.7C). Likewise, single-site mutants of zrMmm1 (L315S or L327S) interacted with scMdm12 in a less stable manner (Figure 2.7D). Furthermore, to confirm the effect of the L315S mutation in solution, we titrated purified native and L315S mutant tag-free zrMmm1 proteins with purified scMdm12 over a wide protein concentration range and analyzed their interactions using native PAGE. As shown in Figure 2.8B, wild-type zrMmm1 interacted with scMdm12 and formed a heterotetramer in a concentration-dependent manner, while the L315S mutant did not interact with scMdm12 at even higher concentrations, suggesting that the observed hydrophobic contacts are critical for the Mdm12–Mmm1 interaction.
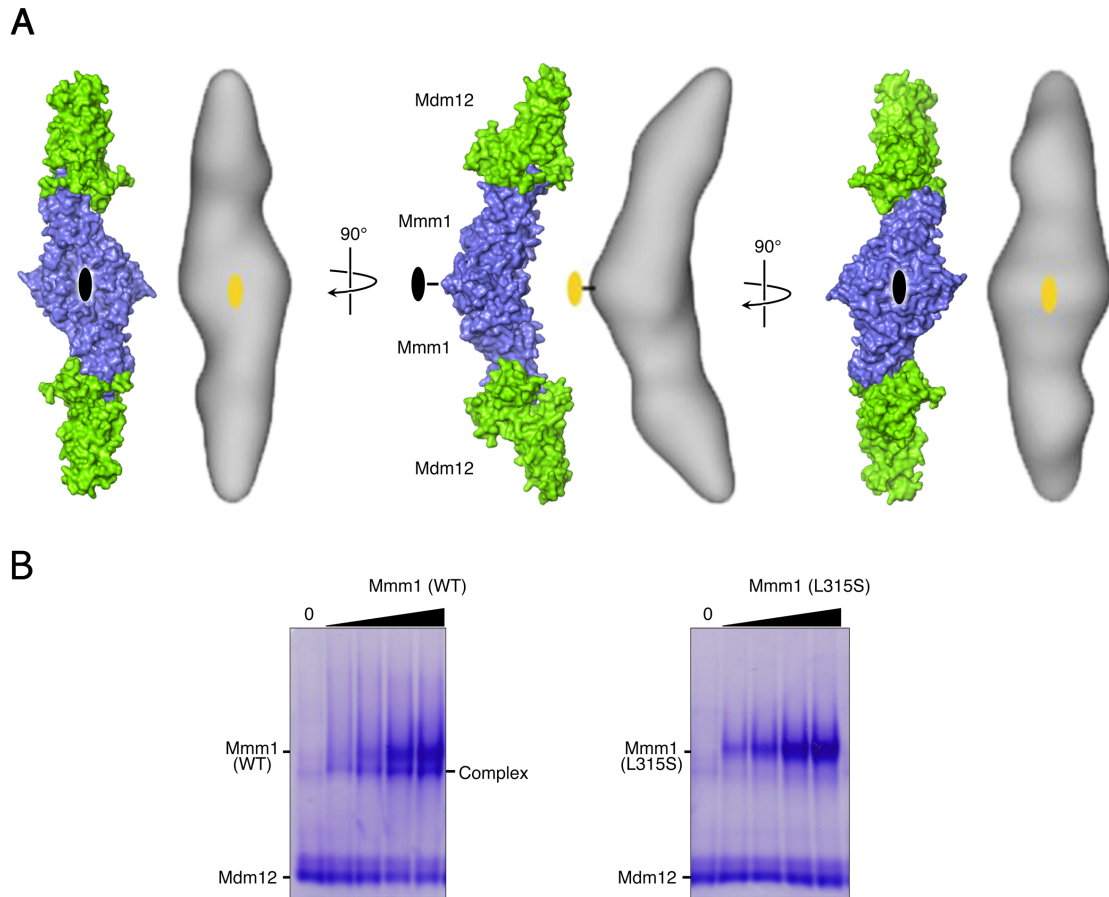
Figure 2.8. Structural alignment of the crystal structure and EM structure of the Mdm12–Mmm1 complex.

(A) Comparison of the 3.8 Å crystal structure of the scMdm12–zrMmm1 complex determined in this study and the 17 Å resolution negative-staining EM map of the Mdm12–Mmm1 complex presented previously [19]. Both structures revealed that the SMP domains of the Mmm1 dimer are located at the center and capped by two Mdm12 molecules, one at each end. The zrMmm1 and scMdm12 are colored blue and green, respectively. Twofold symmetry axes are indicated with yellow and black circles. For complete comparison, the structure of scMdm12Δ in the scMdm12Δ–zrMmm1 complex was replaced with that of the full-length scMdm12 (PDB ID code 5GYD) in this figure.

(B) Purified zrMmm1 [wild-type (WT) and L315S mutant] proteins were incubated with purified scMdm12 at different concentrations, and mixtures were separated by 8% native PAGE and stained with Coomassie Blue.

2.3.6. The scMdm12Δ–zrMmm1 Complex Has an Extended Hydrophobic Tunnel Mediating Lipid Trafficking.

Structural comparison between zrMmm1 and scMdm12 alone, and as part of the scMdm12Δ–zrMmm1 complex, revealed that the structure of zrMmm1 was changed slightly upon complex formation. Interestingly, the structural changes appear to be functionally relevant regarding phospholipid trafficking between the two distinct SMP domains. First, the G-loop of zrMmm1 undergoes a conformational change to form a more extended form that can plug into the scMdm12Δ head region and completely covers the solvent-exposed concave surface of scMdm12Δ (Figure 2.9A). Second, the β4 strand of zrMmm1 is extended by two residues (Leu387 and Ile388) in the complex, and these residues are part of a flexible loop and are solvent-exposed in the structure of zrMmm1 alone. By interacting with scMdm12Δ, Ile388 is projected inward toward the center of the SMP domain and contributes to the formation of a hydrophobic boundary at the junction of the two SMP domains (Figure 2.9B). Third, the conserved loop formed between β4 and α4, which are well ordered in the structure of zrMmm1 alone, becomes disordered upon forming a complex with scMdm12Δ. In particular, three hydrophilic residues (Arg391, Ser392, and Lys393) are not visible in the scMdm12Δ–zrMmm1 complex (Figure 2.9B). Finally, the α4 helix of zrMmm1 and the loop formed between α3 and β1 are pushed outward, generating a wider space inside the cavity that might be important for phospholipid trafficking (Figure 2.9 C and D). Taken together, the formation of the scMdm12Δ–zrMmm1 complex generates a continuous hydrophobic tunnel ~210 Å long through the elongated SMP domains of scMdm12Δ and zrMmm1, which could conceivably translocate phospholipids harboring nonpolar hydrocarbon chains between two components without consuming energy (Figure 2.9E). These results strongly indicate that the Mdm12–Mmm1 complex acts as a lipid-transferring vehicle in addition to tethering molecules to physically connect two distinct subcompartments.
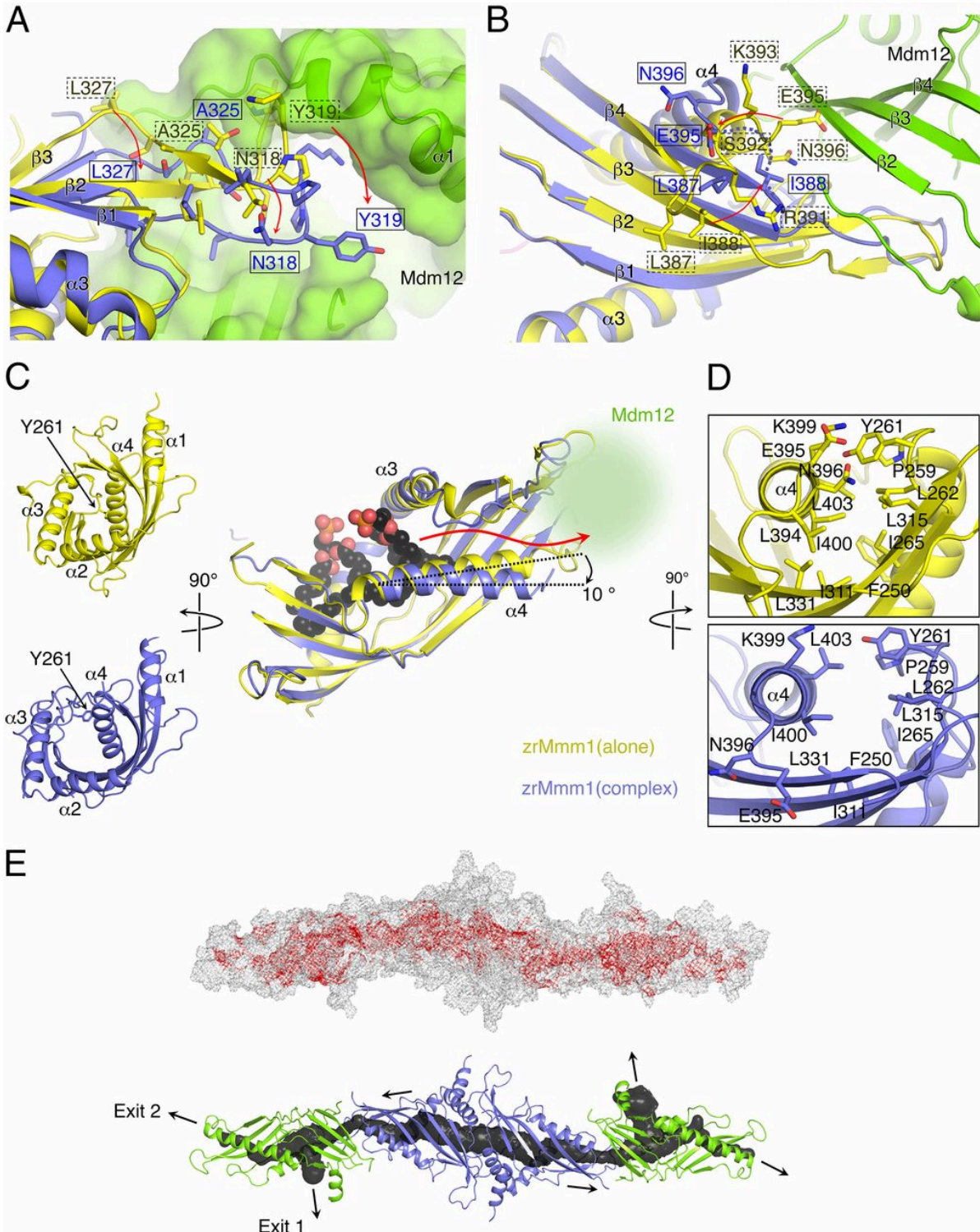
64

Figure 2.9. Direct association of zrMmm1 and scMdm12Δ generates a hydrophobic tunnel for phospholipid trafficking.

(A) Ribbon diagram showing superposition of zrMmm1 (yellow) and the scMdm12Δ (green)–zrMmm1 (blue) complex. To analyze structural changes in zrMmm1 upon association with scMdm12Δ, the structure of zrMmm1 was aligned with the zrMmm1 structure in the scMdm12Δ–zrMmm1 complex. The scMdm12Δ is shown in surface representation. The G-loop of zrMmm1 undergoes conformational changes following interaction with scMdm12Δ, forming an extended structure that covers the solvent-exposed region of scMdm12Δ. Residues of zrMmm1 undergoing this structural reorganization are shown, and their directions are indicated with red arrows.

(B) Structural changes in zrMmm1 occurring upon association with scMdm12Δ further highlighted (more information is provided in the main text) in a diagram colored the same as in A. The dotted line indicates zrMmm1 residues that become disordered upon forming the complex. (C, Right) Direct association of zrMmm1 and scMdm12Δ moves the α4 helix of zrMmm1 by ∼10° outward, vacating enough space to accommodate and transfer phospholipids. Phospholipids bound to zrMmm1 are shown in surface-filling representation. The red arrow indicates the putative pathway of phospholipids from zrMmm1 to scMdm12Δ.

(C, Left**)** Ribbon diagrams compare the overall structure of zrMmm1 in the apo (yellow) and complexed (blue) forms viewed from the left side of the figure **(C**, Right**)**. Loops, including Tyr261, in the complexed form are shifted outward, generating an open space in the process. The scMdm12Δ is omitted for clarity. The overall color scheme is the same as in A.

(D) Structures of zrMmm1 in the apo (yellow) and complexed (blue) forms viewed from the right side of the picture (C, Right).

(E) Overall structure of the scMdm12Δ–zrMmm1 complex shown in meshed line (Top) and ribbon (Bottom) representations. (Top) Red mesh representing hydrophobic amino acids inside the tunnel was superimposed on the figure. (Bottom) Channel (cavity) through the scMdm12Δ–zrMmm1 complex was analyzed by Mole 2.0 [43], and is shown in black tubule representation. Black arrows indicate the putative pathway for phospholipid trafficking.

2.3.7. The scMdm12–zrMmm1 Complex Binds All Glycerophospholipids Except for PE *in Vitro*.

To identify differences in binding priority to phospholipids between the scMdm12–zrMmm1 complex and zrMmm1 or scMdm12 alone, we performed a lipid displacement experiment using the scMdm12–zrMmm1 complex. Interestingly, NBD-PE bound to the scMdm12–zrMmm1 complex could be displaced only by PA, PG, PC, or PS (Figure 2.10A). In the case of PA, high concentrations resulted in band shifts above those of the NBD-PE preloaded scMdm12–zrMmm1 complex alone on native PAGE. No such changes have been observed using NBD-PE–preloaded scMdm12 alone [20]. However, high concentrations of PA also resulted in similar band shifts of NBD-PE–preloaded zrMmm1 alone, indicating that PA binding to zrMmm1 might affect the overall conformation of zrMmm1 or the scMdm12–zrMmm1 complex.

One of the most striking differences between zrMmm1 and the scMdm12–zrMmm1 complex was the absence of scMdm12-zrMmm1 binding to PE (Figure 2.10A). Even though both scMdm12 alone and zrMmm1 alone bound to PE with noticeable efficiency [20] (Figure 2.6D and Figure 2.10B), the scMdm12–zrMmm1 complex did not bind PE at all, suggesting that the association between scMdm12 and zrMmm1 affects the binding preferences of zrMmm1 and scMdm12 to phospholipids. Although the tests were performed using purified proteins in vitro, these results could have important biological implications. The PE component of the mitochondrial membrane might not be directly transferred from the ER but might be synthesized within the mitochondrial matrix via the conversion of PS to PE. Furthermore, the PE generated outside mitochondria via the Kennedy pathway might not be efficiently transferred to mitochondria for unknown reasons [40]. Consistent with this, the scMdm12–zrMmm1 complex did not engage in PE binding *in vitro*.

PS transfer to mitochondria is required for the synthesis of PE in mitochondria. Because scMdm12 alone could not bind PS [20] (Figure 2.10B), we inferred that the PS that displaced NBD-PE from scMdm12 in the scMdm12–zrMmm1 complex might have been directly transferred from zrMmm1. To verify this, we generated an Y261W mutant of zrMmm1. The Y261 residue is located at the interface between zrMmm1 and scMdm12 and is involved in generating a hydrophobic channel. However, the residue does not directly contribute to the interaction between scMdm12 and zrMmm1 (Figure 2.9C and Figure 2.10B). We hypothesized that the conversion of Tyr to Trp would sterically hinder the transfer of phospholipids between zrMmm1 and scMdm12. As expected, the mutation did not affect the association between scMdm12 and zrMmm1(Figure 2.10C), and PS binding by the zrMmm1 (Y261W) mutant was similar to that of wild-type zrMmm1 (Figure 2.11). However, in contrast to the wild type, the NBD-PE bound to the zrMmm1(Y261W)–scMdm12 complex was slowly displaced by PS (Figure 2.10D), suggesting that the bulky side chain of Trp sterically impeded

PS transfer from zrMmm1 to scMdm12 (Figure 2.10E). We also tested whether the mutation affected the displacement of NBD-PE from the zrMmm1(Y261W)–scMdm12 complex by PC and PG, and observed that PC, but not PG, resulted in slightly slow displacement (Figure 2.10D). Since scMdm12 alone could efficiently bind to PC and PG unlike PS [20] (Figure 2.10B), the effect of the mutation might not be significant in vitro. In summary, from these observations, we confirmed that the direct association of SMP domains in the scMdm12–zrMmm1 complex generates a hydrophobic tunnel for lipid trafficking.
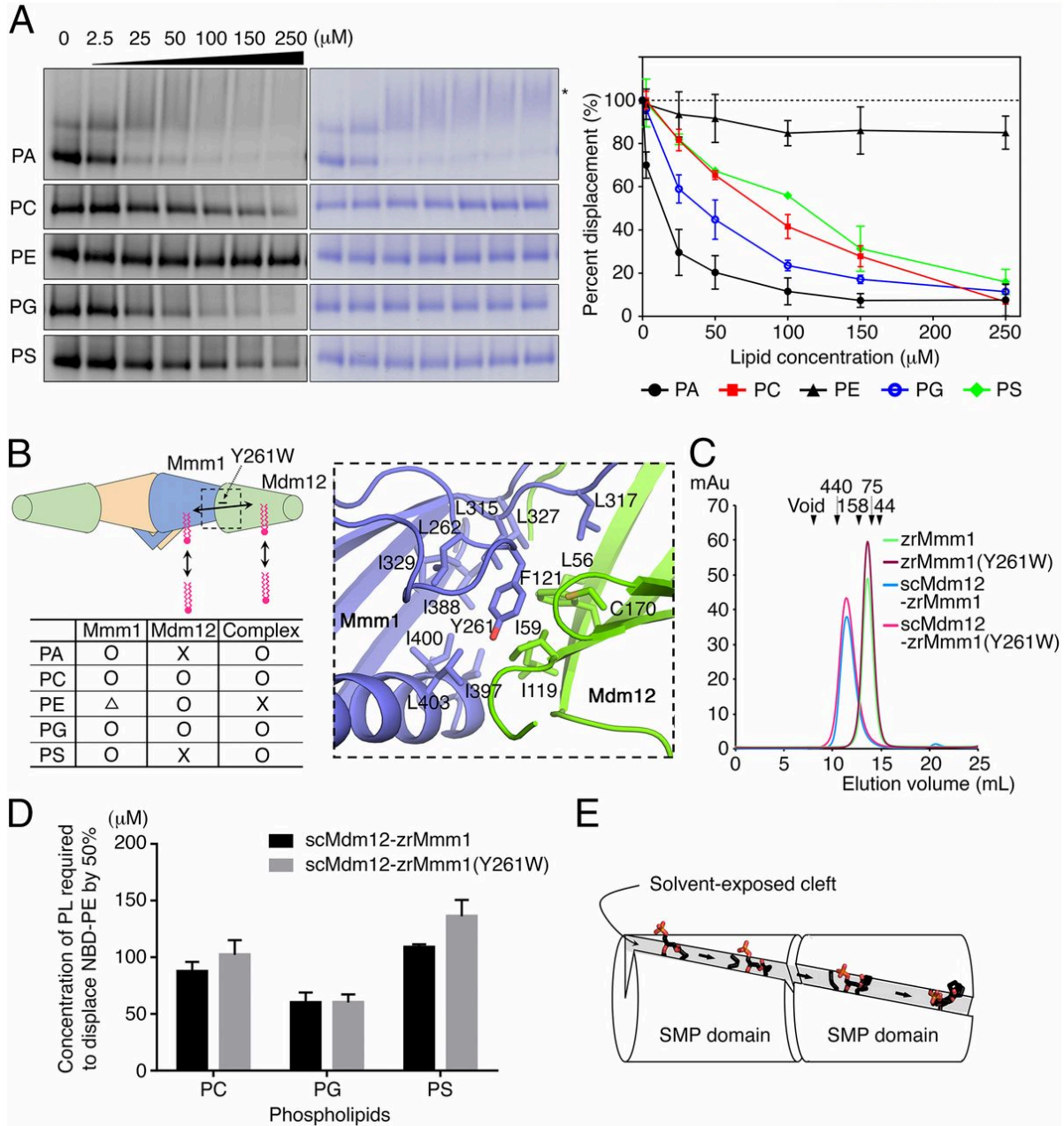
Figure 2.10. The scMdm12–zrMmm1 complex does not bind PE in vitro, and acts as a lipid transfer module.

(A) In vitro phospholipid displacement experiments using the scMdm12–zrMmm1 complex. NBD-PE–preloaded scMdm12–zrMmm1 complexes were mixed with increasing concentrations of phospholipids (PA, PC, PE, PG, and PS). Decreasing fluorescence was used to measure NBD-PE displacement by each phospholipid. (Left) Fluorescence and Coomassie staining of clear-native PAGE gels are shown side by side. (Right) Graph shows quantification data. Experiments were performed in triplicate, independently. Means ± SD are given.

(B, Left**)** Schematic diagram shows possible routes for phospholipid access to Mdm12 or Mmm1 in the Mdm12–Mmm1 complex. The table below shows a summary of the results of the phospholipid displacement experiment using Mmm1, Mdm12–Mmm1 complex (from this study), and Mdm12 [20]. The symbols X, Δ, and ○ indicate that the fluorescence reduction rate is within the range of 0–35%, 35–70%, and 70–100% at 250 μM, respectively, of each phospholipid. **(B,** Right**)** Ribbon diagram highlights the role of the zrMmm1 Y261 residue at the interface between scMdm12Δ and zrMmm1.

(C) SEC analysis shows that the Y261W mutant of zrMmm1 can still associate with scMdm12. Molecular weight standards are indicated above the chromatogram. mAu, milliabsorbance unit.

(D) In vitro phospholipid displacement experiment with the scMdm12–zrMmm1 complex (wild-type and Y261W mutant). The graph indicates the concentration of a phospholipid required to reduce the NBD-PE fluorescence signal by 50%. The bar graph shows means ± SD (n = 3).

(E) Schematic representation highlights the role of the SMP domain in phospholipid transport. The SMP domains in the two distinct subunits directly associate with each other, generating a successive hydrophobic tunnel through which phospholipid transfer can occur from one subunit to the other.
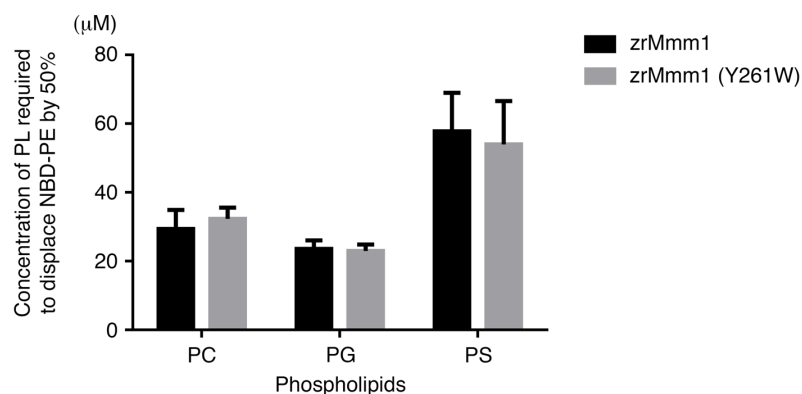
Figure 2.11. In vitro phospholipid displacement of wild-type and mutant (Y261W) zrMmm1.

To confirm Y261W mutant did not affect lipid-binding properties of zrMmm1 alone, in vitro phospholipid displacement experiments were performed using wild-type zrMmm1 and the Y261W mutant of zrMmm1. The graph indicates the concentration of phospholipid (PC, PG, and PS) that reduced NBD-PE fluorescence by 50%. The bar graph shows means ± SD (n = 3).

2.4. Discussion

SMP domains in ERMES and tubular lipid-binding superfamily complexes are believed to have a common role in binding and transferring lipids [41]. However, molecular recognition of specific phospholipids by SMP domains is not conserved among SMP-containing proteins. For example, scMdm12 has a binding preference for phospholipids harboring positively charged head groups, while the SMP domain of zrMmm1 broadly binds to most phospholipids, although zrMmm1 preferentially binds to PS, PA, PG, and PC. In addition, our previous work revealed that scMdm12 binds one molecule of phospholipid [20], while the zrMmm1 SMP domain binds two phospholipids in distinct regions (Figure 2.5B). Interestingly, the phosphate group of the distal phospholipid is specifically coordinated by conserved residues in zrMmm1 (Figure 2.6C). Specifically, two pairs of Arg-Trp residues (Arg415/Trp411 and Arg432/Trp430 from the opposing molecule of the zrMmm1 dimer), which are absolutely conserved among other Mmm1 orthologs, form an extensive H-bonding network with the phosphate ion and carboxyl oxygen of the phospholipid (Figure 2.6C). From this observation, we proposed that the Arg and Trp residues act as a filter for screening phospholipids among the pool of cellular lipids. This represents a unique feature of Mmm1 because most SMP domains bind hydrocarbon chains of phospholipids through nonpolar contacts with hydrophobic residues inside the cavity of the SMP domain.

Regarding phospholipid trafficking at the ER-mitochondria contact site, it is well established that PC is synthesized from PS via PE through the action of two enzymes that are distinctly located in the ER and mitochondria. The conversion of PS to PE is catalyzed by enzymes resident in mitochondria, whereas PA, an important intermediate in the formation of PG and cardiolipin in mitochondria, is synthesized in the ER [11]. PS, PA, and PG must therefore be transferred from the ER, their site of synthesis, to mitochondria. Furthermore, PC synthesized in the ER must be eventually translocated to mitochondria for maintenance of membrane integrity. Because Mmm1 is the only ER resident protein among ERMES components, and since Mmm1 might be involved in phospholipid selection from the ER, the specific and favored recognition of phospholipids by Mmm1 might help to facilitate efficient lipid trafficking. In this study, we structurally and biochemically demonstrated that zrMmm1 alone and the scMdm12–zrMmm1 complex preferentially bind to phospholipids. This apparent selective extraction of phospholipids, facilitated by the surface charge and phospholipid filter of Mmm1, might be critical to the initiation of cooperative phospholipid synthesis at ER-mitochondria contact sites.

The proximal surfaces of membrane proteins are often positively charged, and we therefore suggest that the positively charged concave inner surface in the SMP domain of zrMmm1 might interact closely with the ER membrane. The concave structure of zrMmm1 might complement membrane curvature in terms of shape and size. In addition, the adjacent circumference of a positively

charged patch composed of hydrophobic residues, including Y245, W238, P354, P357, and Y406, with the side chains of these residues exposed to the surface of zrMmm1, indicates that these residues might play a role in tight docking to the ER membrane (Figure 2.12 A and B). Interestingly, we observed that unlike the head groups of phospholipids bound to Mdm12, which are distal from the concave surface of Mdm12, the head groups of phospholipids bound to zrMmm1 project into the concave surface of zrMmm1 (Figure 2.12C). Moreover, the concave surface in the scMdm12–zrMmm1 complex precisely conforms to that generated by zrMmm1, strongly supporting the possibility that the concave inner surface of zrMmm1 binds to a convex membrane region.

Mmm1 interacts with Mdm34 through Mdm12 via relatively weak or transient interactions [19, 20]. Additionally, we previously suggested that the N terminus of Mdm34 might be involved in the interaction with Mdm12 [20]. Based on these findings, we propose two putative models for the organization of the ERMES complex. First, the N terminus of Mdm34 might interact with the N terminus of Mdm12 via β-strand swapping, as shown in the Mdm12 dimer [20]. Second, the head of the Mdm34 SMP domain might interact with the tail of the Mdm12 SMP domain, as shown in the Mdm12–Mmm1 interaction (Figure 2.7A). At present, it remains difficult to test these models because the interaction is likely to be transient. Interestingly, the scMdm12Δ–zrMmm1 structure demonstrates that it is possible to generate a continuous hydrophobic tunnel through both the head and tail of Mdm12 (Figure 2.9E), suggesting that the head and tail of Mdm12 might interact directly with the head of Mdm34. Future work is required to address exactly how the SMP domain of Mdm34 is organized in the Mmm1–Mdm12–Mdm34 ternary complex.

In conclusion, the Mdm12–Mmm1 complex establishes a molecular basis for protein-mediated MCSs between the ER and mitochondria, and for phospholipid trafficking through the ERMES complex.
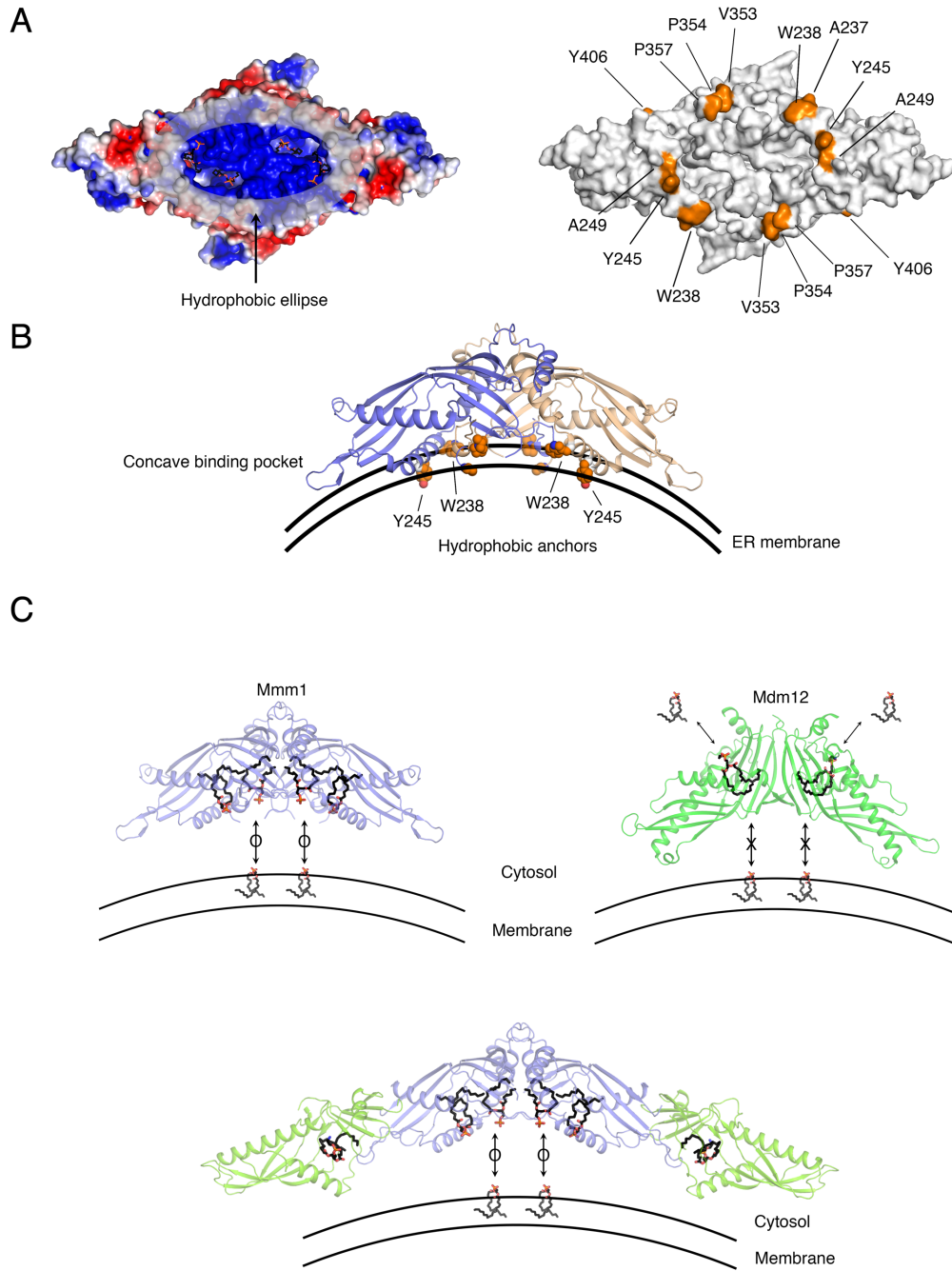
A

Y406
P357
P354 V353
W238 A237
Y245
A249
Hydrophobic ellipse
A249
Y245
W238
V353 P354
P357 Y406

B

Concave binding pocket
Y406 W238 W238 Y245
Hydrophobic anchors
ER membrane

C

Mmm1
Mdm12
Cytosol
Membrane
Cytosol
Membrane

Figure 2.12. Concave surface of the Mmm1 SMP domain apposes the ER membrane.

(A, Left**)** Surface charge representation of zrMmm1 viewed from the concave surface. **(A,** Right**)** Positively charged patch in the center is surrounded by conserved hydrophobic residues (yellow) that might be involved in anchoring to the ER membrane.

(B) Diagram showing the overall structure of the zrMmm1 dimer. This view is rotated 90° about the horizontal axis relative to A. Black lines indicate the putative curvature of the ER membrane. Side chains of the hydrophobic residues indicated in A are shown in surface-filling representation.

(C, Top**)** Ribbon diagrams show the arch-shaped dimeric SMP structure of the zrMmm1 (Left) and scMdm12 (Right, PDB ID code 5GYD). The view is the same as in B. The figures highlight the positions of phospholipids bound to zrMmm1 or scMdm12. Head groups of phospholipids bound to zrMmm1 face the ER membrane, whereas those bound to scMdm12 project toward the opposite side of the ER membrane, suggesting that zrMmm1 might take phospholipids from the ER. **(C,** Bottom**)** Concave surface shown in the scMdm12–zrMmm1 complex corresponds to the concave inner surface of zrMmm1 alone.

Table 2.1. Data collection and Refinement Statistics

	zrMmm1		scMdm12Δ-zrMmm1
Dataset	Native	Se-SAD	Native
PDB accession #			
X-ray source	Beamline 5C, PAL	Beamline 5C, PAL	Beamline 5C, PAL
Temperature (K)	100	100	100
Space group	$P3_221$	$P3_221$	$P6_5$
Cell dimensions			
a, b, c (Å)	125.50, 125.50, 60.88	125.60, 125.60, 60.90	87.56, 87.56, 436.88
α, β, γ (°)	90.00, 90.00, 120.00	90.00, 90.00, 120.00	90.00, 90.00, 120.00
Data processing			
Wavelength (Å)	0.97949	0.97950	0.97950
Resolution (Å)	50.0-2.80	50.0-3.10	50.0-3.80
	(2.85-2.80)	(3.15-3.10)	(3.87-3.80)
R_{merge} (%)	7.4 (39.5)	8.5 (39.0)	4.6 (83.6)
CC1/2	0.999 (0.354)	0.999 (0.847)	0.999 (0.741)
I / σI	26.8 (1.81)	16.6 (2.09)	27.5 (1.43)
Completeness (%)	99.2 (98.5)	99.3 (97.3)	99.8 (99.4)
Redundancy	9.4 (4.8)	6.7 (4.7)	5.8 (4.9)
Measured reflections	130987	130066	107706
Unique reflections	13895	19357	18583
Refinement statistics			
Data range (Å)	41.1-2.80		39.14-3.80
Reflections	13887		18456
R-factor (%)	19.36		24.77
R_{free} (%)	23.49		25.97
No. of Non-hydrogen atom	2059		6736
R. m. s. deviations			
Bond lengths (Å)	0.008		0.005
Bond angles (°)	1.387		0.906
Ramachandran plot, residues in			
Most favored (%)	92.4		87.6
Additional allowed (%)	7.2		11.0
Generously allowed (%)	0.4		1.4
Disallowed (%)	0		0

*Values in parenthesis are for the respective highest-resolution shells.

2.5. Materials and Methods

2.5.1. Plasmid Construction.

The DNA fragment encoding the SMP domain of Mmm1 (*Z. rouxii*, residues 190–444) was generated by PCR amplification from genomic DNA and cloned into the pET28b-SMT3 expression vector with BamHI and SalI restriction enzymes. To construct scMdm12Δ, residues 74–114 and residues 183–211 from full-length Mdm12 were substituted to GGSGG (E73-GGSGG-S115) and GG (D182-GG-S212), respectively, and cloned into the pCDF-duet vector with NdeI and XhoI. All mutants were generated by PCR-based mutagenesis, and mutations were confirmed by DNA sequencing.

2.5.2 Protein Expression and Purification.

All proteins in this study were expressed by transforming the expression plasmids into E. coli BL21 (DE3) bacterial cells. Cells were grown to an $OD_{600\,nm}$ of ∼0.7 at 37 °C with vigorous shaking and induced overnight at 18 °C with 0.3 mM isopropyl-β-D-thiogalactoside. Cells were collected by centrifugation at 3,200 × g for 15 min; resuspended in buffer A containing 25 mM sodium phosphate (pH 7.8), 400 mM sodium chloride, and 10 mM imidazole; and flash-frozen in liquid nitrogen for later use. The zrMmm1 proteins were purified by Ni^{2+}-immobilized metal affinity chromatography (Ni^{2+}-IMAC). His_6-SMT3 tags were removed by adding Ulp1 protease at a ratio of 1:1,000 (wt/wt), and proteins were dialyzed overnight against buffer B comprising 25 mM Tris·HCl (pH 7.5), 150 mM sodium chloride, and 5 mM β-mercaptoethanol at 4 °C. Digested proteins were passed through an Ni2+-chelating column a second time to remove SMT3 tags and undigested protein, followed by SEC with a Superdex 200 (16/60) column (GE Healthcare) preequilibrated with buffer C comprising 25 mM Tris·HCl (pH 7.5), 150 mM sodium chloride, and 5 mM DTT.

For the scMdm12Δ–zrMmm1 complex, pET28b-SMT3-zrMmm1 and pCDF-duet-scMdm12Δ plasmids were simultaneously transformed into *E. coli* BL21 (DE3) cells. The scMdm12Δ–zrMmm1 complex proteins were purified using Ni^{2+}-IMAC. After Ulp1 digestion, proteins were further purified by HiTrap Q HP (GE Healthcare) and Superdex 200 columns in buffer C. Purified zrMmm1 and scMdm12Δ–zrMmm1 complex proteins were concentrated to 12.5 mg/mL and 5 mg/mL, respectively, using Amicon ultra-15 centrifugal filters (Merck Millipore), and were flash-frozen at −80 °C for later use.

For selenomethionine-substituted proteins, the zrMmm1 plasmid was transformed and expressed in the *E. coli* B834 (DE3) methionine auxotrophic strain. Cells were grown in M9 minimal media supplemented with L-selenomethionine, and proteins were purified as described above.

2.5.3. Crystallization and Structure Determination.

For crystallization of zrMmm1, 1 μL of protein solution was mixed with an equal volume of reservoir solution containing 25% (wt/vol) polyethylene glycol (PEG) 10,000 and 100 mM Hepes (pH 7.5), and crystals were grown by hanging drop vapor diffusion at 4 °C. To obtain diffraction-quality single crystals of Se-Met zrMmm1, microseeds of native crystals were added into drops containing a mixture of Se-Met zrMmm1 protein solution and crystallization buffer under the same reservoir conditions. Crystals were cryoprotected by soaking in buffer containing crystallization solution supplemented with 30% (vol/vol) glycerol and flash-frozen in liquid nitrogen. X-ray diffraction data were collected from a single crystal at 100 K at the 5C beamline at the Pohang Accelerator Laboratory with a Pilatus M detector. Data were indexed, integrated, and scaled with the HKL2000 suite [44]. Crystals of native and Se-Met zrMmm1 diffracted to 2.8 Å and 3.1 Å resolution, respectively. Crystals grew in space group P3$_2$21 with one molecule in the asymmetric unit. The structure of the SMP domain of zrMmm1 was determined by selenium single-wavelength anomalous dispersion at a wavelength of 0.97949. Phenix AutoSol [45] found two selenium sites, refined these to give a mean figure of merit of 0.44, and yielded an initial electron density map of excellent quality. The model of zrMmm1 was refined to R/R$_{free}$ values of 0.194/0.235 via iterative rounds of refinement and rebuilding using Phenix [45] and Coot [46]. The final model has good geometry, with 99.6% and 0.4% of residues in favored and generously allowed regions of the Ramachandran plot. The following residues of zrMmm1 were not modeled because of disordered electron density: residues 190–193, residues 357–364, and residues 440–444.

The scMdm12Δ–zrMmm1 complex was crystallized at 18 °C by hanging drop vapor diffusion by mixing 1 μL of the complex with 1 μL of reservoir solution comprising 14% (wt/vol) PEG 4000, 100 mM Hepes (pH 6.5), and 100 mM ammonium sulfate. Because initial crystals diffracted to low resolution (~6.5 Å) using synchrotron radiation, crystals were dehydrated by gradually increasing the percentage of PEG 4000 up to 30%. Crystals were flash-frozen in harvest buffer supplemented with 25% (vol/vol) ethylene glycol. Crystals diffracted to a maximum resolution of 3.8 Å, and diffraction data were processed as previously described. The structure of the scMdm12Δ–zrMmm1 complex was solved by molecular replacement with Phaser-MR [47] using the structures of zrMmm1 (determined in this study) and scMdm12 (Protein Data Bank ID code 5GYD) as search models. The tetramer organized in an scMdm12Δ-zrMmm1-zrMmm1-scMdm12Δ arrangement was found as a molecular

replacement solution with a translation-function Z-score of 17.9 in space group P6$_5$. Model building and refinement were completed with Coot [46] and Phenix [45], respectively. The refined model contains residues 194–347, residues 369–390, and residues 395–439 of zrMmm1 as well as and residues 1–73, residues 116–182, and residues 212–265 of Mdm12. All molecular images in figures were generated using PyMOL (https://pymol.org/2/, version 1.7.4.3). Details of crystallographic data and refinement statistics are summarized in Table S1.

2.5.4. SEC.

To analyze relative molecular weight and assay for interactions between native or truncated scMdm12 and zrMmm1 (Figure 2.1B), protein samples were prepared in buffer C. Proteins at 1 mg/mL were applied to a Superdex 200 16/60 column (GE Healthcare) at a flow rate of 1 mL/min at 4 °C. In Figure 2.10C, 300 μg of wild-type proteins (His-zrMmm1 and His-zrMmm1–scMdm12 complex) or mutant proteins [His-zrMmm1 (Y261W) and His-zrMmm1 (Y261W)–scMdm12 complex] were subjected to chromatography on a Superdex 200 10/300 GL (GE Healthcare) column at a flow rate of 0.5 mL/min at 4 °C. A GE Healthcare gel-filtration calibration kit was used with protein standards (ferritin, 440 kDa; aldolase, 158 kDa; conalbumin, 75 kDa; ovalbumin, 44 kDa; carbonic anhydrase, 29 kDa; and ribonuclease A, 13.7 kDa).

2.5.5. Pull-Down Assay.

For GST pull-down, wild-type zrMmm1 and mutants zrMmm1 (L315S and L327S) were cloned into the pGEX-6p1 vector, and scMdm12 (wild-type, L56S, I59S, I119S, and F121S) was cloned into the pCDF-duet vector using NdeI and XhoI. Supernatants from *Escherichia coli* coexpressing wild-type or mutant scMdm12 and zrMmm1 were incubated with 10 μL of glutathione Sepharose 4B beads (GE Healthcare) preequilibrated with buffer A at 4 °C for 1 h. Beads were washed three times with buffer A containing 0.5% (vol/vol) Nonidet P-40 and 0.1% (vol/vol) Triton X-100. Proteins were eluted with 4× SDS sample buffer, and analyzed by SDS/PAGE and Coomassie Blue staining.

2.5.6. *In Vitro* Lipid Displacement Experiments.

For the lipid displacement experiments shown in Figure 2.6D and Figure 2.10A, the N-terminal His-tagged zrMmm1 (His-zrMmm1) or His-zrMmm1–scMdm12 complex was incubated with a twofold molar excess of NBD-PE purchased from Avanti Polar Lipids overnight on ice in buffer D (buffer C containing 0.3 mM N,N-dimethyldodecylamine N-oxide; Sigma–Aldrich). To remove

excess unbound NBD-PE, the mixture was incubated with Ni-nitrilotriacetic acid agarose beads (QIAGEN) for 30 min, and washed three times with buffer D. NBD-PE bound to His-zrMmm1 or His-zrMmm1–scMdm12 complex was eluted with buffer D containing 200 mM imidazole, and the protein solution was dialyzed against buffer D overnight and concentrated to 1 mg/mL. His-zrMmm1 or His-zrMmm1–scMdm12 complex (8 μL) preloaded with NBD-PE was mixed with 11 μL of buffer D and 1 μL of phospholipids dissolved in methanol. Reaction mixtures were further incubated for 2 h on ice, and analyzed by native PAGE as described previously [20]. Lipid displacement experiments involving mutants, His-zrMmm1 (Y261W) or His-zrMmm1 (Y261W)–scMdm12 complex, were performed in the same way as described above. All phospholipids were purchased from Avanti Polar Lipids: PA (1,2-dioleoyl-sn-glycero-3-phosphate), PC (1,2-dioleoylsn-glycero-3-phosphocholine), PE (1,2-dioleoyl-sn-glycero-3-phosphoethanolamine), PG (1,2-dioleoyl-sn-glycero-3-phospho-[1′-rac-glycerol]), and PS (1,2-dioleoyl-sn-glycero-3-phospho-L-serine). Nonphospholipid ligands, cholesterol (Sigma–Aldrich), ergosterol (Tokyo Chemical Industry), and ceramide (N-oleoyl-D-erythrosphingosine; C18:1 Ceramide [d18:1/18:1(9Z)]; Avanti Polar Lipids) were used.

2.5.7. Lipid-Binding Assays.

For the lipid-binding assays shown in Figure 2.6E, 19 μL of 0.5 mg/mL His-zrMmm1 (wild-type or mutants) in buffer D was mixed with 1 μL of 1 mg/mL 18:1 NBD-PE on ice. After 2 h, reaction products were subjected to 12% blue native (BN)-PAGE and analyzed as described above. BN-PAGE was carried out using the method of Schägger and von Jagow [48].

2.6. Reference

[1] Elbaz Y, Schuldiner M (2011) Staying in touch: The molecular era of organelle contact sites. *Trends Biochem Sci* 36:616–623.

[2] Helle SC, et al. (2013) Organization and function of membrane contact sites. *Biochim Biophys Acta* 1833:2526–2541.

[3] Phillips MJ, Voeltz GK (2016) Structure and function of ER membrane contact sites with other organelles. *Nat Rev Mol Cell Biol* 17:69–82.

[4] Kornmann B, Walter P (2010) ERMES-mediated ER-mitochondria contacts: Molecular hubs for the regulation of mitochondrial biology. *J Cell Sci* 123:1389–1393.

[5] Rowland AA, Voeltz GK (2012) Endoplasmic reticulum-mitochondria contacts: Function of the junction. *Nat Rev Mol Cell Biol* 13:607–625.

[6] Kornmann B (2013) The molecular hug between the ER and the mitochondria. *Curr Opin Cell Biol* 25:443–448.

[7] Lang A, John Peter AT, Kornmann B (2015) ER-mitochondria contact sites in yeast: Beyond the myths of ERMES. *Curr Opin Cell Biol* 35:7–12.

[8] Csordás G, et al. (2006) Structural and functional features and significance of the physical linkage between ER and mitochondria. *J Cell Biol* 174:915–921.

[9] Friedman JR, et al. (2011) ER tubules mark sites of mitochondrial division. *Science* 334:358–362.

[10] Tatsuta T, Scharwey M, Langer T (2014) Mitochondrial lipid trafficking. *Trends Cell Biol* 24:44–52.

[11] Flis VV, Daum G (2013) Lipid transport between the endoplasmic reticulum and mitochondria. *Cold Spring Harb Perspect Biol* 5:a013235.

[12] Lev S (2010) Non-vesicular lipid transport by lipid-transfer proteins and beyond. *Nat Rev Mol Cell Biol* 11:739–750.

[13] Kornmann B, et al. (2009) An ER-mitochondria tethering complex revealed by a synthetic biology screen. *Science* 325:477–481.

[14] Kornmann B, Osman C, Walter P (2011) The conserved GTPase Gem1 regulates endoplasmic reticulum-mitochondria connections. *Proc Natl Acad Sci USA* 108: 14151–14156.

[15] Murley A, et al. (2013) ER-associated mitochondrial division links the distribution of mitochondria and mitochondrial DNA in yeast. *Elife* 2:e00422.

[16] Stroud DA, et al. (2011) Composition and topology of the endoplasmic reticulum-mitochondria encounter structure. *J Mol Biol* 413:743–750.

[17] Belgareh-Touzé N, Cavellini L, Cohen MM (2017) Ubiquitination of ERMES components by the E3 ligase Rsp5 is involved in mitophagy. *Autophagy* 13:114–132.

[18] Kopec KO, Alva V, Lupas AN (2010) Homology of SMP domains to the TULIP superfamily of lipid-binding proteins provides a structural basis for lipid exchange between ER and mitochondria. *Bioinformatics* 26:1927–1931.

[19] AhYoung AP, et al. (2015) Conserved SMP domains of the ERMES complex bind phospholipids and mediate tether assembly. *Proc Natl Acad Sci USA* 112:E3179–E3188.

[20] Jeong H, Park J, Lee C (2016) Crystal structure of Mdm12 reveals the architecture and dynamic organization of the ERMES complex. *EMBO Rep* 17:1857–1871.

[21] Toulmay A, Prinz WA (2012) A conserved membrane-binding domain targets proteins to organelle contact sites. *J Cell Sci* 125:49–58.

[22] Kojima R, Endo T, Tamura Y (2016) A phospholipid transfer function of ER-mitochondria encounter structure revealed in vitro. *Sci Rep* 6:30777.

[23] Nguyen TT, et al. (2012) Gem1 and ERMES do not directly affect phosphatidylserine transport from ER to mitochondria or mitochondrial inheritance. *Traffic* 13:880–890.

[24] Elbaz-Alon Y, et al. (2014) A dynamic interface between vacuoles and mitochondria in yeast. *Dev Cell* 30:95–102.

[25] Hönscher C, et al. (2014) Cellular metabolism regulates contact sites between vacuoles and mitochondria. *Dev Cell* 30:86–94.

[26] Lahiri S, et al. (2014) A conserved endoplasmic reticulum membrane protein complex (EMC) facilitates phospholipid transfer from the ER to mitochondria. *PLoS Biol* 12: e1001969.

[27] Ellenrieder L, et al. (2016) Separating mitochondrial protein assembly and endoplasmic reticulum tethering by selective coupling of Mdm10. *Nat Commun* 7:13021.

[28] Meisinger C, et al. (2007) The morphology proteins Mdm12/Mmm1 function in the major β-barrel assembly pathway of mitochondria. *EMBO J* 26:2229–2239.

[29] Hobbs AE, Srinivasan M, McCaffery JM, Jensen RE (2001) Mmm1p, a mitochondrial outer membrane protein, is connected to mitochondrial DNA (mtDNA) nucleoids and required for mtDNA stability. *J Cell Biol* 152:401–410.

[30] Meeusen S, Nunnari J (2003) Evidence for a two membrane-spanning autonomous mitochondrial DNA replisome. *J Cell Biol* 163:503–510.

[31] Berger KH, Sogo LF, Yaffe MP (1997) Mdm12p, a component required for mitochondrial inheritance that is conserved between budding and fission yeast. *J Cell Biol* 136:545–553.

[32] Mao K, Klionsky DJ (2013) Participation of mitochondrial fission during mitophagy. *Cell Cycle* 12:3131–3132.

[33] Mao K, Wang K, Liu X, Klionsky DJ (2013) The scaffold protein Atg11 recruits fission machinery to drive selective mitochondria degradation by autophagy. *Dev Cell* 26:9–18.

[34] Böckler S, Westermann B (2014) Mitochondrial ER contacts are crucial for mitophagy in yeast. *Dev Cell* 28:450–458.

[35] AhYoung AP, Lu B, Cascio D, Egea PF (2017) Crystal structure of Mdm12 and combinatorial reconstitution of Mdm12/Mmm1 ERMES complexes for structural studies. *Biochem Biophys Res Commun* 488:129–135.

[36] Beamer LJ, Carroll SF, Eisenberg D (1997) Crystal structure of human BPI and two bound phospholipids at 2.4 angstrom resolution. *Science* 276:1861–1864.

[37] Qiu X, et al. (2007) Crystal structure of cholesteryl ester transfer protein reveals a long tunnel and four bound lipid molecules. *Nat Struct Mol Biol* 14:106–113.

[38] Schauder CM, et al. (2014) Structure of a lipid-bound extended synaptotagmin indicates a role in lipid transfer. *Nature* 510:552–555.

[39] Baker NA, Sept D, Joseph S, Holst MJ, McCammon JA (2001) Electrostatics of nanosystems: Application to microtubules and the ribosome. *Proc Natl Acad Sci USA* 98:10037–10041.

[40] Bürgermeister M, Birner-Grünberger R, Nebauer R, Daum G (2004) Contribution of different pathways to the supply of phosphatidylethanolamine and phosphatidylcholine to mitochondrial membranes of the yeast Saccharomyces cerevisiae. *Biochim Biophys Acta* 1686:161–168.

[41] Alva V, Lupas AN (2016) The TULIP superfamily of eukaryotic lipid-binding proteins as a mediator of lipid sensing and transport. *Biochim Biophys Acta* 1861:913–923.

[42] Ashkenazy H, Erez E, Martz E, Pupko T, Ben-Tal N (2010) ConSurf 2010: Calculating evolutionary conservation in sequence and structure of proteins and nucleic acids. *Nucleic Acids Res* 38:W529–W533.

[43] Sehnal D, et al. (2013) MOLE 2.0: Advanced approach for analysis of biomacromolecular channels. *J Cheminform* 5:39.

[44] Otwinowski Z, Minor W (1997) Processing of X-ray diffraction data collected in oscillation mode. *Methods in Enzymology*, ed Carter CW, Jr (Academic, New York), Vol 276, pp 307–326.

[45] Adams PD, et al. (2010) PHENIX: A comprehensive Python-based system for macromolecular structure solution. *Acta Crystallogr D Biol Crystallogr* 66:213–221.

[46] Emsley P, Lohkamp B, Scott WG, Cowtan K (2010) Features and development of Coot. *Acta Crystallogr D Biol Crystallogr* 66:486–501.

[47] McCoy AJ, et al. (2007) Phaser crystallographic software. *J Appl Cryst* 40:658–674.

[48] Schägger H, von Jagow G (1991) Blue native electrophoresis for isolation of membrane protein complexes in enzymatically active form. *Anal Biochem* 199:223–231.

Acknowledgements

5 년 간의 학위 과정 (2014-2018), 울산과학기술대학교 2 학년, 학부생 부터 시작된 8 년 간의 실험실 생활 (2011-2018) 을 끝으로 이제 유니스트 에서의 졸업을 앞두고 있습니다. 20 대 대부분의 시간을 파이펫을 손에 쥐고 밤 늦은 시간까지 실험실에서 보냈지만, 누구보다 최선을 다해 열심히 살아왔다고 생각하기에 후회는 없습니다. 졸업을 눈 앞에 둔 이제서야 연구가 무엇인지, 논문은 어떻게 쓰는지, 조금이나마 알 것 같습니다. 그 동안 정말 많은 분들께서 물심양면으로 도와주셔서 이 자리까지 올 수 있었습니다. 학위 논문을 마무리하며 짧게 감사의 인사를 전해 봅니다.

8 년전, 생화학 수업으로 처음 만난 이창욱 교수님. 아무것도 모르던 학부생인 저를 데리고 파이펫팅 부터 시작해서 모든 것을 가르쳐 주신 교수님, 교수님이 계셨기에 지금의 저도, 앞으로의 저도 있을 수 있습니다. 때로는 고민을 나눌 수 있는 편한 형처럼, 때로는 자상한 아버지처럼 대해 주시던 교수님이 계셨기에 힘든 과정 중에도 즐겁게 이겨낼 수 있었습니다. 항상 어디에 있던지 교수님의 가르침을 기억하며 좋은 제자, 좋은 과학자가 될 수 있도록 노력 하겠습니다.

그리고 바쁘신 일정 가운데도 흔쾌히 논문 심사 위원을 허락해 주신 강병헌 교수님, 박태주 교수님, 임정훈 교수님, 김은희 교수님께도 깊은 감사를 드립니다. 교수님께서 해주신 많은 말씀과 조언들, 앞으로 연구 하고 좋은 과학자가 되는데 있어서 값 진 밑거름으로 삼겠습니다.

긴 시간 동안 함께 지낸 실험실 식구들, 학봉, 주미, 동영, 현우, 서황 그리고 막내 혜진이 까지 모두 감사합니다. 교수님의 가르침을 잘 따라서, 모두 노력한 만큼 좋은 결과 나오길 바랄게.

그리고 대학원 학위 기간 동안 항상 옆에서 응원해주고 격려해주고 힘들 때 힘이 되어준 동료이자 여자친구인 주미, 항상 고맙고 사랑한다.

마지막으로 사랑하는 우리 가족, 멀리서 공부하는 아들 위해서 항상 기도와 격려해준 아빠, 엄마, 동생 모두 감사합니다. 가족이 있기에 웃을 수 있었습니다. 감사합니다. 사랑합니다.

한 분 한 분 전부 다 언급하지는 못했지만, 긴 실험실 생활 동안 도움을 주신 많은 분들께도 전부 감사의 말씀을 전합니다. 감사합니다.

Call to Me and I will answer you and tell you great and unsearchable things you do not know

Jeremiah 33:3